Title
PCR-free nucleic acid detector based on nanopore sensing

Author
Esfandiari, Leyla

Publication Date
2014

Peer reviewed|Thesis/dissertation

UNIVERSITY OF CALIFORNIA

Los Angeles

PCR-free sequence specific nucleic acid detector based on nanopore sensing

A dissertation submitted in partial satisfaction of the

requirements for the degree Doctor of Philosophy

in Biomedical Engineering

by

Leyla Esfandiari

2014

ABSTRACT OF THE DISSERTATION

PCR-free sequence specific nucleic acid detector based on nanopore sensing

by

Leyla Esfandiari

Doctor of Philosophy in Biomedical Engineering

University of California, Los Angeles, 2014

Professor Jacob J. Schmidt

The development of a rapid, sensitive, and cost-effective nucleic acid (NA) detection platform is highly desired for a range of diverse applications. We designed and developed an optical label free, PCR independent and potentially low-cost device for sequence-specific nucleic acid detection. The detection is based on conductance change measurement of a pore blocked by electrophoretically mobilized bead-(peptide nucleic acid (PNA) probe) conjugates upon hybridization with target nucleic acid. As the target NAs hybridize to the complementary PNA-beads, the beads acquire negative charge and become electrophoretically mobile. An applied electric field guides these NA-PNA-beads toward the pore, which they obstruct, leading to an indefinite, electrically detectable blockade of the pore. In the present of noncomplementary NA,

even to the level of single base mismatch, permanent pore blockade was not seen. We show application of this platform to detection of the anthrax lethal factor sequence.

Next, we demonstrated the operation of our device with longer DNA targets, and we described the resulting improvement in the limit of detection (LOD). We investigated the detection of DNA oligomers of 110, 235, 419, and 1613 nucleotides at 1 pM to 1 fM and found that the LOD decreased as DNA length increased, with 419 and 1613 nucleotide oligomers detectable down to 10 fM. Also, target DNA fragments at 10 fM concentration (approximately 6×10^5 molecules) were detected against a DNA background simulating the non-complementary genomic DNA present in real sample. In addition, no false positive responses were obtained with non-complementary, control DNA fragments of similar length. The 1613-base DNA oligomer is similar in size to 16S rRNA, which suggests that our device may be useful for detection of pathogenic bacteria at clinically relevant concentration based on recognition of species-specific 16S rRNA sequences. To investigate that we detected the specific sequence of 16S rRNA of non pathogenic *E.Coli* K-12 at 10fM detection limit. Two different non-pathogenic bacteria were used as negative experimental control and the universal PNA probe complementary to all three bacteria was used as positive experimental control. We could successfully detect *E.Coli* K-12 16S rRNA with no false negative and only one false positive at 3.5×10^4 colony forming units (CFU). This detection limit is below the threshold concentration limit for detecting the pathogenic *E.Coli* in urine and therefore our device has a potential to be used for detecting the clinically significant pathogens.

The dissertation of Leyla Esfandiari is approved.

Harold Monbouquette

Dino Di Carlo

Giovanni Zocchi

Jacob J. Schmidt, Committee Chair

University of California, Los Angeles

2014

Dedication

This work is lovingly dedicated to my aunt Shahla Esfandiari.
The memories of her endless love and kindness have strengthened my soul and made my heart warm throughout the difficult times of my life.
I promise to live the life that you deserved.

May rest in peace…

TABLE OF CONTENTS

1 Introduction 1

1.1 Significance 1

1.2 Optical readout 2

1.2.1 Optical fibers 2

1.2.2 Surface Plasmon Resonance . . . 3

1.2.3 Colorimetric detection 4

1.2.4 Quantum dot 4

1.2.5 Electrochemiluminescene 5

1.2.6 Microarray technology 5

1.3 Mechanical readout 6

1.3.1 Piezoelectric quartz crystal microbalance . . 7

1.3.2 Surface acoustic wave 7

1.3.3 Cantilever beams 8

1.4 Electrochemical readout 9

1.4.1 Enzyme indirect detection 9

1.4.2 Label-based electrochemical detection . . 10

1.4.3 Label-free detection 11

1.4.3.1 Capacitive detection method . . . 11

1.4.3.2 Impedimetry detection method . . 11

1.4.3.3 Field effect transistors 11

1.5 Magnetic readout 12

1.5.1 Substrate-based magnetic sensor . . . 12

1.5.2 Substrate-free magnetic sensor . . . 13
1.6 Summary 14

2 Background and proposed design 16
2.1 Design background 16
2.1.1 Coulter Counter 16
2.1.2 Nanopore Sensing 17
2.1.3 Nanopore and DNA Sequencing . . . 17
2.1.4 Nanopore sensors for sequence- specific NA detection 19
2.1.5 Proposed nanopre based sensor . . . 20
2.2 Project design 21
2.2.1 First element of the design 22
2.2.2 Second element of the design 26
2.2.3 Third element of the design 27
2.3 Experimental Procedure 28
2.3.1 Material 28
2.3.2 Probe coupling to microspheres . . . 29
2.3.3 Hybridization assay 29
2.3.4 Zeta potential, Electrophoretic mobility, Size measurements 30
2.3.5 Sensor apparatus and electrical measurements . 31

3 Proof of concept and sensor operations 33
3.1 Proof of concept 33
3.1.1 Model 42
3.2 Detecting the target nucleic acid 46
3.2.1 Model 51

3.3 Investigating the selectivity and sequence specificity of the system 52

4 Improving the concentration detection limit of the biosensor . 61

4.1 Hypothesis and experimental design 61

4.2 Procedure 63

4.2.1 Material 63

4.2.2 Sample preparation 63

4.2.2.1 Plasmid preparation 63

4.2.2.2 Plasmid digestion, DNA isolation and purification 64

4.3 Results and discussion 66

4.4 Conclusion 85

5 Detecting 16S rRNA species specific sequence . . . 87

5.1 Introduction 87

5.2 Sample preparation 91

5.2.1 Cell culturing and counting 91

5.2.2 RNA extraction and purification 92

5.2.3 Hybridization assay 92

5.3 Results and discussion 93

6 Conclusion and future work 101

6.1 Summary 101

6.2 Future work 104

References 109

ACKNOWLEDGEMENTS

First and foremost I would like to express the deepest appreciation to my adviser Prof. Schmidt for supporting me over the years of my graduate studies and teaching me to become an independent researcher. This research and dissertation could not have been completed without his insightful ideas and guidance. I would also like to extend my gratitude to my co-adviser Prof. Monbouquette for his support and valuable advice throughout. I am sincerely grateful to Prof. Weiss for encouraging me to pursue my research interest and his kind support. I would also like to thank my committee members Prof. Di Carlo and Prof. Zocchi for their time and constructive comments.

I wish to acknowledge that this research is supported by the National Institution of Health (NIH) and National Science Foundation (NSF).

I would like to express my warm thank to the dedicated and bright undergraduate reaserchers who assisted me in conducting experiments: Micheal Lorenzini, Gayane Kocharyan, Siqing Wang, Siqi Wang, and Anisha Banda, this work wouldn't be as comprehensive without your help. Also I would like to thank my collaborators in Prof. Monbouquette group: Allison Yorita and Bonhye Koo for their sincere endeavor and hard work. I would like to show my sincere appreciation to all Schmidt group members and alumni with special thanks to: Ahmad El-Arabi, Abha Jeurkar, Peter Du, Bin Lu and Dr. Takashi Nisisako. I was very fortunate to work with the greatest people at UCLA.

I like to give a special recognition to my special friend Dr. Ehsan Tarkesh Esfahani for his scientific consultation and help throughout my graduate school. Also, I would like to thank my great friend Adria Sherman for proof reading my dissertation.

Finally I would like to express my warm thanks to all my close family and friends for always being there for me. I also would like to express my gratitude to my strong, loving and devoted mother Dr. Shekoufeh Hosseini Barzi and to my tough loving, kind, and courageous father Dr. Mehrdad Esfandiari for encouraging me to pursue my dreams with no fear and always having my back. I can never repay you for everything you have given me throughout my life. Also, I would like to thank my departed grandfather Sattar Esfandiari and my generous loving uncle Dr. Bijan Esfandiari for their inspiration and support.

Leyla Esfandiari

Los Angeles

September 2014

VITA

2006	B.S., California State University of, Long Beach, Electrical Engineering
2008	M.S., University of California, Irvine, Biomedical Engineering
2014	Ph.D. Candidate, University of California, Los Angeles, Biomedical Engineering

PUBLICATIONS

L. Esfandiari , H. G. Monbouquette , J. J. Schmidt, "*Sequence-specific Nucleic Acid Detection from Binary Pore Conductance Measurement*" Journal of American Chemical Society (JACS), 2012, 134 (38), pp 15880–15886.

L. Esfandiari, M. Paff, W. C. Tang, "*Initial studies of mechanical compression on neurogenesis with neonatal neural stem cells*" 2012 Nanomedicine: Nanotechnology, Biology and Medicine, May 2012, 8(4), pp 415–418

L. Esfandiari , J.J. Schmidt, H. G. Monbouquette , "*PCR-Independent, Reagent-Free, Binary-Mode Nucleic Acid Detection*" 2012 American Institute of Chemical Engineers (AIChE), Oct 28th-Nov 3rd, 2012-Pittsburgh, PA.

L. Esfandiari, W.C .Tang, "*PDMS stretchable platforms for studies of mechanical compression on neurogenesis*" 2010 IEEE international Conference on Nano/Molecular Medicine and Engineering, 5-9 Dec 2010-Hong Kong.

CHAPTER 1

INTRODUCTION

1.1 Significance

Nucleic acids (NA) are the most fundamental building blocks of all organisms in nature. Hereditary genetic information embedded in DNA defines cellular function and structure and it determines the characteristics of species. Organisms vary from one another because their DNA molecules have different nucleotide sequences and consequently carry different biological messages. Therefore, reading and analyzing nucleic acid sequences can provide insight into the inner working of an organism. Moreover, molecular diagnostics play an important role in global health. It has been reported that 95% of deaths in the developing world result from limited access to proper diagnostics for infectious diseases[1].One promising option for detecting infectious diseases is to identify the pathogen-specific nucleic acids. As a result, there have been substantial attempts to develop a rapid, robust, portable, low-cost, and point-of-care diagnostic tool based on NA detection.

One of the revolutionized DNA analysis technologies took place in early 1970s by Sanger and Coulson. They developed the first generation of DNA sequencing [2] by using radioactively labeled dideoxynucleotide triphosphates (ddNTPs) as a chain terminator to stop DNA replication, resulting in DNA fragments which were then sequenced by electrophoresis. To date, most conventional DNA sequencing methods are based on Sanger's approach. Although sequencing a species' genome gives information on genetic function, many diagnostic

applications that detect the desired nucleic acid by sequencing it one nucleotide at a time resulting in a slow and inefficient process. Sequence-specific NA detection is a primary interest for a range of diverse applications such as screening for genetic diseases (detecting single polymorphosis (SNPs))[3,4], identifying harmful pathogens in food and water[5,6], paternity testing in forensic science[7], and detecting biological-warfare agents in homeland security[8]. The majority of conventional sequence-specific NA detection platforms rely on base pairing interaction between two single-strands of complementary nucleic acids. Generally, short single-stranded nucleic acids, termed probe molecules, are immobilized on a solid surface. As the complementary target NA molecules come in to contact with the probe molecules, hydrogen bonds are formed between each base pair which provide a specific and strong interaction that can be detected by optical, mechanical, electrochemical, or magnetic readouts[9].

In this chapter we explore various sequence-specific NA detection methods in detail and overview the advantages and shortcomings of these tools to address the motivation and significance of designing our novel sequence-specific NA detection platform.

1.2 Optical readout

There are a few optical methods for the detection of target nucleic acid specific sequence which are listed in this section.

1.2.1 Optical fibers

Optical fibers have been used as biosensors to propagate the signal emitted by fluorescently labeled target single-stranded DNA after hybridization to the tethered probe molecule at the end of the fiber. A fiber-optic array for multiplexing of oligonucleotide sequences was developed by

Fregusson et al. which tethered individual tip of the fiber-optic bundles to microspheres coated with various DNA probes and were detected by combinations of different fluorescent labels. This fiber optic microarray had low concentration detection limit in the range of zeptomolar[10]. In another study by Ying et al., a fiber optic approach for DNA hybridization detection was developed by fabricating layer by layer ultra-thin films on the surface of a thin-core fiber modal interferometer, which showed high sensitivity and specificity[11]. Although fiber optic biosensors are suitable for miniaturization, they have poor stability in presence of environmental light and require fluorescent labels. Another drawback of this technique is that the quartz optical fibers for UV light transmission are very costly[9].

1.2.2 Surface Plasmon Resonance

Surface plasmon resonance (SPR) is another optical method for sensing biomolecular binding events. SPR is based on changes in the optical reflectivity of a thin metal film when a target molecule binds to the probes on its surface. In a study by Buhl and coworkers, a SPR biosensor chip was developed to detect pathogenic double-stranded DNA auto-antibodies produced by patients with systematic lupus erythematosus[12]. The SPR biosensor and a DNA-RNA antibody-based assay was used for detecting microriobonucleic acids (miRNAs) in less than 30 minutes at concentrations down to 2 pM[13]. SPR based biosensors are optical label-free, have high specificity, and a short analysis time of around 10 minutes[14]. However, their low sensitivity requires up to 10μg per milliliter of nucleic acid for detection in addition to needing expensive and bulky optical instrumentations for operation[15].

1.2.3 Colorimetric detection

Colorimetric biosensors have been used as an alternative to the fluorescent labeling method for nucleic acid detection. Gold nanoparticle assays are a popular colorimetric detection tool that produces a visual readout based on varying inter-particle distances when target NA molecules bind to the conjugated probe molecules on the nanoparticles. Pioneered work by Mirkin's group has shown that the gold nanoparticles decorated by thiolated probe molecules can detect synthetic DNA[16]. In recent years, Kalidasan et al. used the same approach to detect Salmonella genome sequence at 37fM without PCR amplification[17]. In a study by Zeng and coworkers, a lateral flow biosensor based on gold nanoparticles and isothermal strand-displacement polymerase reaction was designed for visual detection of NAs with a limit of detection (LOD) of 0.01 fM[18]. The same group developed a hairpin DNA probe and gold nanoparticle assay for multiplex DNA detection with a 0.1fM LOD[19]. Although gold nanoparticles are valuable colorimetric biosensors for detecting NAs, they suffer from loss of reactivity when the ligands are covalently conjugated to their surface[20].

1.2.4 Quantum dot

Another optical label that has been used for NA detection is quantum dot (QD). Quantum dots are used for fluorescence tagging of probe biomolecules. They are brighter and are more photostable compared to the conventional organic fluorophores. Their color is directly correlated with their size and they have broad absorption spectra and narrow emission spectra with large emission shifts, which make this method a powerful tool for multiplex detection of different target molecules[9]. Feng and colleagues used QDs as biomarkers to functionalized nanotubes for enhanced sensitivity of DNA detection[21]. Giri et al. adapted a QD barcode platform to detect

infectious agents with a 10fM concentration limit[22]. An ultrasensitive single QD-based DNA nanosensor and the fluorescence resonance energy transfer (FRET) technique was reported by Wang's group for detecting un-amplified DNA molecules at low concentrations of ~50 copies of target DNA[23]. QD-based NA detection methods suffer from insolubility of the QDs in water when compared to classical fluorescent dyes[24].

1.2.5 Electrochemiluminescene

Electrochemiluminescene is a semi-optical method based on both optical and electrochemical readouts that has been used for sequence-specific NA detection in several studies[25,26,27]. This technique takes advantage of non radioactive, stable labels that emit light when electrochemically simulated. In the majority of electrochemiluminescence assays, the target nucleic acids needs an extra step of amplification prior to detection at low concentration of analytes. For example, in a study by Zhou et al. an electrochemiluminescence DNA sensor combined with isothermal circular amplification exhibited a 5 aM detection limit[28]. The extra amplification step is time consuming and expensive and therefore, there is a significant effort in the scientific community for eliminating this step in sequence-specific NA detection assays[29].

1.2.6 Microarray technology

DNA microarray (chip) technology offers state-of-the-art NA detection by hybridization. Similar to other NA hybridization based detection methods, the probe molecules are immobilized on a solid surface and make hydrogen bonds when fluorescently or enzymatically labeled complementary target NA strands come into contact with probe molecules. To reduce non-specific binding several wash steps are performed after hybridization. Subsequently, the captured

optically tagged NA targets can be detected by fluorescent microscopy or another non-fluorescent technique such as SPR. Microarray technology has been used in broad range of gene-based applications such as gene expression profiling, genotyping, single nucleotide polymorphosis (SNP) detection, nucleic acid diagnostic applications and protein-DNA interaction studies[30]. When integrated with microfluidic platform channels, microarray techniques advance to a high throughput assay, which can be used as a fast powerful tool for genomic sequencing[31]. This platform has been successfully commercialized in industry; examples being the GeneChip high density microarray from Affymetrix (Santa Clara, Ca, USA) and the BeadXpress array system from Illumina (San Diego, CA, USA). Besides the advantages of this method, DNA chip microarray suffers from several shortcomings. In this technique, real time polymerase chain reaction (RT-PCR) is required for labeling and amplifying the target NA molecule prior to detection which is time consuming and expensive as mentioned previously. Moreover, this technique utilizes sophisticated optical instrumentations for detection which are bulky, expensive and difficult to operate[32]. Furthermore, the labeled fluorophore molecules can photobleach and quench at non-uniform rates which can cause inaccurate readouts during optical detection.

1.3 Mechanical readout

Mechanical readout is another sequence-specific nucleic acid detection tool which is sensitive to changes in mass as the target nucleic acid molecules are captured by the tethered probes on a surface.

1.3.1 Piezoelectric quartz crystal microbalance

Piezoelectric quartz crystal microbalance (QCM) is a common mechanical readout technique that is based on a decrease in resonance frequency of an oscillating crystal surface upon hybridization of the target NA to immobilized probe molecules. QCM has been used for nucleic acid, protein and whole cell detection in many studies[33]. In one example of NA detection in a study by Chen et al., a circulating-flow piezoelectric biosensor based on gold nanoparticle amplification and verification method is used for real-time detection of pathogenic *E. Coli* O157:H7 [34]. In another study, detection of a cancer-causative mutation in the human TP 53 gene was reported using QCM [35]. Mascini's group has also shown the application of QCM for simultaneous detection and genotyping of 16 strains of the human papilloma virus[36].

1.3.2 Surface acoustic Wave

Another type of piezoelectric biosensor is a surface acoustic wave (SAW) platform and is similar to the QCM scheme. SAW is based on surface acoustic wave modulation that occurs as the result of an accumulation of mass on the surface when target NA hybridizes to immobilized probe molecules. This technique operates as follows: 1) an array of electrodes generates an input electrical signal which is transduced into mechanical waves, 2) the mechanical waves are influenced by physical phenomena such as changes in mass upon DNA hybridization, 3) the electrical signal is transduced back to receiver electrode arrays for analysis. The changes in SAW speed and amplitude are used to quantify the changes in mass and consequently the detection of target nucleic acid[37]. In a study by Xu et al. a surface acoustic wave biosensor in combination with DNA ligation and enzymatic signal amplification was used to detect Japanese encephalitis virus (JEV) with high specificity of single-nucleotide polymorphisms (SNPs) and 1pM detection

limit[38]. Roh and coworkers used a SAW biosensor that was coated with thin gold layer for detecting a 15 nucleotide long mutated DNA sequence that is known to cause Hunter Syndrome[39]. The main challenge of piezoelectric biosensors is that the sensor has to operate in liquid phase since the target bioanalyte is dispersed in solution, which will introduce multiple interfacial parameters to the system. Some of these parameters are the viscosity, ionic strength and dielectric constant of the solution which needs to be taken into account during the measurements. Therefore, accurate measurements of frequency shifts is challenging and the sensitivity of the piezoelectric biosensor decreases[40,41].

1.3.3 Cantilever beams

Microcantilever beam detection platform overcomes the piezoelectric sensor challenges by measuring not only the changes in resonance frequency of laser beam deflection but also by measuring the surface stress caused by the force involved in the DNA adsorption[42]. A study by the IBM Zurich research laboratory showed the clear detection of single based mismatch in 12 nucleotides long DNA by nanocantilever beams[43]. Moreover, in another study, Oakridge National laboratory reported the detection of SNP by cantilever based optical deflection assays[44]. Illic et al. demonstrated the detection of a single-stranded DNA molecule that was 1,587 base pairs long by the fabricated nanomechanical oscillator[45]. Although cantilever beams have better sensitivity compared to piezoelectric biosensors, reducing the non-specific binding by surface modification and treatment of nano-cantiliver beams remains challenging and tedious[46].

1.4 Electrochemical readout

Electrochemical DNA detection tools are based on changes in electrical parameters such as current, potential, conductance, impedance and capacitance upon hybridization of target NA molecules and probes tethered on an electrically active surface, such as electrode. Sequence-specific NA detection based on electrochemical readouts is a cost-effective, highly selective and sensitive tool and can be categorized into three different detection methods: enzyme indirect detection, label-based detection, and label-free detection methods[9].

1.4.1 Enzyme indirect detection

In the enzyme indirect detection method, DNA probe molecules are labeled by enzymes. The enzymes trigger the catalysis of a redox reaction upon hybridization of the target DNA. The electrochemical changes are detected by electrodes. Walter et al. demonstrated an electrochemical DNA detection method with a 1.2nM detection limit in which signal amplification was achieved by a heated gold electrode and enzymes labels[47]. In another study by the Willner group, a PCR-independent technique utilizing a hybrid electrochemical impedance spectroscopy and the QCM method was developed for the detection of the Tay-Sachs genetic disorder with LOD of 10fM[48]. Rapid and sensitive detection of *E.Coli* genome was investigated by the Zhang group where horseradish peroxidase (HPR) enzyme was used for amplified electrochemical detection on a microchip platform. The DNA probe was designed such that biotin conjugated DNA reacted with avidin-HPR for electrochemical signal enhancement, which improved the concentration detection limit to picomolar range[49]. Electrochemical readout by the enzyme amplification technique is the most successful tool for PCR-independent sequence-

specific nucleic acid detection. However, the drawbacks of this technique include the presence of background noise and the extra enzymatic labeling step when preparing the probe.

1.4.2 Label-based electrochemical detection

In the label-based electrochemical detection method, electroactive hybridization indicators bind to the captured single-stranded DNA target or to the double-stranded DNA immobilized on the electrode surface. This binding occurs by electrostatic attraction to the negatively charged DNA backbone or intercalation and groove-binding to the dsDNA with different affinities. The variation of affinity binding near the electrode surface can be indicated by electrochemical signals. Examples of electroactive hybridization indicators are heterocyclic dyes such as ethidium bromide or ferrocene derivatives and organometallic complexes. The label-based electrochemical strategy by impedance readout and dual amplification by polymerase reaction and hybridization chain reaction (HCR) enabled an 8fM concentration limit of detection of target NA[50]. In another study, ferrocene hybridization indicator was used to detect yeast DNA which was tethered to a self assembly monolayer (SAM)-functionalized gold electrode[51]. Takenaka et al. utilized an indicator with a higher electrochemical sensitivity, one that had better affinity to dsDNA and less affinity to ssDNA, and researched the zeptomole detection sensitivity[52]. The electrochemical readout has also been used as an alternative method in DNA chip to replace fluorescence microscopy[53]. The main shortcoming of this method is that some of these hybridization indicators, such as ethidium bromide, are mutagens and carcinogens and require specialized personnel training before operation.

1.4.3 Label-free detection

The last category of electrochemical readout is the label-free (direct) detection. In this technique, the intrinsic DNA electroactivity after hybridization is directly measured by electrical signals such as capacitive, impedance or conductance. This method is simple and time-efficient compared to the other two electrochemical readout techniques.

1.4.3.1 Capacitive detection method

In the capacitive detection method, the dielectric layer of electrode-solution thickens as the target molecule hybridizes to the probe molecule that is tethered to the surface of an electrode, which is detectable by a capacitance measurement. A genosensor was reported by Guiducci and coworkers that utilizes this capacitive detection method of DNA with thiolated and SAM-immobilized probes on gold electrodes[54].

1.4.3.2 Impedimetry detection method

Impedimetry DNA detection is based on an increase of impedance as the hybridization occurs between the target NA and immobilized probe on the surface of the electrode. Electrochemical impedence spectroscopy combined with magnetic nanoparticles is used for detection of 50 picomole HBV DNA and 160 picomole HIV DNA in 20 µl sample reaction volume[55].

1.4.3.3 Field effect transistors

Another attractive direct electrochemical detection subcategory is field effect transistors (FET). In this method, the silicon-based device indicates an increase in surface charge after DNA hybridization happens on the sensor surface. In a study by Bangar et al. a conducting nanowire

with a LOD of 0.1fM was fabricated to detect a 19 base pair breast cancer gene[56]. Gao and coworkers reported the detection of microRNA by a conducting polymer coated nanowire and the enzymatically catalyzed method to achieve a 5 fM detection limit[57]. In another study by the same group, arrays of n-type silicon nanowire (SiNW) were fabricated and peptide nucleic acids (PNA) were used as probe molecules to detect the complementary DNA target at 10fM LOD[58]. The nanowire technology is a sensitive and label-free DNA detection strategy; however, the device fabrication steps are tedious and costly and device-to-device uniformity, yield and scalability variations hinder further development of these biosensors into practical systems [59].

1.5 Magnetic readout

Magnetic bead bioassays are a powerful tool for detecting and separating biomolecules such as nucleic acids, proteins, cells and bacteria[60]. In general, NA detection by magnetic bead based bioassays involve a magnetic sensor detecting changes in static and dynamic properties of magnetic beads when target NAs hybridize to tethered probe molecules. Magnetic bead-based sensors can be categorized to substrate-based (sensor on chip) or substrate free platforms[9].

1.5.1 Substrate-based magnetic sensors

In substrate-based sensors, the surface of an electronic device is sensitive to changes in magnetic fields and therefore can detect the presence of magnetic particles on device's surface. Magnetoresistive platforms, micro-Hall devices, and magnetic force microscopy belong to substrate-based biosensors[61]. Hybrid substrate-based magnetic sensors with high sensitivity have been used for detecting DNA and RNA in several studies. For instance, Gabig-Ciminska and co-workers used an enzyme direct electrochemical detection method by silicon chip microelectrode

arrays and magnetic bead-based sandwich hybridization (BBSH) assay to detect artificially synthesized RNA and extracted 16S rRNA in amounts ranging from 10^{11} to 10^{10} molecules [62].

In a study by Mulvaney and co-worker, a magnetic-based biosensor was used without any amplification step for femtomolar detection of DNA and proteins. In this method, fluid force discrimination (FFD) assays combined with chip-based magnetoelectronic detection enabled for rapid and sensitive detection of analytes[63].

1.5.2 Substrate-free magnetic sensors

Substrate-free magnetic biosensors take advantage of the decrease in the magnetic bead's Brownian relaxation frequency as a result of the hydrodynamic size increase upon probe-target hybridization[61]. Micro/nano-scale magnetic BBSH assays based on this substrate-free scheme have been used for sequence-specific NA detection. For example, dual labels of metal nanoparticles and magnetic beads in a sandwitch based assay were used for high-sensitivity of DNA detection [64].

Furthermore, various amplification techniques such as rolling cycle amplification (RCA) or PCR have been coupled with substrate-free magnetic bead assays to achieve a low concentration detection limit. Magnetic particles mediated aggregation combined with RCA was utilized to detect specific NAs with a 124 fM detection limit[65]. In another approach a PCR based magnetic assembled sensor was developed for DNA detection at 4.26 aM[66]. Lee et al. developed an integrated system using antibody-conjugated magnetic beads and RT-PCR amplification step on a microfluidic platform to accelerate the detection of RNA viruses with sensitivity around 10-100 plaque forming units (PFU)[67].

Use of the magnetic bead bioassay can improve the sensor's LOD by preserving the small number of beads in hybridization and washing steps. During the washing steps small number of magnetic beads can be easily collected by a strong magnetic field in comparison to centrifugation steps in non-magnetic bead assays. Rapid magnetic bead collection can also decrease the time-duration of NA detection from hours to minutes. Magnetic bead biosensing has other significant advantages such as absence of background noise in magnetic readout since there is no magnetic background in most biological samples. Moreover, magnetic nanoparticles have high physical and chemical stability which is attractive when designing the biomolecular sensors[60]. Despite the many advantages of magnetic-based biosensors, nonspecific interactions of magnetic particles can occur with each other and with other materials present in the solution being analyzed. Aggregation of magnetic particles in the solution or absorption of clusters onto the sensor surface can result in false-positives or misleading measurements[61].

1.6 Summary

In summary, molecular diagnostics play an important role in global health, homeland security, criminology and discovering new species. Consequently, there is a significant demand for the development of hand-held, point of care (POC), fast molecular diagnostic devices where the signal can be readily detected and the overall cost of the device is low. As overviewed in this chapter, there are numerous biosensors with substantial specifications that have been developed in the past few decades for the detection of sequence-specific nucleic acids. However, these platforms contain a series of shortcomings which make NA detection expensive, time-consuming, bulky and complex. These shortcomings can include: PCR-dependency, labeling requirement, background noise /non-specific binding and the need of sophisticated and expensive

instrumentation. Therefore, there is a need for a DNA sequence detection technology that can surpass these shortcomings.

To overcome the difficulties of the current techniques, we proposed a sensitive, optical label free, cost-effective and easily measurable specific sequence nucleic acid detector. Our approach is PCR-independent and is based on the nanopore sensor concept. The idea behind this method is to generate an easily detectable on/off ionic current signal with high signal to noise ratio, in the absence/presence of the target NA macromolecule. The resulting decrease in ionic current in the presence of a target can be detected by a simple operational amplifier and indicated by a low power light emitting diode (LED). This sequence-specific NA sensor addresses many of the shortcomings of the conventional approaches and has remarkable biotechnological applications. Components of the sensor's design will thoroughly be discussed in the following chapter.

CHAPTER 2

BACKGROUND AND PROPOSED DESIGN

2.1 Design background

2.1.1 Coulter counter principle

The inspiration behind the proposed research project is based on the work of Coulter Counter[68]. In mid 1950s, the Coulter brothers invented a sensitive device that counted and sized individual microscopic particles. The principle behind their method is called "resistive-pulse sensing". In this approach, particles suspended in an electrolyte solution are forced to flow through a small current carrying aperture when a pressure difference is applied. As particles pass through the aperture, the electrolyte solution is displaced, causing a momentary increase of electrical resistance of the pore and a corresponding drop in conductance. The size of the change in ionic current signal is directly proportional to the volume of the particles, allowing size measurements to be taken. Furthermore, the concentration of the particles can be determined by analyzing the pulse frequency distribution. Since the 1950s, the Coulter counter principle has been widely used in clinical applications such as counting and analyzing blood cells, protein, and viruses[69].

In 1970, DeBlois et al. used the Coulter principle to improve the detection limit of the minimum particle size. They had observed larger noise in detection of smaller particles; therefore, to compensate for the high level of noise, they scaled the pore size down in their apparatus. Uniform pores of 10nm diameter were etched in non-conducting materials such as Laxan

Polycarbonate plastic sheets. Electrophoretic force was used to drive the charged polystyrene spheres of 90nm in diameter across the pore. The minimum particle size that their resistive pulse sensing apparatus could detect was ~60nm in diameter[70].

2.1.2 Nanopore sensing

The work of the Coulter brothers and DeBlois et al. established the foundation for the nanopore sensing field. The nanopore based sensors are inherently single-molecule-sensing devices and therefore hold particular promise for creation of practical, label-free and PCR-independent NA detectors. The field of nanopore sensing for NA detection was first commenced in 1996, when Kasianowicz et al. developed the first nanopore sensor for single-stranded DNA detection[71]. In their pioneer work, they used α-hemolysin (α-HL) embedded in a lipid bilayer membrane as a biological pore to which single-stranded DNA was electrophoretically driven through. The passage of each strand through the pore was detected as a transient decrease of ionic current across the pore and the transient pulse duration was proportional to the single stranded DNA length. These distinguishable electrical signals led to speculation that the system could be used for single-molecule nucleic acid sequencing.

2.1.3 Nanopore DNA sequencing

Following the pioneer work performed by Kasianowicz and coworkers, there has been a great effort for detecting and ultimately sequencing DNA by implanting the nanopore-based sensor. Solid-state nanopores have been created in substrate materials such as quartz, SiO_2/Si, and SiN. Also, biological protein pores imbedded in lipid bilayer such as α-HL and *Microbacterium Smegmatis* porin A (MspA) were used for DNA detection[72]. The first solid-state nanopore DNA

detection was reported by Saleh and Sohn. In this study, a synthetic pore of 200μm in diameter and 3μm in length embedded in PDMS was utilized for sensing the single molecules of ƛ-phage DNA as they electrophoretically passed through the pore[73].

In the past two decades many groups have attempted to sequence DNA by using this nanopore sensor approach[74]. However, despite the great effort of many research groups for nanopore DNA sequencing, this method has proven to be technically challenging. One of the substantial challenges of this method is the low sensitivity of the sensor to detect conductance changes as each nucleotide passes through the pore. This happens as a result of fast translocation (~ μ second) of small nucleotides through the pore under applied electric field. Additionally, the electrical current change across the nanopore is measured to be on the scale of pA and, therefore, expensive amplifiers with high bandwidths, are required for the detection of such a small signal. To overcome these limitations, researchers have designed numerous techniques to the slow down the DNA translocation through the pore[75,76] and have implemented sensitive, micro-scaled electrical current measurements using high bandwidth amplifiers[77]. To slow down the DNA translocation across the protein pore, Manrao et al. used the phi29 DNA polymerase along with MspA pore to pull the single stranded DNA through the pore and slow down the DNA translocation duration to 28 ms[78]. In another study by the Dekker group, lithium was replaced potassium in the electrolyte solution to act as a counter ion to bind to single- and double-stranded DNA. This decreased the rate of DNA translocation through a solid-state nanopore and therefore enhance the sensing resolution up to 10-fold[79]. In recent years, Rosenstien and coworkers developed a CMOS integrated nanopore platform to amplify the short DNA translocation (microsecond duration) signal when the DNA passes through a solid-state nanopore which enhanced the single molecule detection resolution[80]. Regardless of these appreciable endeavors,

DNA sequencing by the nanopore scheme has not been achieved and the issue of improving the single nucleotide resolution of the sensor is still under investigation.

2.1.4 Nanopore sensors for sequence-specific nucleic acid detection

In addition to a multitude of research studies regarding DNA sequencing by nanopore technology, there has been a great effort by other researchers to detect the sequence-specific nucleic acids utilizing nanopores[72]. For instance, Singer et al. used a solid state nanopore for single molecule detection of specific DNA sequences. In this method, double-stranded DNA was hybridized to peptide nucleic acid (PNA) probes for specific sequence detection. As the individual DNA molecules were translocated through the pore, the traces of the ionic current were measured electronically[81]. In another study by Balagurusamy et al., the resistive pulse sensing principle was used for detection of DNA hybridization. To slow down the translocation of the target DNA through the solid-state pore, a polystyrene sphere was attached to the hybridized DNA[82].

Additionally, protein pores imbedded in lipid bilayers have been used for sequence-specific NA detection. Bayley's group has engineered a "DNA-nanopore" for detecting a specific sequence of single-stranded DNA with single-base resolution. In this technique an individual DNA oligonucleotide was covalently attached to the lumen of the α-HL pore. Binding of the target single-stranded DNA to the tethered DNA strand caused detectable changes in the ionic current flow through the pore[83].Benner et al. reported the sequence-specific detection of individual DNA polymerase complexes using an α-HL pore. In this study, discrimination among unbound DNA, binary DNA/polymerase complexes, and ternary DNA/polymerase/deoxynucleotide triphosphate complexes was achieved in real time[84]. In recent years, Wang et al. showed the detection of

circulating microRNA strands in lung cancer patients using the α-haemolysin protein pore and complementary signal probes. The concentration detection limit of the sensor was sub-picomolar level and the sensor could distinguished the single-nucleotide differences between micro-RNA family members[85]. However, the key drawback of the biological pore systems is the instability of proteins in lipid bilayers and as a result these sensors are not satisfactory as point of care diagnostic devices.

2.1.5 Proposed nanopore based sensor

The majority of these techniques, both solid-state and protein based nanopore sensing devices, the target molecule was detected by measuring small transient changes in current (~pA) over a short period of time (μs to ms), and therefore translocation of each target through the pore required fast and sensitive amplification with large bandwidth measurements of a small signal. To overcome these drawbacks, a binary, sequence-specific NA detection concept based on permanent attenuation of nanopore conductance by electrophoretically mobile beads has been developed in the Schmidt and Monbouquette laboratory at University of California, Los Angeles and is the subject of this thesis. In the design, there is no need for fast, sensitive and expensive amplifiers since the signal is intrinsically amplified by the bead to ~μA and extends its duration indefinitely in response to the presence of target NA. This device also differs from other nanopore-based NA sensing systems in the sense that it is not directed at NA sequencing or concentration determination, rather it is designed for a binary-mode (yes/no) detection of the presence of NA molecules containing specific sequence. For many of the diagnostic applications, if not most, the importance is for a yes or no answer (binary response) regarding the presence or absence of the NA sequence of interest in a sample rather than a quantitative determination of

concentration. The advantages of our design greatly simplify device electronics and readout and are a key aspect of our approach to ultimately advance into a POC diagnostic tool.

2.2 Project design

The overarching goal of this research project is to design, construct, and demonstrate a nanopore-based device for target nucleic acid detection based on electrical detection of a hybridized polystyrene bead. The device consists of an electrically neutral bead-capture probe conjugate to which target NA can complementarily bind with sequence specificity. Upon binding, the bead becomes negatively charged and electrophoretically mobile. If this charged bead is driven toward a conical pore smaller than the bead diameter by an applied potential difference across the pore, the bead can occlude the pore, signified by a large reduction in the pore conductivity. If the NA in the solution is non-complementary and does not bind to the bead, the bead stays immobile under the applied potential difference and does not block the pore (Figure 2.1). In this approach, the bead effectively amplifies the physical size of the NA, giving it a much larger and more easily detected reduction in current when it is inside the pore. Further, because the bead is larger than the pore, the blockade is permanent and does not require rapid data acquisition to capture and display the detection event.

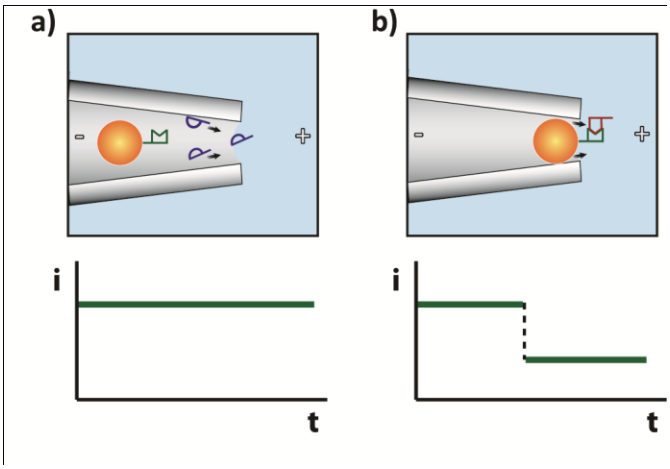

Figure2.1 a) In an applied electric field (+ and – symbols), charge neutral bead conjugated with probe molecule (PNA) in a conical capillary are electrophoretically immobile in the presence of non-complementary NA, which passes through the capillary pore without significantly altering the measured current. **b)** Complementary NA binds to the PNA-bead, making the complex negatively charged and electrophoretically mobile, thereby resulting in the NA-PNA-bead blocking the capillary, which results in a large and persistent reduction in conductance.

The design of the present device is classified into three main elements: a solid-state pore, a functionalized polysterene bead that serves as the probe substrate, and the peptide nucleic acid (PNA) probe molecule.

2.2.1 First element of the desing

The pores used in our system are the capillary openings formed at prepulled glass micropipette tapered to a 2µm diameter (Figure 2.2).

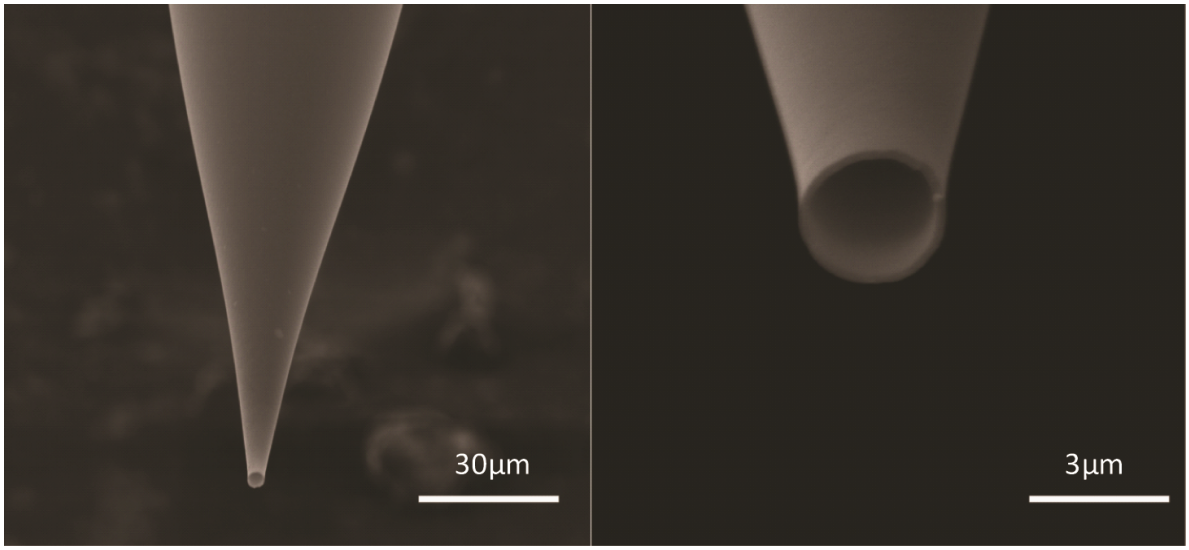

Figure 2.2 SEM image of the prepulled glass micropipetts

The glass micropipette has several advantages over solid-state pores fabricated on a plane substrate such as SiN: the glass capillary can withstand considerable longitudinal hydraulic pressure necessary to wet the channel containing the electrolyte solution and the fabrication of the micropipette requires relatively inexpensive laser puller and a one-step fabrication process. Similar glass capillary pores with a diameter of 50nm have been used to detect the translocation of single DNA molecules attached to a 10 nm gold nanoparticle[86]. In a study by Steinbock et al. the detection of the folding state of double-stranded DNA in a nanocapillary with a diameter of 45nm was shown by the resistive pulse technique[87]. Moreover, functionalized nanopipettes were used as label-free, single cell biosensors in many studies[88]. Additionally, nanopipettes have been used as electrochemical biosensors for detecting nucleic acids and proteins. For instance, nanopipette tips functionalized with antibodies were used for detecting antigens[89]. When the target antigen binds to the tethered antibody, the ionic current passing through the nanopipette rectifies as a result of partial blockage of current by captured antigen and this current rectification indicates the detection of the target molecule. In another study, dendrimer modified

nanopipette was used to detect hybridization of a specific DNA sequence by the same concept[90]. Pourmand's group has improved this technology for quantitative detection of thrombine by decorated aptamers on the tip of nanopipette[91]. The massive use of micro/nano capillaries in molecular biosensors confirms the validity of micropipette application in our sensor design.

However, there might be some challenges when utilizing glass micropipettes in the operation of this novel nanopore based system which will be discussed here. One of the possible challenges is electroosmotic flow (EOF) that could oppose the electrophoretic movement of hybridized charged bead (DNA-PNA-sphere) and prevent pore blockage. Electroosmosis occurs when silanol (Si-OH) groups on the surface of silica (or Si) are ionized to negatively charged silanoate (Si-O-) groups at pH > 3. As a result, positively charged cations will be attracted to the negatively charged silanoate groups, forming two inner layers. The first layer is referred to as the fixed layer (or double layer) since it is held tightly to the silanoate groups. The outer layer is called the mobile layer as it is farther from the silanoate groups. When an electric field is applied, the mobile cation layer is pulled in the direction of the negatively charged cathode, dragging the bulk buffer solution with it to result in electroosmotic flow. For thin electric double layers, the electro-osmotic velocity of the fluid (u_{EOF}) can be described by Helmholtz-Smoluchowski (HS) model [92] which yields to a simple equation shown as Equation 1.

$$u_{EOF} = -\frac{\varepsilon \zeta E}{4\pi\mu} \tag{1}$$

In Equation 1, ε is dielectric constant of the fluid, E is the applied electric field, μ is the fluid viscosity and ζ is zeta-potential at the electrolyte/substrate interface. The zeta-potential is a function of the thickness of double-layer (δ) and the charge density (σ), which is shown as Equation 2.

$$\zeta = -\frac{\delta \sigma}{\varepsilon_0 \varepsilon_r} \tag{2}$$

Charge density of the surface σ, depends on pH of electrolyte.

The thickness of the double layer δ, described by Equation 3.

$$\delta = \sqrt{\frac{\varepsilon_0 \varepsilon_r RT}{2cF^2}} \tag{3}$$

Where ε_0 and ε_r are the permittivity of a vacuum and relative permittivity of the eluent, respectively, *R* is the universal gas constant, *T* is the absolute temperature, *F* is the Faraday constant, and *c* is the molar concentration.

As an example, for a monovalent electrolyte at a concentration of 1mM in water the thickness of the electric double layer would be 10nm. Likewise, at a concentration of 0.1M it would be 1nm. Thus, by increasing the concentration of electrolyte, the thickness of the double layer will decrease. This results in a smaller zeta-potential and consequently a reduction in electro-osmotic velocity of the fluid.

However at high concentrations of electrolyte, the electrophoretic velocity of the particles decreases due to a smaller Debye length, described in Equation 4,

$$u_{ep} = \frac{QE}{4\pi\mu r}\frac{\lambda_D}{r} \tag{4}$$

where *Q* is the particle surface charge, λ_D is the Debye length, and *r* represents the particle radius. Therefore, increasing the concentration of electrolyte decreases the electro-osmotic flow but also electrophoretic mobility.

An alternative solution for EOF suppression is eliminating the surface charge. Surface modifications with PEG-Silane in capillary electrophoresis applications have been used for neutralization of glass surface charges in water[93]. PEG (polyethyleneglycol) is an inert,

hydrophilic polymer that can eliminate the surface charge when conjugated to the surface without reducing the wettability of pore surface with electrolyte solution. The same technique can be employed here to modify the surface of silica and reduce the opposing electroosmotic flow.

2.2.2 Second element of the desing

The second element of our design is carboxylate functionalized polystyrene spheres with a 3μm diameter as the probe substrate. We have intentionally chosen this dimension so that the bead's diameter would be larger than the diameter of micropipette's tip (2μm) and therefore, under the applied electrical potential, the bead blocks the pore and consequently the electrical current. Microspheres have been used in many biomolecular detection assays including sequence-specific NA detection schemes[94]. For instance, in a study by Cao et al. quantum dot (QD) optical encoded carboxyl functionalized polystyrene beads with 100μm diameters were used as a multiplex analysis technology for detecting the target DNA with a concentration detection limit of 0.2μg/mL[95]. Fan and coworkers designed a colloidal gold-polystyrene bead hybrid for chemiluminescent detection of sequence-specific target DNA down to a 100 amol level[96]. A microfluidic system has been designed by the Lin group to integrate both microfluidic mixing of 16μm diameter mobile microbeads and hydrodynamic bead arrays to simultaneously detect multiple DNA oligonucleotide sequences from the Hepatitis C Viral (HCV) genome by immobilized molecular beacon probes attached to microbeads with single base-pair mismatch sensitivity[97].

2.2.3 Third element of the desing

The third element and the key component of our design is the use of peptide nucleic acid (PNA) capture probes. The PNA is an artificial synthetic polymer which was invented in 1991 by Nielson et.al[98]. Unlike the deoxyribose backbone in DNA, PNA's backbone is composed of repeating N-(2-aminoethyl)-glycine units linked by peptide bonds. The various bases are linked to the backbone by methylene carbonyl bonds. Since the PNA backbone contains no phosphate groups, PNA is uncharged and has stronger binding affinity to complementary NA sequences at relatively lower and higher salt concentrations than NA-NA binding due to the lack of electrostatic repulsion. Further, PNAs are stable under acidic conditions and are resistant to enzyme-catalyzed hydrolysis. Finally, the stability of PNA-DNA duplexes is affected much more by base mismatches than their DNA-DNA counterparts causing a more substantial decrease in melting temperature[99].As a result of these remarkable characteristics, PNA have been used in many biotechnological and medical applications, particularly in genetic research and diagnostic techniques[100]. PNA has also been used previously for sequence specific DNA detection in a number of platforms[101] including electrochemical detection of DNA hybridization with PNA-modified magnetic beads. In this study, biotinylated PNA probes with streptoavidin coated magnetic beads in combination with redox-active intercalator molecule, Meldola's blue (MBD), was used for sequence-specific DNA detection with high specificity of SNP discrimination and LOD of 2pM[102]. Du et al. showed the DNA sequence detection based on electrochemically reduced graphene oxide (ERGO) and peptide nucleic acid probes with concentration detection limit of 5.45×10^{-13} mol/ L [103]. In 2014, Zhang and coworkers reported a reduced graphene oxide (RGO) based field effect transistor (FET) biosensor for label-free detection of DNA via PNA-DNA hybridization with LOD of 100fM[104]. Furthermore, a solid state nanopore decorated with

PNA probes was used for the detection of a specific sequence of DNA target molecules by the rectification of current across the pore when the DNA molecules hybridized to the complementary tethered PNA probes. As the control experiment, DNA strands with a single base mismatch were incubated with probes to investigate the specificity of the sensor and as a result SNP discrimination was successfully reported in this paper[105].

Here we take particular advantage of the electrical neutrality of PNAs to ensure that the beads are uncharged and electrophoretically immobile until the target NA is complexed. Hybridization of complementary target NAs to the PNA-beads impart sufficient negative charge to the beads, enabling them to be driven electrophoretically to the pore. The beads are then able to physically occlude the pore, leading to a large decrease in conductance. The coupling of target NA to the PNA-bead conjugate thereby leads to an electromechanical amplification phenomenon that gives rise to a large, easily detected, binary modulation of electrical current.

2.3 Experimental procedures

2.3.1 Material

All chemicals were purchased from Sigma-Aldrich (St. Louis, MO) unless otherwise noted. Amine and carboxylic acid-functionalized 3 μm diameter polystyrene microspheres were purchased from Polysciences, Inc. (Warrington, PA). All oligonucleotides (PNA and single stranded DNA) were purchased from Bio-Synthesis, Inc. (Lewisville, TX) as HPLC purified. Pre-pulled borosilicate micropipettes with 2 μm pore diameter were purchased from World Precision Instruments, Inc. (Sarasota, FL). Methoxy-polyethylene glycol amine, CH_3O-$(CH_2CH_2O)_3$-NH_2, MW 350, was obtained from Nanocs, Inc. (New York, NY).

2.3.2 Probe coupling to microspheres

Fifty μL of 3-μm-diameter, carboxylic acid-functionalized polystyrene microspheres at 1.69 × 10^9/mL were washed three times with MES buffer (60 mM 2-(N-morpholino) ethanesulfonic acid, pH 5.5). After each wash, the microspheres were centrifuged at 14,000 rpm for 15 min; after the third wash, the beads were resuspended in 0.6 mL coupling buffer (100 mM 1-[3-(dimethylamine) propyl]-3-ethylcarbodiimide (EDC) in MES buffer) and incubated at 50 °C for 45 min. Ten nmol of amine-functionalized PNA probes were added to the coupling buffer and incubated with the beads at 50 °C for two hours. mPEG-amine (100 mM) was added to the reaction mixture and incubated at 50 °C for one hour to reduce nonspecific binding of nucleic acids to the beads. 100 mM ethanolamine was added to the beads to cap residual carboxyl groups and incubated at 50 °C for an additional hour. Finally, the beads were washed four times in 0.4× SSC buffer (60 mM NaCl, 6 mM trisodium citrate, 0.1% Triton X-100, pH 8) and stored in PBS buffer (137 mM NaCl, 2.7 mM KCl, 10 mM Na_2HPO_4, 2 mM KH_2PO_4, pH 7.4) at 4 °C.

2.3.3 Hybridization assay

Prior to DNA incubation, PNA-beads were washed twice in 0.4× SSC buffer and once in hybridization buffer (750 mM NaCl, 10 mM Tris-HCl, pH 7.0), and were resuspended in 100 μL of hybridization buffer. The PNA-beads were divided between two separate 1.5 mL centrifuge tubes; one for target complementary DNA hybridization and the other for incubation of non-complementary DNA sequence as control experiment. The tubes were placed on a mechanical rotator and incubated overnight at room temperature. After incubation, the beads were washed with 0.4× SSC buffer 3 times.

2.3.4 Zeta potential, Eletrophoretic mobility, and Size measurements

Prior to hybridization, the zeta potentials of PNA-bead batches were measured in 1 mM KCl, 10 mM HEPES (pH 7.0) to assure the near electroneutrality of the beads. The Zetasizer Nano-ZS (Malvern Instruments) was used to characterize their zeta potential and electrophoretic mobility as well as their size using dynamic light scattering.

Zeta potential or electrokinetic potential in colloidal dispersions is the electric potential in the slipping plane boundary. The slipping plane is the boundary between stern layer (the stationary liquid layer attached to the particle) and the dispersion medium around the particle. Zetasizer measures the electrophoretic mobility by performing an electrophoresis experiment on the sample and measuring the velocity of the particles using Laser Doppler Velocimetry (LDV) and then calculate the zeta potential by applying the Henry equation (equation 5).

$$U_E = \frac{2\varepsilon z f(ka)}{3\eta} \tag{5}$$

Where U_E is electrophoretic mobility, z is zeta potential, ε is dielectric constant, η is viscosity and $f(ka)$ is Henry's function which is 1.5 in case of aqueous media and modest electrolyte concentration and is refer to Smoluchowski approximation.

The magnitude of the zeta potential gives an indication of the potential stability of the colloidal system and is highly dependent on solution pH. If all the particles in suspension have a large positive or negative zeta potential then they will tend to repel each other and there is no aggregation of particles in solution and the particles are considered as stable. However, if the particles zeta potential will be between +30 mV and -30 mV then the particles are unstable and flocculate in solution. In our experiments, we measure the zeta potential of our samples after PNA conjugation and after the incubation of PNA-beads with target and control DNA molecules. Measuring the beads zeta potential after PNA conjugation indicates the neutrality of the beads

prior to DNA hybridization. Also, the zeta potential value after DNA incubation with PNA-beads qualitatively indicates the capture of DNA molecules by PNA-beads.

2.3.5 Sensor apparatus and electrical measurements

Two identical chambers made of polydimethylsiloxane (PDMS) connected by a 1 mm diameter opening were sealed to a glass microscope slide following activation with oxygen plasma. A pre-pulled borosilicate micropipette with outer diameter of 1 mm and nominal inner tip (pore) diameter of 2 µm was placed in the opening between the two chambers and sealed with vacuum grease so that the micropipette is the only connection between the two chambers (Figure 2.2). The platform was mounted on an inverted optical microscope (Leica DMIRB).

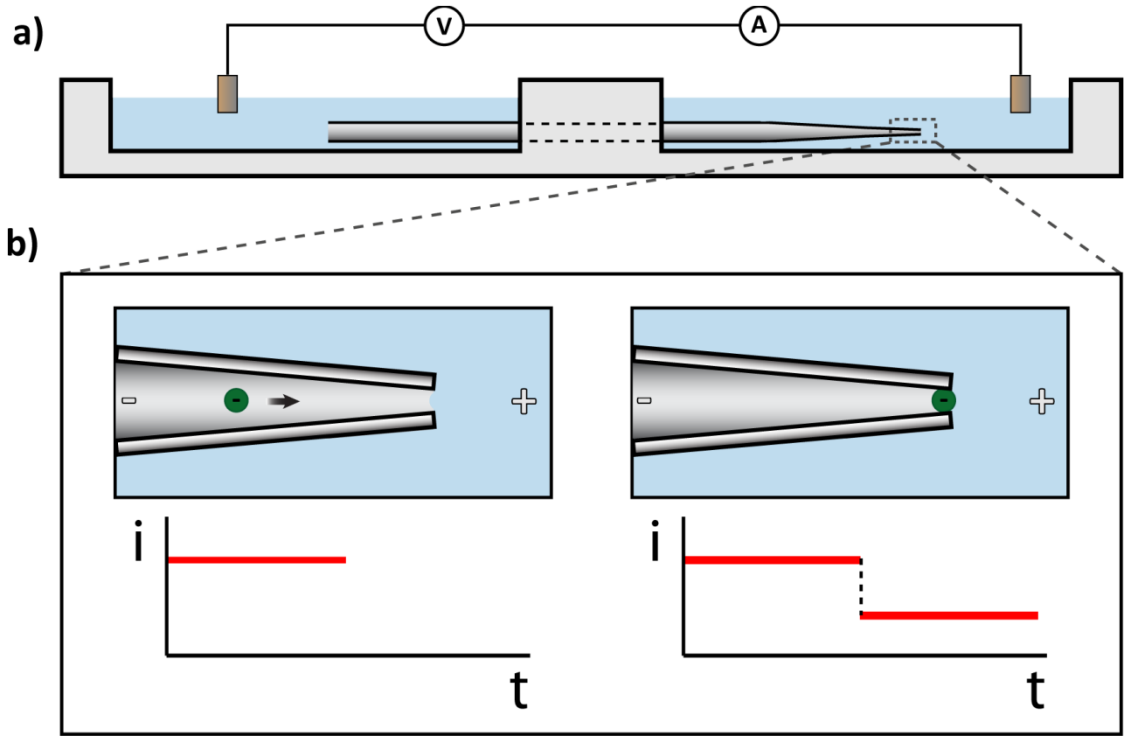

Figure 2.2 a) Cross-sectional diagram of the pipette and measurement chamber. **b)** Depiction of pipette tip and measured current before bead blockade (left) and after (right).

The chambers were filled with identical volumes of buffer (1 mM KCl, 10 mM HEPES, pH 7.0); Pt electrodes were placed in each chamber, away from the pipette entrances. A potential difference of 25 V was applied between the electrodes, and the resultant current was amplified by a transimpedance amplifier and logged using acquisition hardware at 1 kHz (PCI 6052E, National Instruments) and LABView software (National Instruments). Data shown in figures through this thesis was processed in MATLAB with a 5^{th} order Butterworth 100 Hz lowpass filter. After initial set up and baseline current recording, 100 μL of the bead suspension (in 1 mM buffered KCl pH 7.0) were injected into the micropipette and were observed optically while the system was monitored electrically. In the absence of applied voltage, motion of the beads within the capillaries was not observed.

In the following chapter, the performance of the proposed sensing platform will be demonstrated by initially detecting charged polystyrene beads for the proof of concept and then detecting the target nucleic acid. Furthermore, the selectivity and sensitivity of the system to discriminate between fully complementary NA target sequence and single nucleotide polymorphisms (SNPs) will be investigated.

CHAPTER 3

PROOF OF CONCEPT AND SENSOR OPERATION

3.1 Proof of concept

A series of preliminary experiments using a micropipette as the synthetic pore have been conducted to demonstrate the proof of concept. These initial experiments relied on pH to modulate the charge of carboxylic acid- or amine-terminated polystyrene beads thereby manipulating their electrophoretic mobility and ability to effect pore blockage. At pH 7.0, the carboxylic acid beads carried substantial negative surface charge (zeta potential = -87 mV) due to the deprotonation of carboxylic acid groups (pK_a ~ 4.5) thereby making the beads responsive to an electric field. With the capillary tip at high electric potential (positively charged electrode at tip), we observed the beads to move inside the capillary toward the pore ("sensing zone") and block it stably and indefinitely. Reversal of the applied potential caused the bead to move in the opposite direction, re-opening the pore and returning the magnitude of the measured current to the initial value (Figure 3.1 a).

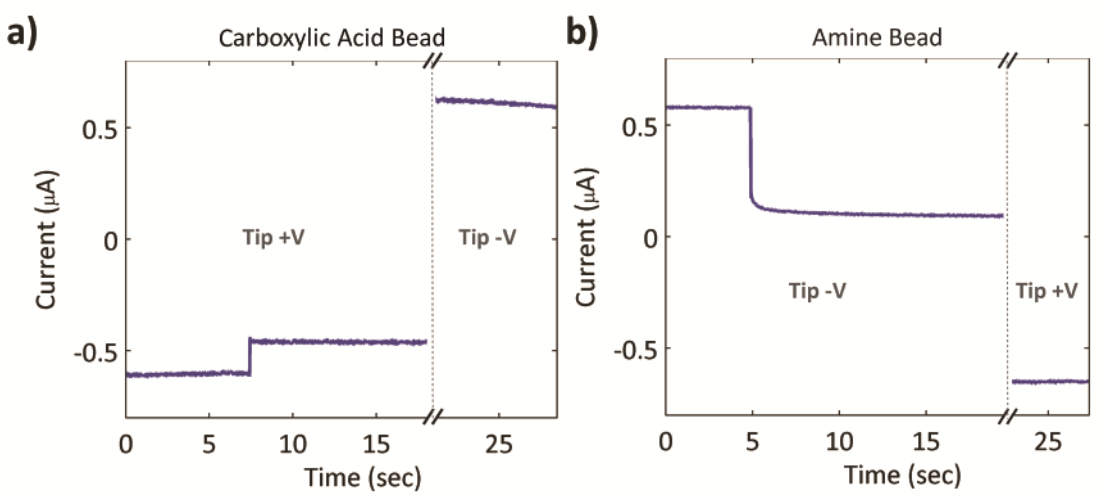

Figure 3.1 a) Ionic current drop caused by pore blockade from a carboxylic acid-functionalized bead at pH 7.0. The blockade was reversible, as seen from the increase in current measured following reversal of the applied voltage (dashed line). **b)** Ionic current drop caused by pore blockade from an amine-functionalized bead at pH 7.0. The blockade also was reversible, as seen from the increase in current measured following reversal of the applied voltage (dashed line).

This behavior was consistent and repeatably measurable, with some variation in the magnitudes of open capillary current and blocked current observed with different capillaries (Table 3.1).

Table T3.1 Repeated carboxylic acid bead blockade current measurements for four capillaries

Capillary 1

	I_{open} (μA)	I_{block} (μA)	$(I_o - I_b)/ I_o$	R_{open} (Ω)	ΔR (Ω)	ΔR/R
	-0.583	-0.437	0.250	4.29E+07	1.43E+07	0.334
	-0.594	-0.466	0.216	4.21E+07	1.16E+07	0.276
	-0.594	-0.479	0.193	4.21E+07	1.01E+07	0.239
	-0.609	-0.479	0.213	4.11E+07	1.11E+07	0.271
	-0.565	-0.478	0.154	4.43E+07	8.07E+06	0.182
Average	-0.589	-0.468	0.205	4.25E+07	1.10E+07	0.261
Std. Dev.	0.016	0.018	0.035	1.19E+06	2.29E+06	0.056

Capillary 2

	I_{open} (µA)	I_{block} (µA)	$(I_o - I_b)/ I_o$	R_{open} (Ω)	ΔR (Ω)	ΔR/R
	-0.583	-0.452	0.224	4.29E+07	1.24E+07	0.289
	-0.602	-0.458	0.240	4.15E+07	1.31E+07	0.315
	-0.605	-0.461	0.238	4.13E+07	1.29E+07	0.312
	-0.610	-0.463	0.241	4.10E+07	1.30E+07	0.317
	-0.630	-0.577	0.084	3.97E+07	3.62E+06	0.091
	-0.629	-0.470	0.252	3.97E+07	1.34E+07	0.337
	-0.630	-0.472	0.250	3.97E+07	1.32E+07	0.333
	-0.633	-0.583	0.079	3.95E+07	3.40E+06	0.086
	-0.635	-0.585	0.078	3.94E+07	3.33E+06	0.084
	-0.631	-0.586	0.072	3.96E+07	3.08E+06	0.078
	-0.632	-0.591	0.064	3.96E+07	2.73E+06	0.069
	-0.627	-0.590	0.059	3.99E+07	2.50E+06	0.063
	-0.625	-0.589	0.058	4.00E+07	2.45E+06	0.061
	-0.628	-0.585	0.069	3.98E+07	2.95E+06	0.074
	-0.630	-0.592	0.060	3.97E+07	2.54E+06	0.064
Average	-0.622	-0.537	0.138	4.02E+07	6.97E+06	0.172
Std. Dev.	0.015	0.063	0.087	1.00E+06	5.11E+06	0.124

Capillary 3

	I_{open} (µA)	I_{block} (µA)	$(I_o - I_b)/ I_o$	R_{open} (Ω)	ΔR (Ω)	ΔR/R
	-0.595	-0.522	0.123	4.20E+07	5.87E+06	0.140
	-0.509	-0.485	0.047	4.91E+07	2.42E+06	0.049
	-0.556	-0.447	0.195	4.50E+07	1.09E+07	0.242
	-0.508	-0.437	0.141	4.92E+07	8.10E+06	0.165
	-0.647	-0.504	0.220	3.87E+07	1.09E+07	0.283
	-0.663	-0.505	0.238	3.77E+07	1.18E+07	0.312
	-0.677	-0.536	0.207	3.69E+07	9.66E+06	0.261
	-0.771	-0.473	0.387	3.24E+07	2.05E+07	0.631
	-0.769	-0.641	0.166	3.25E+07	6.50E+06	0.200
Average	-0.633	-0.506	0.192	4.04E+07	9.62E+06	0.254
Std. Dev.	0.099	0.060	0.094	6.37E+06	5.04E+06	0.163

Capillary 4 (Experiment ended after 3rd event, which did not reverse with reversed voltage.)

	I_{open} (µA)	I_{block} (µA)	$(I_o - I_b)/ I_o$	R_{open} (Ω)	ΔR (Ω)	ΔR/R
	-0.613	-0.211	0.656	4.08E+07	7.79E+07	1.910
	-0.600	-0.220	0.634	4.16E+07	7.22E+07	1.733
	-0.594	-0.241	0.594	4.21E+07	6.17E+07	1.465
Average	-0.602	-0.224	0.628	4.15E+07	7.06E+07	1.703
Std. Dev.	0.009	0.016	0.031	6.48E+05	8.24E+06	0.224

The bead blockade in capillary 4 could not be reversed after the third blockade, but the other three capillaries were repeatably reversible and measured as long as desired. When the same experiments were conducted at pH 2.5 (below the carboxylic acid bead pK_a, measured zeta potential = -1.79 mV) the beads were observed to be immobile and no pore blockade could be achieved. Bead blockades were observed for applied potentials between 5 and 25V; all measurements described below were conducted with an applied potential of 25V.

Similar experiments were conducted with amine-terminated beads that are positively charged at pH 7.0 (pK_a ~ 9.5, zeta potential = +69 mV at pH 7.0). When a potential of sign opposite to that used in the carboxylic acid bead experiments above was applied, the amine beads were observed to move toward the pore and block it, also producing stable, indefinite, and reversible reduction in the measured current (Figure 3.1b) and the summary of data is presented in Table T3.2.

Table T3.2 Repeated amine bead blockade measurements for three capillaries

Capillary 1

	I_{open} (μA)	I_{block} (μA)	$(I_o - I_b)/ I_o$	R_{open} (Ω)	ΔR (Ω)	ΔR/R
	0.608	0.103	0.831	4.11E+07	2.02E+08	4.905
	0.585	0.118	0.798	4.27E+07	1.69E+08	3.951
	0.565	0.136	0.759	4.43E+07	1.39E+08	3.150
	0.626	0.128	0.796	3.99E+07	1.56E+08	3.894
	0.626	0.117	0.812	4.00E+07	1.73E+08	4.332
	0.615	0.113	0.816	4.07E+07	1.80E+08	4.425
	0.645	0.120	0.814	3.87E+07	1.69E+08	4.364
	0.600	0.124	0.793	4.17E+07	1.59E+08	3.825
	0.594	0.120	0.799	4.21E+07	1.67E+08	3.963
	0.610	0.078	0.872	4.10E+07	2.78E+08	6.787
	0.556	0.079	0.857	4.50E+07	2.70E+08	6.000
Average	0.603	0.113	0.813	4.16E+07	1.87E+08	4.509
Std. Dev.	0.027	0.019	0.031	1.87E+06	4.55E+07	1.045

Capillary 2

	I_{open} (μA)	I_{block} (μA)	$(I_o - I_b)/ I_o$	R_{open} (Ω)	ΔR (Ω)	ΔR/R
	0.624	0.071	0.886	4.01E+07	3.10E+08	7.738
	0.580	0.058	0.901	4.31E+07	3.91E+08	9.073
	0.616	0.053	0.914	4.06E+07	4.34E+08	10.679
	0.493	0.057	0.884	5.07E+07	3.86E+08	7.600
	0.484	0.054	0.889	5.17E+07	4.13E+08	7.989
	0.557	0.056	0.900	4.49E+07	4.06E+08	9.034
	0.567	0.054	0.905	4.41E+07	4.20E+08	9.519
	0.572	0.060	0.894	4.37E+07	3.70E+08	8.467
Average	0.561	0.058	0.897	4.49E+07	3.91E+08	8.763
Std. Dev.	0.051	0.006	0.010	4.26E+06	3.85E+07	1.035

Capillary 3

	I_{open} (μA)	I_{block} (μA)	$(I_o - I_b)/ I_o$	R_{open} (Ω)	ΔR (Ω)	ΔR/R
	0.621	0.091	0.854	4.03E+07	2.35E+08	5.834
	0.601	0.214	0.644	4.16E+07	7.51E+07	1.806
	0.633	0.274	0.567	3.95E+07	5.17E+07	1.309
	0.611	0.317	0.481	4.09E+07	3.80E+07	0.928
	0.491	0.151	0.692	5.10E+07	1.14E+08	2.242
	0.563	0.226	0.598	4.44E+07	6.61E+07	1.488
Average	0.586	0.212	0.639	4.30E+07	9.67E+07	2.268
Std. Dev.	0.053	0.082	0.127	4.27E+06	7.26E+07	1.803

When repeated at pH 11.5, above the bead pK_a, the deprotonated and neutral amine beads (zeta potential = +6.3 mV) still moved in the same direction, but more slowly and with insufficient driving force to block the pore. This most likely resulted from electroosmotic flow caused by the deprotonated silanol (Si-OH) groups (pK_a ~ 4) on the capillary surface. To confirm this, we microscopically examined the same beads and solution above the planar surface of a borosilicate glass petri dish, and observed that the beads moved only when close to the glass surface, where the electroosmotic flow is largest. This is also consistent with the complete immobility of the carboxylic acid beads at acidic pH, since both the silanol groups on the capillary surface and the carboxylic acid groups on the beads are protonated and neutral. We presume that, in the experiments with the carboxylic acid beads at neutral pH, the force on the beads due to the

electric field acting on the charged beads is greater than the opposing force due to electroosmotic flow, thereby enabling the beads to be driven to the pore.

Figure 3.3 shows a larger fraction of blocked current obtained with the amine beads compared to the carboxylic beads (81% vs. 24%). In general, from measurements of the carboxylic acid beads in four capillaries and amine beads in three capillaries, the amine beads resulted in higher blockages (48% - 91%) than the carboxylic acid beads (4.7% - 66%) (Tables T3.1 and T3.2 and Figure 3.2), with some exception (Capillary 4 for carboxylic acid beads and Capillary 3 for amine beads).

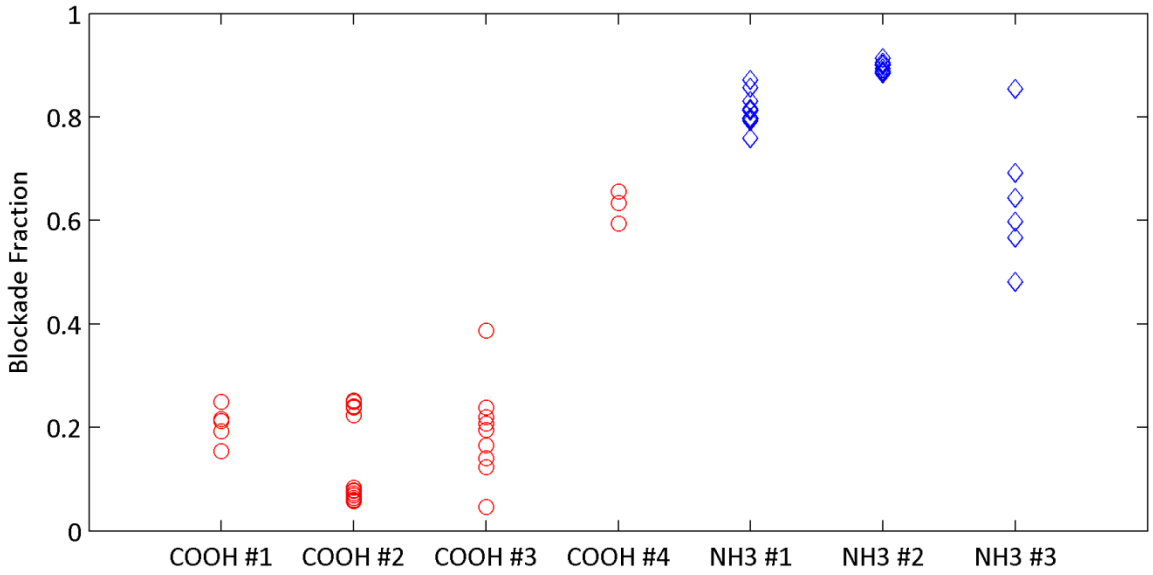

Figure3.2 Plot of blockade fractions measured for all capillaries listed in Tables T3.1 and T3.2

Optical observations indicated that the amine beads were typically immobilized closer to the capillary tip than the carboxylic acid beads and it was common to observe some of the amine beads passing completely through the capillary tip. We measured the average size of amine beads and carboxylic acid beads using DLS (Figure 3.3). These measurements indicate that the diameter of amine beads is smaller than carboxylic acid beads on average.

Since the amine beads were on average smaller than the carboxylic acid beads, this and additional observations suggest that the magnitude of the blockade is highly dependent on the relative sizes of the beads and the capillary tip.

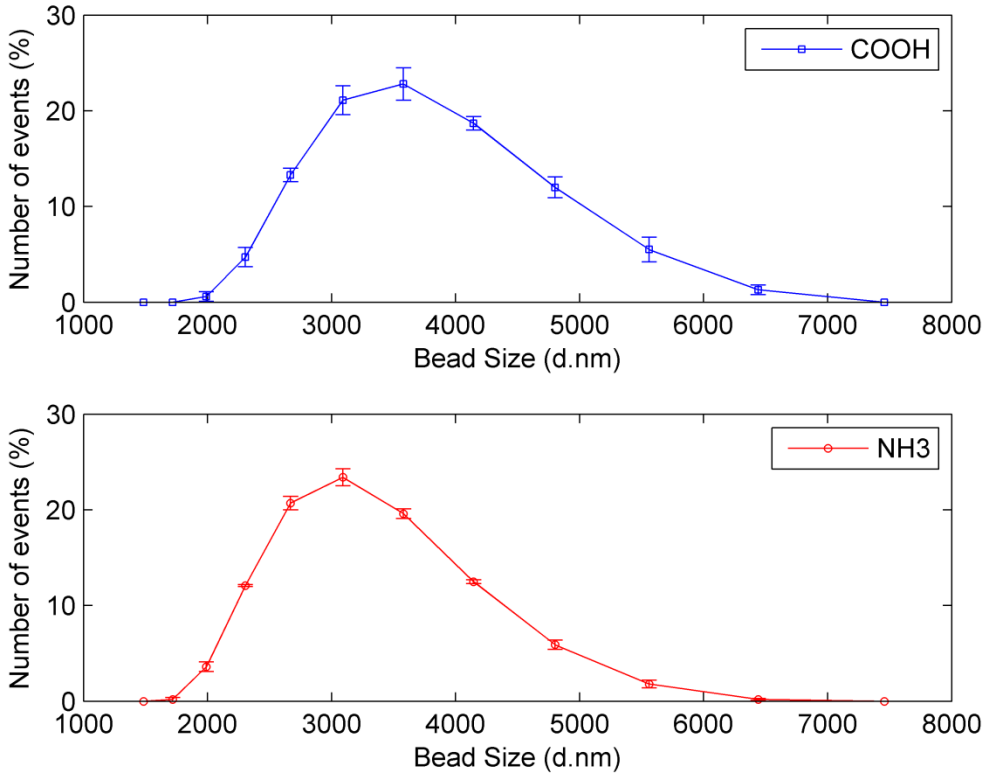

Figure3.3 DLS diameter measurements of the carboxylic acid beads (top) and amine beads (bottom) measured with the Zetasizer Nano-ZS (Malvern Instruments). Diameters and errors bars shown are determined from the averages and standard deviation calculated from 3 measurement runs. The peak and mean of the carboxylic acid distribution are 3580 nm and 3680 nm, respectively. The peak and mean of the amine distribution are 3090 nm and 3250 nm, respectively.

In further support of this, a subsequent experiment with the carboxylic acid beads in a different capillary (with same nominal pore diameter of 2 μm) resulted in microscopic observation of some of the beads passing through the pore and, for those that blocked the pore, a larger

reduction of current (63% average current blockage, Capillary 4, Table T3.1). Since the carboxylic acid beads in this experiment were drawn from the same batch as the carboxylic acid beads in previous experiments, complete passage of the beads through the pore suggests that the tip diameter of the micropipette was larger than the ones used in previous experiments. Additionally, measurement of the carboxylic acid beads in another capillary (Capillary 2 in Table T3.1) showed a reproducible bimodal blockade current (average blockade percentage of 24% and 6.9%) and two reproducible immobilization locations (with the 24% block occurring closer to the capillary tip (Figure 3.4)) as the voltage was reversed and the experiment repeated.

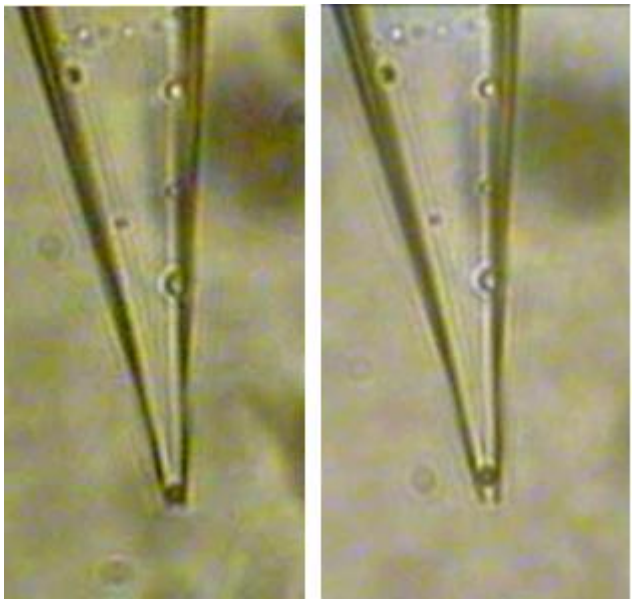

Figure3.4 Microscopic images of 3.6 µm diameter carboxylic acid beads immobilized in Capillary 2. Left: A blockade current of -0.461 µA was measured, a blockade fraction of 0.238 (Entry 3 of Capillary 2 in Table T3.1). Right: A blockade current of -0.591 µA was measured, a blockade fraction of 0.064 (Entry 11 of Capillary 2 in Table T3.1).

Since this measurement was obtained with one capillary, this suggests that beads of two different sizes or shapes were separately participating in the blockade.

Next we explore the current measured for carboxylic acid beads passing completely through the tip of Capillary 4 (Figure 3.5) displayed similar characteristics to previous reported measurements of beads traversing conical capillaries[106,107], specifically with respect to the rapid decrease in blockade current as the bead passes through the tip to the external solution.

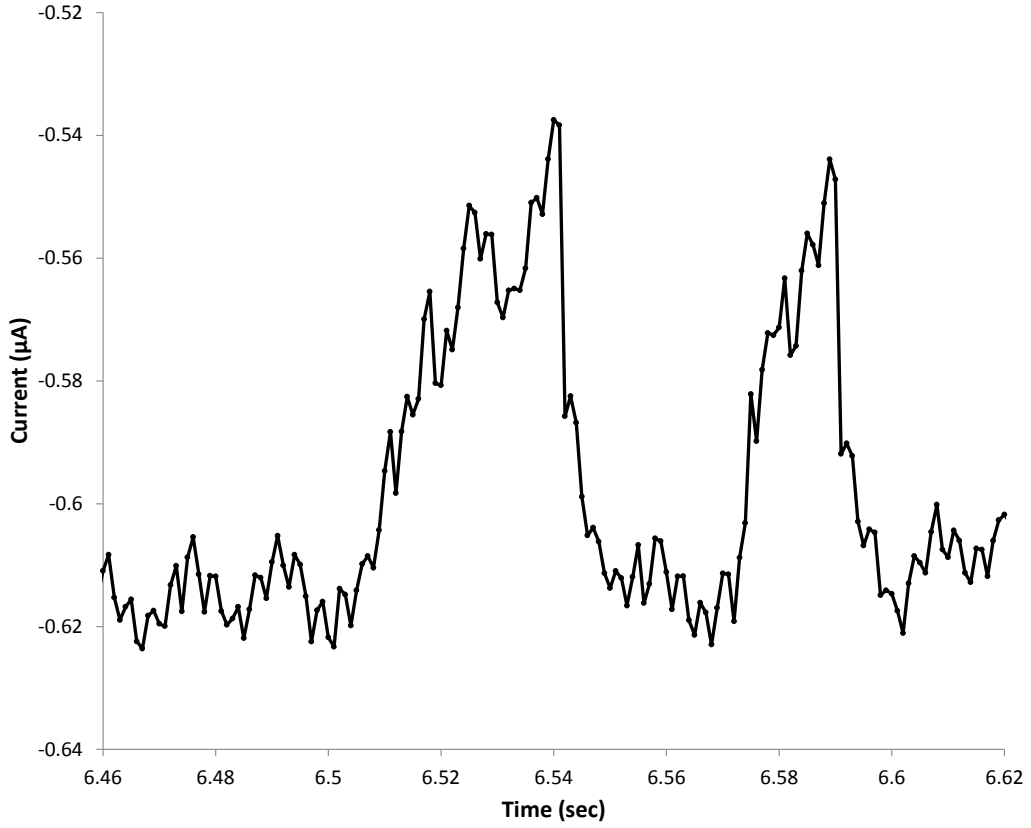

Figure3.5: Measurement of current during passage of two carboxylic acid beads through Capillary 4.

However, we do see a difference from this previous work in that the passage time of the bead through the tip is approximately 40 ms, significantly longer than the 1 ms times previously reported for 2 µm diameter colloids. This is most likely due to the transport of the carboxylic acid beads being slowed by the opposing electroosmotic flow. This is also supported by

experiments with the amine beads, which were observed microscopically to pass through the capillary tip but no blockade currents were able to be resolved with 1 kHz data acquisition. The magnitude of the reduction in current measured during the passage of the carboxylic acid beads (12%, an increase in resistance of 5.65 MΩ) was consistent with previous work reported with similar systems[107,108]. We also developed a simple analytic model calculating the increase in resistance caused by the presence of a spherical particle in a conical channel with circular cross-section based on Gregg and Steidley's model of resistive pulse from particles in a cylindrical channel[109,110].

3.1.1 Model

Gregg and Steidley (Biophys J. 1965 July; 5(4): 393–405) obtained the size of a resistive pulse in a cylindrical channel:

$$\Delta R = \frac{2\rho}{\pi r_c}\left[\frac{\tan^{-1}\left[\frac{r_p}{r_c}\left(1-\left(\frac{r_p}{r_c}\right)^2\right)^{-\frac{1}{2}}\right]}{\sqrt{1-\left(\frac{r_p}{r_c}\right)^2}} - \frac{r_p}{r_c}\right] \quad (6)$$

Extending Gregg and Steidley's derivation to the case of a particle in a conical channel,

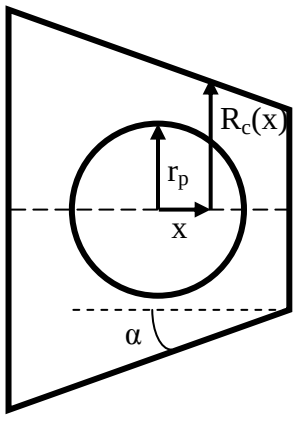

Where x is the distance from the particle center along the capillary axis, r_p is the particle radius, $R_c(x)$ is the capillary radius at position x, and α is the half-angle of the conical capillary. We may write for the resistance of the electrolyte in the space between the particle and the capillary:

$$dR(x) = \frac{\rho dx}{A(x)} = \frac{\rho dx}{\pi\left[R_c^2(x) - \left(r_p^2 - x^2\right)\right]} = \frac{\rho dx}{\pi\left[(r_c - \mathrm{x}\tan a)^2 - \left(r_p^2 - x^2\right)\right]} \qquad (7)$$

Where ρ is the solution resistivity, and r_c is the radius of the capillary at the position of the particle center. Integrating this expression over x from $-r_p$ to $+r_p$ and subtracting the integrated resistance of this same volume without a particle, we find the change in resistance resulting from the presence of the particle:

$$\Delta R = \frac{\rho}{\pi r_c\sqrt{1-\sec^2\alpha\left(\frac{r_p}{r_c}\right)^2}}\left[\tan^{-1}\frac{\left[\tan\alpha+\sec^2\alpha\frac{r_p}{r_c}\right]}{\sqrt{1-\sec^2\alpha\left(\frac{r_p}{r_c}\right)^2}} - \tan^{-1}\frac{\left[\tan\alpha-\sec^2\alpha\frac{r_p}{r_c}\right]}{\sqrt{1-\sec^2\alpha\left(\frac{r_p}{r_c}\right)^2}}\right] - \frac{2\rho\left(\frac{r_p}{r_c}\right)}{\pi r_c\sqrt{1-\tan^2\alpha\left(\frac{r_p}{r_c}\right)^2}} \qquad (8)$$

When α = 0, we obtain Gregg and Steidley's expression. In the case of full contact of the spherical particle with the capillary walls, $r_c = r_p \sec\alpha$, and this expression diverges as expected. α for the capillaries used in these experiments was estimated to be 7.5 degrees, giving a maximum for $\frac{r_p}{r_c}$ of 0.99.

The model predicts increasing blockade resistance with increasing ratio of particle radius to capillary radius $\left(\frac{r_p}{r_c}\right)$. For a spherical particle fully contacting the interior of a conical capillary

with circular cross-section, $\frac{r_p}{r_c}$ is close to unity and the model predicts complete block of the current. None of our measurements showed complete blockades, although one capillary measured with the amine beads showed 90% average block (Capillary 2, Table T3.2). These measurements of incomplete block indicate that the particles did not fully contact the capillary interior, possibly due to non-circular cross-sections of the particle or capillary, presence of asperities on the bead or capillary surfaces, or adherence of the particle to the capillary wall before full contact. Evidence from the previously discussed carboxylic acid beads with Capillary 2 supports variation in bead size or shape in that the bimodal distribution of blocked currents was quite repeatable and correlated with microscopic observations.

Although the model assumes circular particle and conical capillary cross-section, its parameterization in $\frac{r_p}{r_c}$ can be seen alternatively in terms of the particle and capillary cross-sections as $\frac{r_p}{r_c} = \frac{\sqrt{Area_{particle}}}{\sqrt{Area_{capillary}}}$ or $\frac{r_p}{r_c} = \sqrt{1 - \frac{Area_{gap}}{Area_{capillary}}}$ and therefore as $\frac{r_p}{r_c}$ increases, $\frac{Area_{gap}}{Area_{capillary}}$ decreases. In this way, we may understand that spherical particles blocking a conical capillary with elliptical cross-section would create larger blockades for smaller particles (thus also blocking closer to the capillary tip) because the cross-sectional area of the gap would decrease, roughly translating to an increased $\frac{r_p}{r_c}$ in our model. Therefore in our model, the size of the resistance increase depends on eccentricity of the particle or capillary cross-sections and the particle size. For beads plugging pores, we experimentally observed resistance increases in the range of 38 - 430 MΩ for amine beads (48% - 91% block) and 2 - 78 MΩ for carboxylic acid beads (4.7% - 66% block) (Tables T3.1 and T3.2). For the smaller 3150 nm diameter amine

beads, the model yields resistance increases of 38 - 430 MΩ for $\frac{r_p}{r_c}$ of 0.87 to 0.985. For 3600 nm diameter carboxylic acid beads the model yields ΔR of 2 - 78 MΩ for $\frac{r_p}{r_c}$ of 0.54 to 0.93.

To investigate the percentage of pore blockade we conducted additional experiments with various micropipette pore diameters and relative carboxylate sphere sizes. The tip diameters of micropipettes were 1μm, 0.75μm, and 0.5μm and the corresponding sphere sizes were 2μm, 1μm, and 0.75μm respectively. However, in experiments with small pore diameters current blockade by carboxylic beads were not feasible as a result of electroosmosis flow. In all these experiments electroosmosis flow was stronger than electrophoretic force and blocking the tip of the pore by carboxylic acid beads were infrequent compare to the initial experiments with 2μm pores. The strong electroosmosis flow in these capillaries occurred as a result of narrowed capillary walls close to the tip. The percentage of infrequent current blockade obtained by 1μm, 0.75μm capillaries remained roughly the same as the 2μm capillary. Also, we observed no current block using 0.5μm capillary as a result of strong opposing electroosmosis flow.

To reduce the electroosmosis flow in smaller capillaries, we attempted to silanize the glass micropipettes with PEG-Silane purchased from Gelest Inc (Philadelphia PA). However, the tip of capillaries was clogged by PEG-Silane molecules and we were unable to rinse through the capillaries. The silanizing experiment can be further investigated in future work if necessary.

We concluded that the 2μm tip and 3μm carboxylate spheres have given the most consistent electrical readout. Also the micropipettes with 2μm tip are easier to handle (comparing to the smaller sizes) and therefore were chosen for further experiments.

3.2 Detecting the target nucleic acid

Next, nucleic acid detection was measured using 20-mer polyA ssDNA as a simple target sequence and PNA-beads conjugated with 12-mer polyT PNA (Amine-TT TT TT TT TT TT) as the complementary probe (conjugation was described in previous chapter, section2.3.2). The sequence of target and control ssDNA used in these experiments are : polyT (5'-TT TT TT TT TT TT TT TT TT TT-3'), polyA (5'- AA AA AA AA AA AA AA AA AA AA-3'). To assess the PNA conjugation to the carboxylic acid beads, the beads' zeta potential before PNA conjugation was measured to be -87 mV, after ethanolamine capping +5.75 mV, and after three washes with 0.4% SSC buffer -4.39 mV. Following capping and washing, the beads were observed to aggregate. Without incubation DNA, the PNA-beads in the micropipette were seen to follow the electroosmotic flow away from the pipette tip, indicating that the PNA-beads alone were unable to block the pore. Incubation of the PNA-beads with polyA target ssDNA resulted in well-dispersed beads with a measured zeta potential of -71.1 mV, and motion toward the pipette tip in the same applied voltage, ultimately blocking it (Figure 3.6b). These current blockades were stable, indefinite, and reversible.

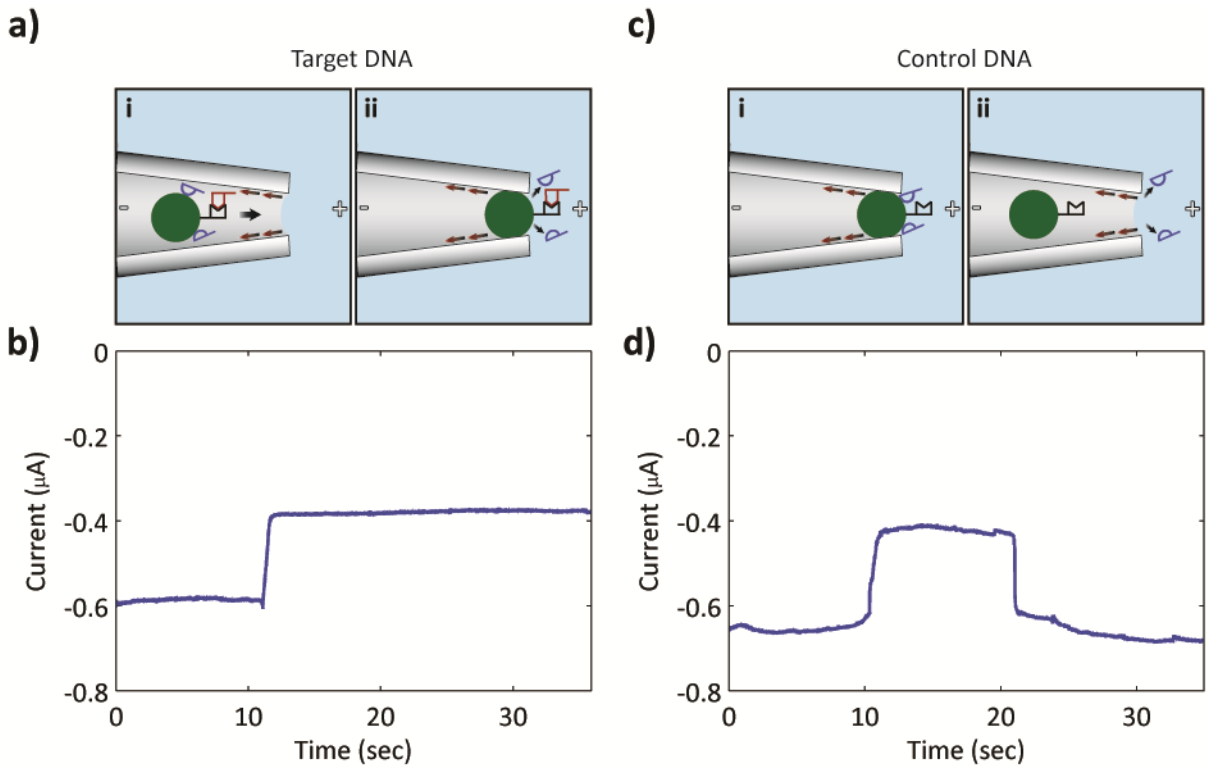

Figure 3.6 Schematic of motion of PNA-bead under an applied potential and resultant measured current. **a)** i) PNA-beads (green) with non-specifically bound ssDNA and specifically bound ssDNA hybridized to PNA on the bead are negatively charged and electrophoretically mobile. ii) In the strong electric field at the pore tip, the non-specifically bound DNA is removed from the bead, but the hybridized DNA is not, leaving the bead with sufficient negative charge to remain blocking the pore indefinitely. **b)** Measured permanent current blockade for PNA-beads incubated with complementary polyA DNA, corresponding to (a). **c)** For PNA-beads incubated with only non-complementary DNA, any DNA bound to the bead is non-specific; the strong electric field at the pore tip removes the non-specifically bound DNA, reducing the beads charge sufficiently so that the electroosmotic flow (red arrows) is able to remove the bead from the pore tip (ii). **d)** Transient current blockade measured for PNA-beads incubated with non-complementary polyT DNA, corresponding to (c).

In a control experiment, the same polyT PNA-beads as above were incubated with non-complementary 20-mer polyT ssDNA, resulting in a bead preparation with a measured zeta potential of -46.7 mV, which indicated a significant amount of non-specific binding of DNA to the beads. Microscopic observation of the control beads showed movement of the beads to the pore, which they temporarily blocked and then moved back down the pipette away from the pore along with the electroosmotic flow. Simultaneous electrical measurement showed a transient current blockade of up to approximately 10 seconds long (Figure 3.6d). This transient blockade was observed infrequently, with most of the control beads unable to block the pore.

The control and target experiments were repeated at least three times; measured zeta potentials and electrophoretic mobilities are listed in Table 3.3 with the qualitative results of the electrical measurements (Data summarized in Tables T3.4 and T3.5).

Table 3.3 Summary of experimental results for target and control samples: Zeta potential and electrophoretic mobility measured after ssDNA incubation and results of micropipette electrical measurements.

Target PolyA			**Control PolyT**		
Zeta potential (mV)	Mobility (10^{-8} m^2/Vs)	Results	Zeta potential (mV)	Mobility (10^{-8} m^2/Vs)	Results
-71.1 ± 4.0	-5.57	Permanent block	-46.7 ± 4.28	-3.66	Transient block
-59.3 ± 5.1	-4.65	Permanent block	-36.8 ± 4.47	-2.88	No block
-59.8 ± 4.7	-4.69	Permanent block	-32.1 ± 5.3	-2.52	No block

Table T3.4 Repeated polyA DNA - polyT bead blockade measurements for three capillaries

Capillary 1

	I_{open} (μA)	I_{block} (μA)	$(I_o - I_b)/ I_o$	R_{open} (Ω)	ΔR (Ω)	ΔR/R
	-0.603	-0.500	0.171	4.14E+07	8.56E+06	0.207
	-0.612	-0.509	0.168	4.08E+07	8.23E+06	0.201
	-0.638	-0.501	0.214	3.92E+07	1.07E+07	0.272
	-0.647	-0.507	0.216	3.86E+07	1.07E+07	0.276
	-0.646	-0.495	0.235	3.87E+07	1.19E+07	0.307
	-0.632	-0.400	0.367	3.96E+07	2.30E+07	0.580
	-0.633	-0.486	0.233	3.95E+07	1.20E+07	0.304
	-0.608	-0.512	0.157	4.11E+07	7.67E+06	0.186
Average	-0.627	-0.489	0.220	3.99E+07	1.16E+07	0.292
Std. Dev.	0.017	0.037	0.067	1.11E+06	4.87E+06	0.125

Capillary 2 (Experiment ended after 5th event, which did not reverse with reversed voltage.)

	I_{open} (μA)	I_{block} (μA)	$(I_o - I_b)/ I_o$	R_{open} (Ω)	ΔR (Ω)	ΔR/R
	-0.543	-0.432	0.204	4.61E+07	1.18E+07	0.257
	-0.601	-0.481	0.199	4.16E+07	1.03E+07	0.248
	-0.618	-0.426	0.312	4.04E+07	1.83E+07	0.453
	-0.616	-0.489	0.205	4.06E+07	1.05E+07	0.258
	-0.610	-0.391	0.359	4.10E+07	2.29E+07	0.560
Average	-0.597	-0.444	0.256	4.19E+07	1.48E+07	0.355
Std. Dev.	0.031	0.041	0.074	2.35E+06	5.61E+06	0.143

Capillary 3

	I_{open} (μA)	I_{block} (μA)	$(I_o - I_b)/ I_o$	R_{open} (Ω)	ΔR (Ω)	ΔR/R
	-0.619	-0.479	0.227	4.04E+07	1.18E+07	0.293
	-0.592	-0.459	0.224	4.23E+07	1.22E+07	0.288
	-0.596	-0.458	0.232	4.19E+07	1.26E+07	0.301
	-0.616	-0.407	0.338	4.06E+07	2.08E+07	0.511
	-0.622	-0.512	0.177	4.02E+07	8.66E+06	0.215
	-0.660	-0.488	0.261	3.79E+07	1.34E+07	0.353
	-0.667	-0.492	0.263	3.75E+07	1.34E+07	0.357
	-0.698	-0.472	0.324	3.58E+07	1.71E+07	0.479
Average	-0.634	-0.471	0.256	3.96E+07	1.37E+07	0.350
Std. Dev.	0.037	0.031	0.054	2.28E+06	3.67E+06	0.100

Table T3.5 polyT DNA - polyT bead blockade measurements for one capillary (Control). Blockades did not occur for the other two capillaries tested.

I_{open} (μA)	I_{block} (μA)	$(I_o - I_b)/ I_o$	R_{open} (Ω)	ΔR (Ω)	ΔR/R	Block duration (sec)
-0.637	-0.427	0.329	3.93E+07	1.93E+07	0.491	7
-0.637	-0.494	0.225	3.92E+07	1.14E+07	0.290	2
-0.650	-0.425	0.345	3.85E+07	2.03E+07	0.528	10

Quantitatively, the magnitude of the blockades measured for the target DNA was consistent between the three capillaries (average blockades: 22.0%, 25.6%, and 25.6%; Table T3.4). The blockade of one of the capillaries could not be reversed after five measurements.

We hypothesize that incubation of the beads with ssDNA results in a significant amount of non-specific binding for both complementary and non-complementary sequences. In the control experiments, the DNA binding to the bead is entirely non-specific and presumably less strongly bound than the complementary DNA. Still, the non-specific DNA beads are negatively charged and electrophoretically mobile, allowing them to be driven to the pore. In the pore, the electric field is sufficiently strong to remove the non-specifically bound DNA from the bead, which causes a reduction in bead charge and electrophoretic mobility, enabling the electroosmotic flow to exceed the electrophoretic force and carry the bead away from the pore. For complementary DNA sequences, the bead likely carries specific and non-specifically bound DNA but that the strong electric field is insufficient to remove the hybridized DNA from the bead (Figures 3.6a and c).

To estimate the electric force on a 20-mer ssDNA on the bead surface, we used the model described below.

3.2.1 Model

The force on the charged nucleic acids on the bead surface can be estimated by finding the change in potential dV with distance dx from the bead center above a bead in the capillary and $dR(x)$ was previously acquired from Equation (7):

$$dV(x) = I_b dR(x) = I_b \frac{\rho dx}{A(x)} = I_b \frac{\rho dx}{\pi\left[R_c^2(x) - \left(r_p^2 - x^2\right)\right]} = I_b \frac{\rho dx}{\pi\left[(r_c - \mathrm{x}\tan a)^2 - \left(r_p^2 - x^2\right)\right]} \quad (9)$$

The force on charge q on the particle surface at position x is:

$$F(x) = qE(x) = -q\frac{dV}{dx} = \frac{-qI_b\rho}{\pi\left[(r_c - \mathrm{x}\tan a)^2 - \left(r_p^2 - x^2\right)\right]} \quad (10)$$

$$F(x=0) = \frac{-qI_b\rho}{\pi\left[r_c^2 - r_p^2\right]} = \frac{-qI_b\rho}{\pi r_p^2\left[\frac{r_c^2}{r_p^2} - 1\right]} \quad (11)$$

To estimate the force on a nucleic acid strand (q = -20e) on the bead surface at x = 0, we take the measured change in resistance ΔR measured for a block event from experimental values in Tables T4 and find a value of $\frac{r_p}{r_c}$ producing it from Eq. 9. With the measured I_b and the particle size, we may calculate the force.

Calculating the force on PolyA ssDNA-polyT beads:

The average ΔR from a bead blockade for all measurements in Table T4 is 11.5 MΩ and the average I_b is -0.497 μA. In our experimental conditions, this ΔR obtains for 3.6 μm diameter COOH beads at a $\frac{r_p}{r_c}$ of about 0.753. Using these numbers in Eq. 11, we obtain 13.9 pN for the

20-mer ssDNA on the bead surface. This force is less than the 57 pN rupture forces measured for 8 bp DNA-PNA with optical tweezers[111]. Therefore, we can conclude that the applied force won't unzip the 20-mer DNA-PNA.

3.3 Investigating the selectivity and sequence specificity of the system

To further investigate the selectivity of the sensor, we detected ssDNA with a non-repeating sequence, a 12-mer portion of a gene encoding the anthrax lethal factor[112]. To allow direct comparison with the previous experiment detecting 20-mer ssDNA, we added an 8-mer polyA tail to the 12-mer anthrax sequence. Single stranded DNA anthrax LF target sequence: (5'-GG AT TA TT GT TA AA AA AA AA-3'). To enhance the binding of complementary ssDNA and minimize non-specific binding, a PEG spacer was added to the amine-functionalized 12-mer complementary PNA capture probe[113]. The PNA probe sequence: Amine-$(CH_2CH_2O)_{12}$- CC TA AT AA CA AT. After PNA conjugation, capping with ethanolamine, and washing, the measured zeta potential of this PNA-bead preparation was -2.75 mV. The PNA-beads were divided into two volumes, one incubated with 20-mer target anthrax ssDNA and the other with control 20-mer polyT ssDNA. Measured zeta potentials after incubation were -56.7 mV for target beads and -39.0 mV for control beads. As with the previous experiments described above, the presence of complementary DNA led to permanent blockades, whereas its absence led to transient or no blockade (Figure 3.7).

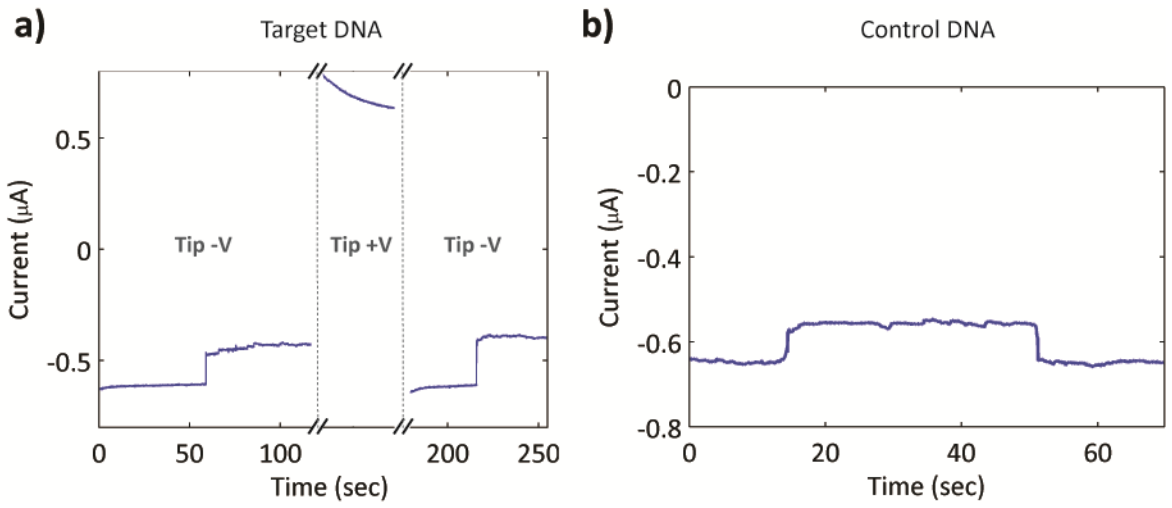

Figure 3.7 a) Permanent ionic current drop caused by beads incubated with target anthrax ssDNA. The blockade was reversible and repeatable, as seen by reversals of the applied voltage (dashed lines). **b)** Transient ionic current drops were seen occasionally with beads incubated with the non-complementary, control ssDNA.

Even in experiments with the control DNA in which transient blockades were measured, only a few beads were seen to transiently block the current, with the majority of the beads being inadequately mobile in the electric field to block the pore. These experiments were repeated three times and the results are summarized in Table 3.6.

Table 3.6. Summary of experimental results for target and control samples: zeta potential and electrophoretic mobility measurements after each hybridization experiment and results of electrical measurements.

Target Anthrax			**Control PolyT**		
Zeta potential (mV)	Mobility (10^{-8} m^2/Vs)	Results	Zeta potential (mV)	Mobility (10^{-8} m^2/Vs)	Results
-56.7 ± 6.4	-4.44	Permanent block	-39.0 ± 6.50	-3.06	Transient block
-53.5 ± 5.1	-4.19	Permanent block	-30.6 ± 5.78	-2.40	No block
-50.6 ± 3.7	-3.96	Permanent block	-32.8 ± 4.50	-2.57	No block

Table 3.7 and 3.8 show the detail of current blockades for detecting Anthrax LF DNA and the Poly-T control experiments.

Table 3.7 Repeated Anthrax LF DNA – Anthrax bead blockade measurements for six capillaries

Capillary 1 (Experiment ended after 5th event, which did not reverse with reversed voltage.)

	I_{open} (µA)	I_{block} (µA)	$(I_o - I_b)/ I_o$	R_{open} (Ω)	ΔR (Ω)	ΔR/R
	-0.605	-0.405	0.330	4.13E+07	2.04E+07	0.493
	-0.596	-0.460	0.228	4.20E+07	1.24E+07	0.295
	-0.607	-0.483	0.205	4.12E+07	1.06E+07	0.258
	-0.605	-0.505	0.166	4.13E+07	8.23E+06	0.199
	-0.601	-0.513	0.147	4.16E+07	7.14E+06	0.172
Average	-0.603	-0.473	0.215	4.15E+07	1.18E+07	0.283
Std. Dev.	0.004	0.043	0.072	3.27E+05	5.25E+06	0.127

Capillary 2

	I_{open} (µA)	I_{block} (µA)	$(I_o - I_b)/ I_o$	R_{open} (Ω)	ΔR (Ω)	ΔR/R
	-0.585	-0.399	0.319	4.27E+07	2.00E+07	0.468
	-0.593	-0.461	0.223	4.22E+07	1.21E+07	0.287
	-0.604	-0.481	0.204	4.14E+07	1.06E+07	0.256
	-0.605	-0.479	0.208	4.13E+07	1.08E+07	0.262
	-0.614	-0.493	0.198	4.07E+07	1.00E+07	0.246
Average	-0.600	-0.463	0.230	4.17E+07	1.27E+07	0.304
Std. Dev.	0.011	0.037	0.050	7.89E+05	4.15E+06	0.093

Capillary 3

	I_{open} (µA)	I_{block} (µA)	$(I_o - I_b)/ I_o$	R_{open} (Ω)	ΔR (Ω)	ΔR/R
	-0.560	-0.418	0.254	4.46E+07	1.52E+07	0.341
	-0.565	-0.360	0.362	4.42E+07	2.51E+07	0.569
	-0.592	-0.497	0.160	4.23E+07	8.06E+06	0.191
	-0.626	-0.461	0.263	3.99E+07	1.43E+07	0.358
	-0.621	-0.475	0.235	4.02E+07	1.24E+07	0.308
	-0.604	-0.472	0.218	4.14E+07	1.16E+07	0.280
	-0.610	-0.471	0.229	4.10E+07	1.21E+07	0.296
Average	-0.597	-0.451	0.246	4.19E+07	1.41E+07	0.335
Std. Dev.	0.026	0.047	0.061	1.86E+06	5.35E+06	0.116

Capillary 4

	I_{open} (µA)	I_{block} (µA)	$(I_o - I_b)/ I_o$	R_{open} (Ω)	ΔR (Ω)	ΔR/R
	-0.637	-0.470	0.263	3.93E+07	1.40E+07	0.356
	-0.630	-0.524	0.168	3.97E+07	7.99E+06	0.201
	-0.585	-0.455	0.222	4.27E+07	1.22E+07	0.286
	-0.599	-0.505	0.156	4.18E+07	7.72E+06	0.185
	-0.621	-0.494	0.204	4.03E+07	1.03E+07	0.257
	-0.632	-0.446	0.294	3.95E+07	1.65E+07	0.417
Average	-0.617	-0.482	0.218	4.06E+07	1.15E+07	0.284
Std. Dev.	0.021	0.030	0.054	1.39E+06	3.46E+06	0.090

Capillary 5

	I_{open} (µA)	I_{block} (µA)	$(I_o - I_b)/ I_o$	R_{open} (Ω)	ΔR (Ω)	ΔR/R
	-0.605	-0.405	0.330	4.13E+07	2.04E+07	0.493
	-0.596	-0.460	0.228	4.20E+07	1.24E+07	0.295
	-0.607	-0.493	0.189	4.12E+07	9.58E+06	0.233
	-0.607	-0.498	0.179	4.12E+07	9.01E+06	0.219
	-0.602	-0.482	0.200	4.15E+07	1.04E+07	0.251
	-0.644	-0.446	0.308	3.88E+07	1.73E+07	0.446
Average	-0.610	-0.464	0.239	4.10E+07	1.32E+07	0.323
Std. Dev.	0.017	0.035	0.064	1.12E+06	4.64E+06	0.117

Capillary 6

	I_{open} (µA)	I_{block} (µA)	$(I_o - I_b)/ I_o$	R_{open} (Ω)	ΔR (Ω)	ΔR/R
	-0.587	-0.437	0.256	4.26E+07	1.47E+07	0.344
	-0.602	-0.456	0.243	4.15E+07	1.33E+07	0.321
	-0.564	-0.478	0.152	4.43E+07	7.94E+06	0.179
	-0.614	-0.454	0.260	4.07E+07	1.43E+07	0.352
	-0.623	-0.533	0.145	4.01E+07	6.82E+06	0.170
Average	-0.598	-0.472	0.211	4.18E+07	1.14E+07	0.273
Std. Dev.	0.023	0.037	0.058	1.66E+06	3.74E+06	0.091

Table 3.8 polyT DNA – Anthrax DNA bead blockade measurements for one capillary (Control). Blockades did not occur for the other two capillaries tested.

I_{open} (µA)	I_{block} (µA)	$(I_o - I_b)/ I_o$	R_{open} (Ω)	ΔR (Ω)	ΔR/R	Block duration (sec)
-0.639	-0.523	0.181	3.92E+07	8.67E+06	0.222	5
-0.640	-0.557	0.130	3.91E+07	5.84E+06	0.150	36

The capillary blockade and its magnitude was highly repeatable. In six capillaries tried, blockades were observed for all six (average blockade: 21.5%, 23.0%, 24.6%, 21.8%, 23.9%, and 21.1%; Table T3.7). In each of the capillaries measured, following blockade, the voltage was reversed to remove the bead from the capillary tip to attempt further blockades. In one of the six capillaries, after five detection events, the bead was not able to be removed from the blockade site with reversal of applied voltage and the experiment was terminated.

To investigate the sequence specificity of the sensor, we created a 20-mer ssDNA with the same sequence as the 20-mer ssDNA for the anthrax LF experiment described above but with a single base mismatch. Here is the sequence of ssDNA Anthrax LF with single base mismatch: 5'-GG AT TC TT GT TA AA AAAA AA-3'. The measured zeta potential after PNA conjugation, capping with ethanolamine, and washing was -7.39 mV. As described above, the PNA-beads were divided into two volumes, one incubated with the anthrax LF ssDNA and one with the single base mismatch ssDNA.

Table 3.9 summarizes the results of three separate experiments, which are consistent with our previous results described above. Occasional transient blockades were observed in the presence of the mismatch DNA sample; permanent blockades were recorded only in the presence of target anthrax ssDNA. Also Table 10 shows the current measurements of Anthrax LF with single-base mismatch in three separate capillaries.

Table 3.9. Summary of experimental results for target and single base mismatch control samples: zeta potential and electrophoretic mobility measurements after each hybridization experiment and results of electrical measurements.

Target Anthrax			**Anthrax LF Single Base Mismatch**		
Zeta potential (mV)	Mobility (10^{-8} m^2/Vs)	Results	Zeta potential (mV)	Mobility (10^{-8} m^2/Vs)	Results
-51.1 ± 5.6	-4.01	Permanent block	-45.3 ± 4.38	-3.55	Transient block
-50.3 ± 4.2	-3.95	Permanent block	-44.8 ± 3.72	-3.52	Transient block
-50.9 ± 3.9	-3.99	Permanent block	-41.4 ± 5.23	-3.24	Transient block

Table T3.10 Repeated Anthrax single mismatch DNA – Anthrax bead blockade measurements for three capillaries

Capillary 1

I_{open} (μA)	I_{block} (μA)	$(I_o - I_b)/ I_o$	R_{open} (Ω)	ΔR (Ω)	ΔR/R	Block duration (sec)
-0.605	-0.519	0.143	4.13E+07	6.88E+06	0.167	2
-0.607	-0.501	0.175	4.12E+07	8.73E+06	0.212	4

Capillary 2

	I_{open} (μA)	I_{block} (μA)	$(I_o - I_b)/ I_o$	R_{open} (Ω)	ΔR (Ω)	ΔR/R	Block duration (sec)
	-0.612	-0.480	0.216	4.08E+07	1.12E+07	0.275	2
	-0.628	-0.494	0.212	3.98E+07	1.07E+07	0.269	1
	-0.584	-0.489	0.163	4.28E+07	8.34E+06	0.195	1
	-0.599	-0.490	0.182	4.18E+07	9.29E+06	0.223	1
	-0.582	-0.475	0.183	4.30E+07	9.62E+06	0.224	3
	-0.591	-0.473	0.199	4.23E+07	1.05E+07	0.248	4
	-0.617	-0.479	0.223	4.05E+07	1.17E+07	0.288	1
	-0.645	-0.502	0.221	3.88E+07	1.10E+07	0.283	1
	-0.612	-0.480	0.216	4.08E+07	1.12E+07	0.275	2
	-0.628	-0.494	0.212	3.98E+07	1.07E+07	0.269	1
Average	-0.607	-0.485	0.200	4.12E+07	1.03E+07	0.251	
Std. Dev.	0.022	0.010	0.022	1.49E+06	1.12E+06	0.034	

Capillary 3

	I_{open} (μA)	I_{block} (μA)	$(I_o - I_b)/ I_o$	R_{open} (Ω)	ΔR (Ω)	ΔR/R	Block duration (sec)
	-0.606	-0.427	0.295	4.13E+07	1.73E+07	0.418	8
	-0.608	-0.423	0.303	4.11E+07	1.79E+07	0.436	4
	-0.584	-0.481	0.177	4.28E+07	9.19E+06	0.215	1
	-0.609	-0.541	0.112	4.11E+07	5.17E+06	0.126	7
Average	-0.601	-0.468	0.222	4.16E+07	1.24E+07	0.299	
Std. Dev.	0.012	0.055	0.093	8.36E+05	6.24E+06	0.153	

Since the melting temperature for the single base mismatched DNA is above room temperature, the mismatched DNA-PNA is stably hybridized following incubation of the DNA with the PNA-beads. The measurement of the transient block could result from the mismatched hybrid having a sufficiently low force of dissociation that the DNA strands are removed in the strong electric field of the pore, or the number of mismatched strands hybridized to the bead could be less and the electric field of the pore is removing non-specifically bound DNA from the bead as described above. With either or both of these mechanisms contributing, there was no permanent blockade resulting from the single base mismatched DNA.

Next we calculated the electric force on ssDNA on Anthrax LF beads as described above:

The average ΔR from a bead blockade for all measurements in Table T3.5 is 12.5 MΩ and the average I_b is -0.467 μA. In our experimental conditions, this ΔR obtains for 3.6 μm diameter COOH beads at a $\frac{r_p}{r_c}$ of about 0.765. Using these numbers in Eq. 11, we obtain 14.1 pN. This value is smaller than the required force for unzipping a double stranded DNA and therefore the hybridized ssDNA-PNA is stable under applied force.

Force on entire bead

Next we modeled the bead electrophoretic force by equating it to the drag force on the bead when it is moving with constant speed. The measured mobility is the proportionality constant between the speed and the electric field. By modeling the capillary as a simple cone, we estimated the electric field in the capillary as a function of position.

The electrophoretic force on the entire bead is estimated as follows: The electrophoretic mobility μ is the proportionality constant between the electric field E and bead speed v:

$$v = \mu E \tag{12}$$

For a sphere electrophoretically moving at constant speed in the fluid, there is a constant Stokes drag force equal and opposite to the drag force:

$$F = 6\pi\eta r v = 6\pi\eta r \mu E \tag{13}$$

Where η is the viscosity of water and r is the sphere radius. The electric field in an empty conical capillary we can find from Eq. 11 with $r_p = 0$:

$$E(r_c) = \frac{I_o \rho}{\pi r_c^2} \tag{14}$$

Using the measured open capillary currents and bead mobilities and the measured sphere radius, we may find the electric fields and forces as a function of the capillary radius. For example, with I_o = 600 nA, μ=4x10^{-8} m^2/Vs, $r_c = 2\ r_p$ we find F = 1.36 nN and with $r_c = r_p$ we find F = 5.44 nN. Therefore, we found forces between 1.36 and 5.44 nN as the capillary radius tapered from two bead radii to one bead radius.

Comparison of beads incubated with complementary target ssDNA in Table 3.3 (target: poly A) and Tables 3.6 and 3.9 (target: Anthrax-LF) shows that the magnitudes of the zeta potentials and mobilities in Table 3.3 were larger than those in Tables 3.6 and 3.9. A possible explanation for

these results is the lack of registration required for the hybridization of polyA ssDNA, compared to the exact registration required for hybridization of Anthrax ssDNA. Longer ssDNA targets may improve the electrophoretic mobility of the hybridized beads, while longer strands of non-specifically bound ssDNA would still be expected to detach from the bead in the strong electric field at the sensing zone to result in only transient ionic current blockades.

The limits of detection were probed by serially diluting the 20-mer target anthrax ssDNA in hybridization buffer and repeating the incubation with PNA beads and nanopore measurement as described above (Table T3.11).

Table T3.11 Zeta potential measurements and blockade results as a function of Anthrax LF ssDNA concentration

Concentration	Zeta Potential (mV)	Result
100µM	-50.9± 3.9	Permanent block
10µM	-48.6± 3.5	Permanent block
1µM	-46.3± 5.1	Permanent block
100nM	-43.9± 5.4	Permanent block
10nM	-47.9± 6.7	Permanent block
1nM	-41.0± 7.1	Permanent block
100pM	-36.8± 7.5	Permanent and transient block
10pM	-35.6± 6.5	Permanent and transient block
1pM	-31.2± 3.3	No block
100fM	-27.2± 4.1	No block

Pore blockade was observed down to a concentration of 10 pM. At this concentration, we observed some beads only transiently blocking the pore before permanent block was achieved, indicating the presence of both non-specific and complementary ssDNA bound to the beads, as well as a smaller amount of bound complementary DNA.

Overall, our system performed as expected for detection of specific DNA sequences. Using the conditions described, polyA or Anthrax were successfully detected in every capillary tried (nine capillaries total), with no false positives (no permanent blockade) observed in any capillary (nine capillaries total), including ssDNA with only a single base mismatch. The lowest DNA concentration successfully detected with our unoptimized system was ~10 pM, an unimpressive detection level compared to other published approaches, including a PNA sandwich-hybridization assay for anthrax with a DNA detection limit of as low as 10 zmol.[31] Yet, this binary detection system could exhibit a very low detection limit and in the next chapter we illustrate the reduction of concentration detection limit through the use of longer target ssDNA oligomers.

CHAPTER 4

IMPROVING THE CONCENTRATION DETECTION LIMIT OF THE BIOSENSOR

4.1 Hypothesis and experimental design

In previous chapter, we utilized our sensor for sequence specific detection of 20-mer DNA containing a portion of the anthrax LF gene with a demonstrated detection limit of 10 pM.

In the work described in this chapter, we explored the ability of our device to detect longer DNA fragments. Many samples of biological origin prepared by shearing or other methods contain DNA of a thousand bases or more[114,115,116]. Additionally, as our method relies on the electrophoretic blockade of a pipette tip by beads that have acquired their electrophoretic mobility through the binding of negatively charged target DNA, use of longer DNA strands would impart more negative charge per bound DNA molecule. We hypothesized that increasing the length of the target DNA and therefore increasing charge added to the bead would enable detection at lower DNA concentration.

To assess the capability of our system to detect DNA of various longer lengths and to investigate the impact of target DNA length on the concentration LOD, we produced DNA of 110, 235, 419, and 1613 nucleotides in length all containing the same 12 base target sequence. Control studies were performed with DNA of similar lengths (125, 184, 309, and 1503 nucleotides) in which the target sequence was not present. For efficient production of target and control DNA[117] we performed controlled restriction enzyme digests of pET21b(+) plasmid DNA produced by a

bacterial expression system. The 12-mer target sequence complementary to our PNA probe with the following sequence: NH_2-$(CH_2CH_2O)_{12}$- GC AA CA GT CT TC was located at the 5'- end of the 110-mer and 1613-mer target strands, but was in the middle of the 235-mer and 419-mer targets (Figure 4.1a). The procedure of sample preparation is described below.

4.2 Procedure

4.2.1 Material

NovaBlue competent *E. coli* K-12 cells and pET-21b (+) plasmid vector were purchased from EMD Millipore, Inc. (Billerica, MA). Restriction endonucleases ScaI, PvuI, PstI, BsaI, and EcoNI were obtained from New England BioLabs, Inc. (Ipswich, MA). QIAprep Spin Miniprep, QIAquickGel Extraction, and MinElute Reaction Cleanup Kits were purchased from QIAGEN (Valencia, CA).

4.2.2 Sample preparation

4.2.2.1 Plasmid preparation

Competent *E. coli* K-12 bacteria (Novablue) were transformed with the pET-21b(+) vector following the Novagen protocol. Novablue cells were removed from freezer and thawed on ice for 2-5 minutes. 20 µL cell aliquots were placed in pre-chilled polypropylene tubes to which 1 µL of purified plasmid DNA was added and incubated on ice for 5 minutes. Then the tubes were heated for 30 seconds in a 42 °C water bath and placed on ice for 2 minutes. 80 µL of room temperature SOC medium (2% tryptone, 0.5% yeast extract, 10 mM NaCl, 2.5 mM KCl, 10 mM $MgCl_2$, 10 mM $MgSO_4$, and 20 mM glucose) was added to each tube. An agar plate containing Luria Broth (LB) (10 g/L tryptone, 10 g/L NaCl, and 5 g/L yeast extract in DI water, pH 7.5) was

coated with 60 µL SOC medium and 100 mg/L ampicillin. 25 µL of the induced cells were spread over this plate and incubated inverted at 37 °C for 15 hours. After incubation, a single colony of plasmid-induced NovaBlue cells was selected from the agar plate and incubated in 10 mL LB media supplemented with 100 mg/L ampicillin at 37 °C for 8 hours to provide a starter culture. Subsequently, 1 mL of starter culture was diluted into 500 mL LB medium and incubated at 37 °C for 14 hours. The bacterial culture was aliquoted into ten 50-mL Falcon tubes and centrifuged at 25000 × g for 15 min at 4 °C. The supernatant was removed and the pellets were stored at -80 °C.

For plasmid extraction, one bacterial pellet was thawed in a 50 °C DI water bath. Plasmid extraction and purification was performed following the QIAprep Spin Miniprep Kit protocol. The concentration of extracted plasmids was measured using a NanoDrop2000 (ThermoScientific) spectrophotometer at 260 nm wavelength.

4.2.2.2 Plasmid digestion and DNA isolation and purification

The isolated plasmid was double digested by selected restriction enzyme pairs from ScaI, PvuI, PstI, BsaI, and EcoNI (Figure 4.1a). The enzyme pairs were selected such that target fragments of different lengths were produced containing the sequence, 3’ – GA AG AC TG TT GC – 5’; and control fragments of different lengths were produced not containing the target sequence. Specifically, ScaI and PvuI, acting at bases 4537 and 4427 on the plasmid respectively, produced a 110-base, target-containing fragment, T1 (Figure 4.1), with the remainder of the plasmid forming a 5332-base, non-target-containing fragment. Similarly, ScaI (4537) and PstI (4302) produced target fragment T2 (235 bases); while ScaI (4537) and BsaI (4118) produced target fragment T3 (419 bases), and PvuI (4427) and EcoNI (598) produced target fragment T4 (1613

bases). Control fragments not containing the target sequence were produced using: PvuI and PstI (C1, 125 bases), PstI and BsaI (C2, 184 bases), PvuI and BsaI (C3, 309 bases), and ScaI and EcoNI (C4, 1503 bases).

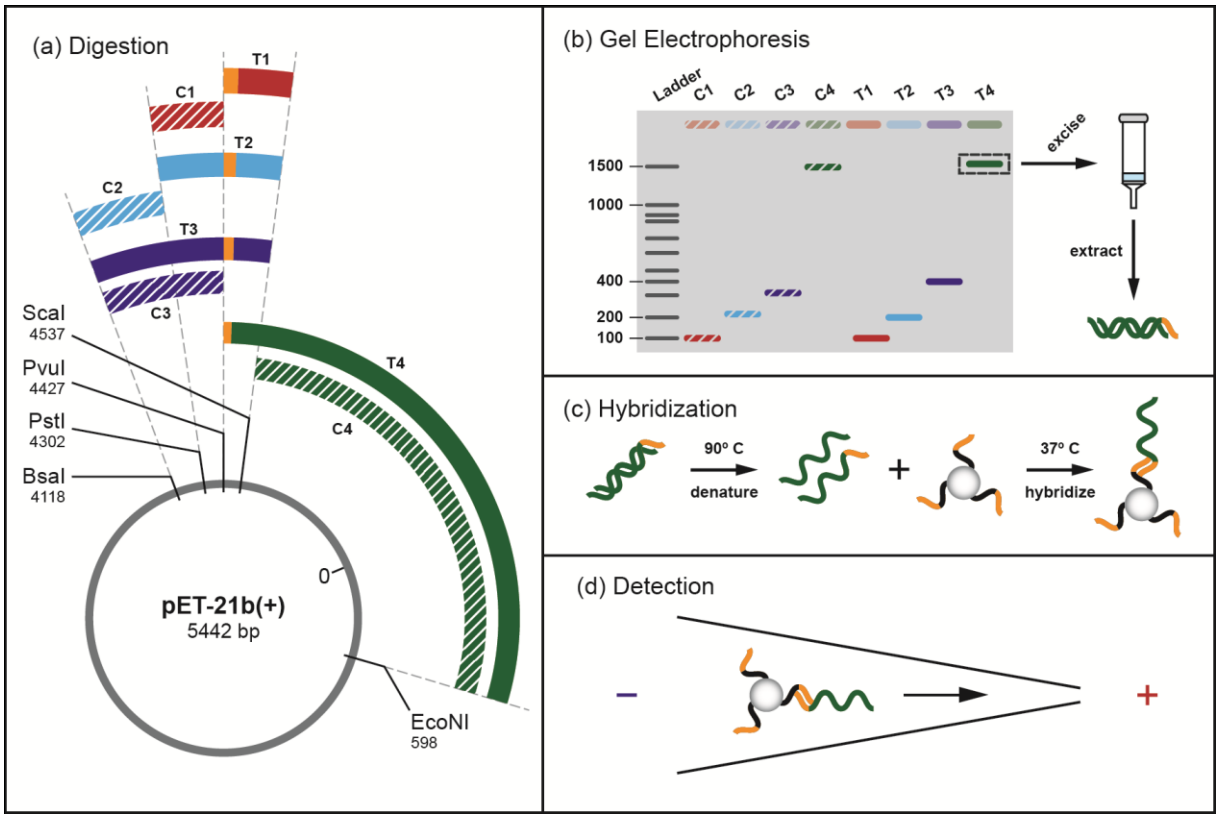

Figure 4.1. Schematic of DNA oligomer preparation. (a) Purified pET-21b plasmids were enzymatically digested by selected pairs of ScaI, PvuI, PstI, BsaI, and EcoNI restriction enzymes, producing fragments of different lengths. The target DNA sequence complementary to the PNA probe is located beginning at plasmid position 4427 (orange band). Plasmid digestion by ScaI and PvuI produced a 110-base, target-containing fragment, T1. Plasmid digestion by PvuI and PstI produced a 125-base, target-free control fragment, C1. Other fragments were produced similarly: T2 (235 bases) using ScaI and PstI, T3 (419 bases) using ScaI and BsaI, T4 (1613 bases) using by PvuI and EcoNI), C2 (184 bases) using PstI and BsaI, C3 (309 bases)

using PvuI and BsaI, and C4 (1503 bases) using ScaI and EcoNI. (b) Following digestion, the DNA was isolated by gel electrophoresis, extracted, and purified. (c) The purified double-stranded DNA was denatured and hybridized with bead-PNA probe conjugates. (d) The DNA-PNA-bead mixture was injected into the micropipette for electrical detection.

After plasmid digestion, target and control DNA fragments were isolated by 1% agarose gel electrophoresis, were excised from the gel, and were purified using QIAquick Gel Extraction and MinElute Cleanup Kits (Figure 4.1b) and eluted into 10 µl Buffer EB (10 mM Tris-Cl, pH 8.5). The DNA concentration of the fragment preparations was measured using the NanoDrop spectrophotometer (260 nm wavelength).

4.3 Results and discussions

Following digestion, gel electrophoresis, excision, purification, and characterization, each of the target and control DNA samples were separately diluted to 1 pM, 100 fM, 10 fM, and 1 fM. The probe conjugation was performed as described before and the zeta potential after four washes typically was ~ -2.4mV.The DNA in each of these solutions was denatured into single strands in a 90 °C water bath for 20 minutes prior to hybridization. Hybridization was performed with 2.1×10^6 PNA-bead conjugates in hybridization buffer at 37 °C overnight (Figure 10 c). Beads incubated with each target and control concentration (1 pM – 10 fM) were injected into a fresh capillary and the resultant current measured during voltage application (Figure 10 d). When a block was observed, the potential was maintained for at least 60 seconds following the block. Blocks that persisted for ≥60 seconds were deemed to be permanent. To show that permanent blocks were a result of electrophoresis and not an adhesion of the bead to the capillary wall, we repeatedly reversed the voltage and reapplied it to open the pore and obtain another block. Some

bead blocks were observed to be transient, where the bead traveled back down the capillary after a short time (average time of 10.8 sec). This was also observed in our previous work, where we hypothesized that removal of weakly attached, non-specifically bound DNA from the bead reduced its charge, reducing the electrophoretic force on the bead and enabling its removal from the tip by the opposing electroosmotic flow.

Beads incubated with the 110-mer target DNA were unable to block the capillaries at any concentration tested (1 pM – 1 fM), except for one observation at 10 fM. To verify that the 110-mer target was functional, we successfully detected it at 10 pM concentration (the lower limit of detection found in our previous work with 20-mer target DNA). Permanent, reversible blocks were successfully detected for the 235-mer targets down to 100 fM and for the 419-mer and 1613-mer targets down to 10 fM. At 1 fM, no blockades were obtained for target or control DNA of any length. Table 4.1 shows the results of the capillary blockade detection for the different target and control DNA lengths as a function of DNA concentration. In each of the three experiments shown, the 1613-mer target DNA was detected at 10 fM.

Table4.1. Summary of Detection results for target and control samples. A positive result indicates a blockade measured for > 60 seconds that was reversible. A negative result is indicated when no block or a transient block (<60 sec) was observed. Measurement details are provided in the Supplemental Information.

	Target		Control	
[DNA]	Length	Detection?	Length	Detection?
1 pM	110	No	125	No
	235	Yes	184	No*
	419	Yes	309	No
	1613	Yes	1503	Yes^
100 fM	110	No*	125	No
	235	Yes	184	No*
	419	Yes	309	No
	1613	Yes	1503	No
10 fM Expt. 1	110	No	125	No
	235	No	184	No
	419	Yes/No%	309	No
	1613	Yes	1503	No*
10 fM Expt. 2	110	Yes%	125	No*
	235	No	184	No
	419	No	309	No
	1613	Yes	1503	No*
10 fM Expt. 3	110	No	125	No
	235	No	184	No*
	419	Yes	309	No
	1613	Yes	1503	No*
1 fM (2 expts.)	110	No	125	No
	235	No	184	No
	419	No	309	No
	1613	No	1503	No

* Transient block observed

^ Permanent block then transient block after reversal

% Transient block observed, followed by permanent block

Measured current traces from all observed blockages for DNA oligomers of each concentration are listed below:

Measurement results for Target and Control DNA from 1 pM to 10 fM

I_{open} is the current measured in the capillary with no obstruction, I_{block} is the current measured with an obstructing bead present, $R_{open} = 25\ V/I_{open}$, $\Delta R = V/I_{block} - R_{open}$. A Permanent block is

noted if the block persisted beyond 60 sec, and was reversible when the sign of the applied voltage was reversed.

1 pM Target

110-mer Target

No capillary blockades observed.

Table 4.2. 235-mer Target

	I_{open} (µA)	I_{block} (µA)	$(I_o - I_b)/ I_o$	R_{open} (Ω)	ΔR (Ω)	ΔR/R	Block duration (Sec)
	-0.518	-0.436	0.158	4.83E+07	9.10E+06	0.200	Permanent
	-0.527	-0.462	0.123	4.74E+07	6.70E+06	0.141	Permanent
	-0.559	-0.488	0.127	4.47E+07	6.51E+06	0.145	Permanent
	-0.577	-0.495	0.142	4.33E+07	7.20E+06	0.200	Permanent
	-0.585	-0.522	0.108	4.27E+07	5.20E+06	0.121	Permanent
Average	-0.553	-0.481	0.132	4.53E+07	6.91E+06	0.152	
Std.Dev.	0.027	0.029	0.017	2.20E+06	1.26E+06	0.022	

Table 4.3. 419-mer Target

	I_{open} (µA)	I_{block} (µA)	$(I_o - I_b)/ I_o$	R_{open} (Ω)	ΔR (Ω)	ΔR/R	Block duration (Sec)
	-0.617	-0.546	0.115	4.11E+07	5.30E+06	0.130	Permanent
	-0.612	-0.512	0.163	4.20E+07	7.98E+06	0.200	Permanent
	-0.609	-0.516	0.153	4.11E+07	7.40E+06	0.180	Permanent
	-0.62	-0.529	0.147	4.03E+07	6.94E+06	0.172	Permanent
Average	-0.615	-0.526	0.144	4.20E+07	6.90E+06	0.169	
Std.Dev.	0.004	0.013	0.018	2.83E+05	1.01E+06	0.024	

Table 4.4. 1613-mer Target

	I_{open} (µA)	I_{block} (µA)	$(I_o - I_b)/ I_o$	R_{open} (Ω)	ΔR (Ω)	ΔR/R	Block duration (Sec)
	-0.576	-0.512	0.111	4.34E+07	5.43E+06	0.125	Permanent
	-0.53	-0.450	0.151	4.72E+07	8.39E+06	0.178	Permanent
	-0.524	-0.447	0.147	4.77E+07	8.22E+06	0.172	Permanent
	-0.523	-0.439	0.161	4.78E+07	9.15E+06	0.191	Permanent
Average	-0.538	-0.462	0.142	4.65E+07	7.79E+06	0.167	
Std.Dev.	0.022	0.029	0.019	1.82E+06	1.41E+06	0.025	

1 pM Control

125-mer Control

No capillary blockades detected.

Table 4.5. 184-mer control

I_{open} (µA)	I_{block} (µA)	$(I_o - I_b)/ I_o$	R_{open} (Ω)	ΔR (Ω)	ΔR/R	Block duration (Sec)
-0.535	-0.458	0.158	4.8E+07	9.10E+06	0.20	7
-0.543	-0.421	0.123	4.7E+07	6.70E+06	0.141	5

419-mer Control

No capillary blockades detected.

Table 4.6. 1503-mer Control

	I_{open} (µA)	I_{block} (µA)	$(I_o - I_b)/ I_o$	R_{open} (Ω)	ΔR (Ω)	ΔR/R	Block duration (Sec)
	-0.608	-0.406	0.332	4.11E+07	2.05E+07	0.498	Permanent
	-0.624	-0.575	0.079	4.01E+07	3.41E+06	0.085	29
	-0.636	-0.523	0.177	3.93E+07	8.49E+06	0.216	16
Average	-0.623	-0.501	0.196	4.02E+07	1.08E+07	0.266	
Std.Dev.	0.011	0.071	0.104	7.42E+05	7.14E+06	0.172	

100 fM Target

Table 4.7. 110-mer Target

I_{open} (µA)	I_{block} (µA)	$(I_o - I_b)/ I_o$	R_{open} (Ω)	ΔR (Ω)	ΔR/R	Block duration (Sec)
-0.610	-0.475	0.222	4.09E+07	1.20E+07	0.286	4
-0.615	-0.550	0.105	4.07E+07	4.78E+06	0.117	16

Table 4.8. 235-mer Target

	I_{open} (µA)	I_{block} (µA)	$(I_o - I_b)/ I_o$	R_{open} (Ω)	ΔR (Ω)	ΔR/R	Block duration (Sec)
	-0.574	-0.485	0.155	4.36E+07	7.99E+06	0.184	Permanent
	-0.552	-0.479	0.132	4.53E+07	6.90E+06	0.152	Permanent
	-0.583	-0.500	0.143	4.29E+07	7.15E+06	0.167	Permanent
Average	-0.570	-0.488	0.143	4.39E+07	7.35E+06	0.168	
Std.Dev.	0.013	0.009	0.009	1.02E+06	4.67E+05	0.013	

Table 4.9. 419-mer Target

	I_{open} (µA)	I_{block} (µA)	$(I_o - I_b)/ I_o$	R_{open} (Ω)	ΔR (Ω)	ΔR/R	Block duration (Sec)
	-0.572	-0.353	0.383	4.37E+07	2.71E+07	0.621	Permanent
	-0.574	-0.358	0.376	4.36E+07	2.63E+07	0.603	Permanent
	-0.576	-0.485	0.158	4.34E+07	8.14E+06	0.188	Permanent
	-0.571	-0.356	0.377	4.38E+07	2.64E+07	0.604	Permanent
	-0.581	-0.4191	0.279	4.303E+07	1.66E+07	0.386	Permanent
Average	-0.575	-0.394	0.315	4.35E+07	2.09E+07	0.480	
Std.Dev.	0.003	0.052	0.087	2.65E+05	7.48E+06	0.170	

Table 4.10. 1613-mer Target

	I_{open} (μA)	I_{block} (μA)	$(I_o - I_b)/ I_o$	R_{open} (Ω)	ΔR (Ω)	ΔR/R	Block duration (Sec)
	-0.676	-0.600	0.112	3.70E+07	4.67E+06	0.126	Permanent
	-0.671	-0.599	0.107	3.73E+07	4.45E+06	0.119	Permanent
	-0.639	-0.571	0.106	3.91E+07	4.66E+06	0.119	Permanent
	-0.636	-0.535	0.159	3.93E+07	7.43E+06	0.189	Permanent
	-0.613	-0.488	0.203	4.08E+07	1.04E+07	0.255	Permanent
Average	-0.647	-0.559	0.137	3.87E+07	6.32E+06	0.162	
Std.Dev.	0.023	0.043	0.038	1.41E+06	2.32E+06	0.054	

100 fM Control

No capillary blockades detected for the 125-mer, 184-mer, 309-mer, and 1503-mer control DNA.

10 fM Target

Experiment 1

110-mer and 235-mer target

No capillary blockades detected

Table 4.11. 419-mer Target

	I_{open} (μA)	I_{block} (μA)	$(I_o - I_b)/ I_o$	R_{open} (Ω)	ΔR (Ω)	ΔR/R	Block duration (Sec)
	-0.597	-0.478	0.199	4.19E+07	1.04E+07	0.249	2
	-0.574	-0.486	0.153	4.36E+07	7.89E+07	0.181	2
	-0.583	-0.465	0.202	4.29E+07	1.09E+07	0.254	Permanent
	-0.579	-0.475	0.180	4.32E+07	9.45E+06	0.219	Irreversible
Average	-0.583	-0.476	0.184	4.29E+07	9.66E+06	0.226	
Std.Dev.	0.009	0.008	0.020	6.23E+05	1.147E+06	0.029	

Table 4.12. 1613-mer Target

	I_{open} (µA)	I_{block} (µA)	$(I_o - I_b)/ I_o$	R_{open} (Ω)	ΔR (Ω)	ΔR/R	Block duration (Sec)
	-0.638	-0.542	0.150	3.92E+07	6.93E+06	0.177	Permanent
	-0.654	-0.518	0.208	3.82E+07	1.00E+07	0.263	Permanent
	-0.603	-0.527	0.126	4.15E+07	5.98E+06	0.144	Permanent
	-0.602	-0.525	0.128	4.15E+07	6.09E+06	0.147	Permanent
	-0.598	-0.524	0.124	4.18E+07	5.90E+06	0.141	Permanent
Average	-0.619	-0.527	0.147	4.04E+07	6.99E+06	0.174	
Std.Dev.	0.023	0.008	0.032	1.45E+06	1.57E+06	0.046	

Experiment 2

Table 4.13. 110-mer Target

	I_{open} (µA)	I_{block} (µA)	$(I_o - I_b)/ I_o$	R_{open} (Ω)	ΔR (Ω)	ΔR/R	Block duration (Sec)
	-0.514	-0.446	0.132	4.86E+07	7.42E+06	0.152	43
	-0.531	-0.451	0.151	4.71E+07	8.35E+06	0.177	Permanent
	-0.543	-0.422	0.223	4.60E+07	1.32E+07	0.287	Permanent
Average	-0.529	-0.440	0.169	4.73E+07	9.66E+06	0.206	
Std.Dev.	0.012	0.013	0.039	1.07E+06	2.54E+06	0.058	

235-mer and 419-mer Target

No capillary blockades detected.

Table 4.14. 1613-mer Target

	I_{open} (µA)	I_{block} (µA)	$(I_o - I_b)/ I_o$	R_{open} (Ω)	ΔR (Ω)	ΔR/R	Block duration (Sec)
	-0.622	-0.548	0.119	4.02E+07	5.43E+06	0.135	Permanent
	-0.614	-0.454	0.261	4.07E+07	1.43E+07	0.352	Permanent
	-0.628	-0.457	0.272	3.98E+07	1.49E+07	0.374	Permanent
	-0.6143	-0.463	0.246	4.07E+07	1.33E+07	0.326	Permanent
	-0.597	-0.454	0.240	4.19E+07	1.32E+07	0.315	Permanent
Average	-0.615	-0.475	0.228	4.07E+07	1.22E+07	0.301	
Std.Dev.	0.010	0.037	0.055	6.97E+05	3.46E+06	0.085	

Experiment 3

110-mer and 235-mer Target

No capillary blockades detected.

Table 4.15. 419-mer Target

	I_{open} (µA)	I_{block} (µA)	$(I_o - I_b)/ I_o$	R_{open} (Ω)	ΔR (Ω)	ΔR/R	Block duration (Sec)
	-0.64	-0.532	0.169	3.91E+07	7.93E+06	0.203	Permanent
	-0.628	-0.536	0.146	3.98E+07	6.83E+06	0.172	Permanent
	-0.614	-0.530	0.136	4.07E+07	6.43E+06	0.158	Permanent
Average	-0.627	-0.533	0.151	3.99E+07	7.07E+06	0.178	
Std.Dev.	0.011	0.002	0.013	6.74E+05	6.33E+05	0.019	

Table 4.16. 1613-mer Target

	I_{open} (µA)	I_{block} (µA)	$(I_o - I_b)/ I_o$	R_{open} (Ω)	ΔR (Ω)	ΔR/R	Block duration (Sec)
	-0.626	-0.506	0.192	3.99E+07	9.47E+06	0.237	Permanent
	-0.632	-0.544	0.139	3.96E+07	6.40E+06	0.162	Permanent
	-0.629	-0.534	0.151	3.97E+07	7.07E+06	0.178	Permanent
	-0.643	-0.547	0.149	3.89E+07	6.82E+06	0.176	Permanent
Average	-0.633	-0.533	0.158	3.95E+07	7.44E+06	0.188	
Std.Dev.	0.006	0.016	0.020	3.98E+05	1.2E+06	0.029	

10 fM Control

Experiment 1

125-mer, 184-mer, and 309-mer control

No capillary blockades detected.

Table 4.17. 1503-mer Control

	I_{open} (μA)	I_{block} (μA)	$(I_o - I_b)/ I_o$	R_{open} (Ω)	ΔR (Ω)	ΔR/R	Block duration (Sec)
	-0.560	-0.484	0.135	4.47E+07	6.98E+06	0.156	20
	-0.592	-0.425	0.283	4.22E+07	1.66E+07	0.394	37
	-0.587	-0.477	0.188	4.26E+07	9.83E+06	0.231	21
Average	-0.580	-0.462	0.202	4.31E+07	1.11E+07	0.260	
Std.Dev.	0.014	0.026	0.061	1.08E+06	4.05E+06	0.099	

Experiment 2

Table4.18. 125-mer Control

I_{open} (μA)	I_{block} (μA)	$(I_o - I_b)/ I_o$	R_{open} (Ω)	ΔR (Ω)	ΔR/R	Block duration (Sec)
-0.557	-0.465	0.165	4.48E+07	8.96E+06	0.201	2

184-mer and 309-mer Control

No capillary blockades detected.

Table 4.19. 1503-mer Control

	I_{open} (μA)	I_{block} (μA)	$(I_o - I_b)/ I_o$	R_{open} (Ω)	ΔR (Ω)	ΔR/R	Block duration (Sec)
	-0.614	-0.497	0.191	4.07E+07	9.60E+06	0.236	14
	-0.622	-0.406	0.347	4.02E+07	2.14E+07	0.532	2
	-0.589	-0.487	0.173	4.24E+07	8.89E+06	0.209	10
Average	-0.608	-0.463	0.237	4.11E+07	1.33E+07	0.326	
Std.Dev.	0.014	0.041	0.078	9.64E+05	5.73E+06	0.146	

Experiment 3

125-mer Control

No capillary blockades detected.

Table 4.20. 184-mer Control

I_{open} (μA)	I_{block} (μA)	$(I_o - I_b)/ I_o$	R_{open} (Ω)	ΔR (Ω)	ΔR/R	Block duration (Sec)
-0.552	-0.483	0.123	4.53E+07	6.46E+06	0.143	2

309-mer Control

No capillary blockades detected.

Table 4.21. 1503mer Control, Ex.3

I_{open} (μA)	I_{block} (μA)	$(I_o - I_b)/ I_o$	R_{open} (Ω)	ΔR (Ω)	ΔR/R	Block duration (Sec)
-0.581	-0.462	0.205	4.30E+07	1.11E+07	0.258	13
-0.572	-0.481	0.159	4.37E+07	8.27E+06	0.189	5

1 fM Target and Control

No permanent or transient blocks observed for any target or control DNA oligomer.

All control experiments showed either transient or no blockade of the pore for all DNA lengths and concentrations measured, with one exception. At 1 pM, the beads incubated with the 1503-mer control initially showed a permanent block, which was not repeated following voltage reversal; instead the previously blocking bead gave a transient block. Thus, the devices yielded essentially no false positive results.

To simulate the detection of our target sequence against a background of genomic DNA, we incubated PNA-beads with a solution containing 10 fM of the 1613-mer target sequence and 30 pM of the 1503-mer control sequence. Thirty picomolar of 1503-mer DNA approximates the 4.6 Mb *E. coli* genome at 10 fM after shearing. Repeatable permanent blocks of the capillary pore were observed (Table 4.22) . As a control experiment, we incubated the PNA-beads with 30 pM of 1503-mer DNA without 10 fM of the 1613-mer target sequence and observed no permanent or transient blocks.

10 fM 1613-mer Target in presence of 30 pM 1503-mer control background

Table 4.22 10fM 1613-mer target in presence of non-specific background

	I_{open} (μA)	I_{block} (μA)	$(I_o - I_b)/ I_o$	R_{open} (Ω)	ΔR (Ω)	ΔR/R	Block duration (Sec)
	-0.565	-0.487	0.138	4.42E+07	7.09E+06	0.160	6
	-0.578	-0.464	0.197	4.33E+07	1.06E+07	0.246	4
	-0.596	-0.433	0.273	4.19E+07	1.58E+07	0.376	4
	-0.579	-0.478	0.174	4.32E+07	9.12E+06	0.211	Permanent
	-0.567	-0.440	0.224	4.41E+07	1.28E+07	0.289	Permanent
	-0.619	-0.475	0.233	4.04E+07	1.22E+07	0.303	3
	-0.623	-0.481	0.228	4.01E+07	1.19E+07	0.295	3
	-0.596	-0.481	0.193	4.19E+07	1.00E+07	0.239	8
	-0.589	-0.493	0.162	4.24E+07	8.23E+06	0.194	Permanent
	-0.587	-0.375	0.361	4.27E+07	2.41E+07	0.566	Permanent
	-0.614	-0.464	0.244	4.07E+07	1.32E+07	0.323	Permanent
	-0.564	-0.413	0.268	4.43E+07	1.62E+07	0.366	Permanent
	-0.625	-0.403	0.355	4.00E+07	2.20E+07	0.551	Permanent
	-0.625	-0.532	0.149	4.00E+07	6.99E+06	0.175	14
	-0.598	-0.484	0.191	4.18E+07	9.85E+06	0.236	7
	-0.597	-0.464	0.223	4.19E+07	1.20E+07	0.287	Permanent
	-0.634	-0.458	0.278	3.94E+07	1.52E+07	0.384	Permanent
	-0.581	-0.486	0.164	4.30E+07	8.41E+06	0.195	Permanent
	-0.592	-0.415	0.299	4.22E+07	1.80E+07	0.427	Permanent
Average	-0.596	-0.459	0.229	4.02E+07	1.28E+07	0.307	
Std.Dev.	0.021	0.040	0.063	1.48E+06	4.64E+06	0.113	

No permanent or transient blocks observed for 30pM 1503-mer control DNA measured alone.

The successful detection of 1613-mer DNA at 10 fM concentration is consistent with our hypothesis that the concentration limit of detection could be lowered from 10 pM found in our previous work by increasing the length of the DNA bound to the bead and therefore the amount of charge imparted to the bead. By increasing the charge per bound strand, we may be compensating for a decrease in electrophoretic mobility resulting from a decreased number of bound DNA oligomers per bead at lower DNA concentrations.

We may estimate the number of bound DNA oligomers per bead using Poisson statistics:

$$P_{\mu}(\nu) = e^{-\mu}\frac{\mu^{\nu}}{\nu!} \quad (15)$$

where μ is the average number of DNA molecules per bead and $P_{\mu}(\nu)$ is the probability of finding ν molecules on one bead. Our 100 μl reaction volume contained 2.1×10^6 beads; and 10 fM DNA in this volume is approximately 6.0×10^5 molecules, which gives a bead-to-DNA ratio of 3.5:1 and a μ of 0.287 DNA/bead. With this μ, we obtain the probability of a bead having zero bound DNA of P(0) = 0.751, probability of one bound DNA, P(1) = 0.215, P(2) = 0.031, etc. Multiplication of these probabilities by the total bead count yields the number of beads having a number of bound DNA (Table 4.23): 1.6×10^6 beads with no DNA, 4.5×10^5 beads with 1 bound DNA, 6.5×10^4 beads with 2 bound DNA, 6190 beads with 3 bound DNA, 443 beads with 4 bound DNA, 25 beads with 5 bound DNA, 1 with 6 bound DNA, and less than 1 with more than 6 bound DNA. This analysis assumes that all DNA molecules are bound to beads and ignores the binding of the non-complementary DNA to the beads (the DNA after purification is double-stranded and denatured before incubation with the beads, giving a complementary and non-complementary population of DNA).

Table 4.23. Poisson distribution calculation for 10 fM DNA concentration ($2.1x10^6$ beads).

DNA concentration	Number of target DNA	Number of beads	Average # of target DNA per bead (μ)	# of bound DNA (ν)	Percent of beads bound to ν target DNA	#of beads with ν bound DNA
10fM	$6.02x10^5$	$2.1x10^6$	0.287	0	75.07619%	1576600
				1	21.52184%	451958
				2	3.084797%	64780
				3	0.29477%	6190
				4	0.021125%	443
				5	0.00121%	25
				6	0.00006%	1

Repeating this analysis with the same number of beads, but for DNA detection at 1 fM gives μ = 0.0287 corresponding to 97.2% of the beads bound to zero DNA molecules, 58498 beads bound to one DNA, 838 beads bound to 2 DNA, 8 beads bound to 3 DNA, and less than 1 on average bound to more than 3 DNA (Table 4.24).

Table 4.24. Poisson distribution calculation for 1 fM DNA concentration ($2.1x10^6$ beads).

DNA concentration	Number of target DNA	Number of beads	Average # of target DNA per bead (μ)	# of bound DNA (ν)	Percent of beads bound to ν target DNA	#of beads with ν bound DNA
1fM	$6.02x10^4$	$2.1x10^6$	0.0287	0	97.17403%	2040654
				1	2.78566%	58498
				2	0.03993%	838
				3	0.00038%	8

Based on this analysis, we suggest two possible reasons why the detection was successful at 10 fM but not 1 fM. 1) Only beads containing 4, 5, or 6 DNA (present at 10 fM but not 1 fM) have electrophoretic mobility sufficient to block the capillary; 2) Beads containing fewer bound DNA (e.g., 3) can produce blockades; but less than 100% yield in bead preparation, combined with the

smaller numbers of these beads present at 1 fM (8 out of 2.1×10^6), combine to give a low probability of blockage by such beads.

The results presented here suggest that it may be possible to obtain a lower concentration LOD with this device by further lengthening the DNA target. However, for shorter DNA lengths, it may also be possible to obtain a lower concentration LOD by decreasing the number of beads used. According to our Poisson calculations, a 10-fold to 100-fold decrease in bead count per experiment would increase μ and therefore increase the number of beads bound to several DNA. For example, 1 fM DNA measured with 2.1×10^5 beads would result in 619 beads with 3 DNA, 44 with 4 DNA, and 2 with 5 DNA. At 1 fM DNA measured and 2.1×10^4 beads thousands of beads bound to 4 or more DNA would result (Table4.25 and 4.26).

Table 4.25. Poisson distribution calculation for 1 fM DNA concentration ($2.1x10^5$ beads).

DNA concentration	Number of target DNA	Number of beads	Average # of target DNA per bead (μ)	# of bound DNA (ν)	Percent of beads bound to ν target DNA	#of beads with ν bound DNA
1fM	$6.02x10^4$	$2.1x10^5$	0.287	0	75.07619%	157660
				1	21.52184%	45195
				2	3.08479%	6478
				3	0.29477%	619
				4	0.02113%	44
				5	0.00121%	2

Table 4.26. Poisson distribution calculation for 1 fM DNA concentration ($2.1x10^4$ beads).

DNA concentration	Number of target DNA	Number of beads	Average # of target DNA per bead (μ)	# of bound DNA (ν)	Percent of beads bound to ν target DNA	#of beads with ν bound DNA
1fM	$6.02x10^4$	$2.1x10^4$	2.87	0	5.68882%	1194
				1	16.30796%	3424
				2	23.37475%	4908
				3	22.33587%	4690
				4	16.00737%	3361
				5	9.17759%	1927
				6	4.38483%	920
				7	1.79569%	377
				8	0.643457%	135
				9	0.204953%	43
				10	0.058753%	12
				11	0.015311%	3
				12	0.0036577%	1

However, in our 100 μl reaction volume, 2.1×10^6 polystyrene beads was the minimum usable aliquot per experiment, given the limitations of pipetting, centrifugation, and zeta potential measurement. In order to overcome the centrifugation limitation and conserve the small number of beads (dilution~ 10^4) during sample preparation step, we used 3μ diameters magnetic beads coated with polystyrene and functionalized with carboxylic acid groups. The advantage of using the magnetic beads is the fast and easy collection of them after conjugation, hybridization and wash steps by a strong magnetic field. We used COMPEL COOH magnetic beads (catalog number UMC3N, Bangs Laboratory Inc, Fishers, IN) which are 2.90μm in diameter. The beads were serially diluted to 10^5 and 10^4 beads per 100μL and counted using a hemocytometer to accurately calculate the number of beads prior to hybridization step. Each dilution was collected with a strong magnet and resuspended in 1mM KCl to replicate the sample collection after the hybridization step. To verify the efficiency of collection, beads were counted using the hemocytometer once more. The number of beads after collection remained the same and

therefore using magnetic bead as surface probe addressed our previous sample collectiong shortcomings. Next, 10^6 carboxylic acid magnetic beads per milliliter were used for zeta a potential measurement and the readout was -47mV. This zeta potential measurement was significantly larger than zeta potential measurement of the non-magnetic polystyrene carboxylic acid beads (~ -80mV). Afterward carboxylic acid magnetic beads were injected into a micropipette for conductance measurements. Under applied electric field, beads blocked the pore but were stuck to the tip of capillary and the blocks were un-reversible by changing the polarity of voltage. We only observed few reversible current blockades by the carboxylic acid magnetic beads. This could be the result of magnetic beads elasticity which results in their deformation under strong applied electric field compare to non-magnetic polystyrene beads. As a magnetic bead deformed and consequently wedged into the pore, it became stuck and irreversible when switching the polarity of applied voltage.

To overcome this challenge we tested two different types of magnetic beads with carboxylic acid functional groups: proMag beads 3 series, average diameter 3.02µm (catalog number PMC3N, Bangs Laboratory Inc, Fishers, IN) and SPHERO carboxyl Magnetic particles with 3.14µm average diameter (catalog number CMS-30-10, Spherotech Inc, Lake Forest IL). The zeta potential measurements of these beads were -7mV and -12mV respectively and the capillary experiments showed no current blockade with any of these particles as a result of few surface charges on the beads. Although conservation of magnetic beads after sample preparation was improved by using a strong magnetic field, the beads material structure and properties prevented us to obtain reversible current blocks in the conductance measurement experiments. An alternative future solution could be the use of a “front-to-end” microfluidic approach to reduce

the volumetric limitation of our current hybridization procedure and reduce our bead-to-DNA ratio which potentially could improve our detection limit beyond 10 fM.

In addition to Poisson statistical analysis, zeta potential measurements were performed to illustrate the charge distribution on beads after the hybridization procedure. Table 4.27 shows the measurement results in 1mM KCl solution pH 7.0.

Table 4.27 Summary of zeta potential measurements for target and control samples

Target			Control		
DNA length	DNA concentration	zeta potential peaks (mV)	DNA length	DNA concentration	zeta potential peaks (mV)
110	1pM	-34.6 /97.5% 6.99 /2.5%	125	1pM	-8.58 /100%
235	1pM	-41.6 /98.6% -0.4/ 1.4%	184	1pM	-4.61 /68.4% -32.8/ 31.6%
419	1pM	-43.6 /100%	309	1pM	-29.6 /80.8% 4.65 / 19.2%
1613	1pM	-35.1 /59.0% -3.31 /38.5% -66.6 /2.5%	1503	1pM	-2.63 /72.7% -34.8 / 27.3%
110	100fM	-37.7 /98.6% -63 / 1.4%	125	100fM	-37.7 /100%
235	100fM	-46.3 /89.2% -5.89/10.8%	184	100fM	-35.7 /100%
419	100fM	-43.6 /98.9% -13.8 /1.1%	309	100fM	-32.5 /97.7% 6.75 / 2.3%
1613	100fM	-41.3 /98.3% 0.098/ 1.7%	1503	100fM	-31.2 /97.9% 6.91 / 2.1%
110	10fM	-5.11 /49.1% -31.3 /28.8% -18.1 /22.1%	125	10fM	-27.7 /73.9% 2.18 /16.9% -8.38 /9.2%
235	10fM	-30.3 /31% -11.3 /28.6% 8.93 /37.3%	184	10fM	-27.9 /96.1% 7.7 /3.9%
419	10fM	-38.6 /52% -2.81 /48%	309	10fM	-21.3 /94.7% -38.6 /4.7% 10.5 /0.6%
1613	10fM	-43.8 /68.6% -14.7 /13.7% 2.84 /8.9%	1503	10fM	-31.3 /51% -1.95/31.5% -44.6 /17.3%
110	10fM	-45.5 /100%	125	10fM	-38.0 /89.9% -5.8 /10.1%
235	10fM	-35.5 /98.4% -4.35 /1.6%	184	10fM	-31.6 /100%
419	10fM	-41.1 /100%	309	10fM	-37.9 /98.9% -0.0236 /1.1%

1613	10fM	-44 /95% -4.73 /5.0%	1503	10fM	-34.1 /100%
110	10fM	-34 /95.3% 1.35 /3.9%	125	10fM	-30.1 /100%
235	10fM	-34.5 /96.1% 8.55 /3.9%	184	10fM	-36.3 /97.3% 2.9 /2.7%
419	10fM	-40.5 /92.6% -13.3 /7.4%	309	10fM	-31 /73.3% 6.44 /26.7%
1613	10fM	-40.7 /86.1% -13.7 /10.6% 0.525 /4.3%	1503	10fM	-30.1 /100%
110	1fM	-5 /99.9% -35.4 /0.1%	125	1fM	-0.268 /100%
235	1fM	-11 /47.5% -26.6 / 27.6% 3.13 /24.8%	184	1fM	4.7 /50.5% -14.3 /49.5%
419	1fM	-2.42 /57.5% -19.7 /30.9% -33.8 /11.5%	309	1fM	-13.6 /57.9% 9.71 /23.6% -35 /16.7%
1613	1fM	-18.1 /74.8% 5.8 /25.2%	1503	1fM	0.418 /68.2% -35.5 /25.3% -18.2 /6.5%
1613 Target 10 fM 1503 Control 30 pM		-22.5mV/53.8% -36.5mV/46.2%	1503	30pM	-21.7mV/100%

These measurements show the decrease in zeta potential values after PNA-beads were incubated with target and control DNA strands as a result of specific and non-specific bindings. Also, the measurements of target DNA hybridized beads showed lower zeta potential value (more negative) for higher percentage of beads compare to the corresponding control ZP values. Therefore, these measurements qualitatively confirmed the presence of higher number of charges per bead after the DNA incubation; which is in line with the sensor's conductance measurement results.

One would expect to see low zeta potential values when beads hybridized with longer ssDNA compare to the beads hybridized with shorter ssDNA. However, the measurement results didn't confirm this prediction. As an example, at 100fM concentration the majority of 1613-mer and 419-mer DNA hybridized beads have almost identical zeta potential values of -41.3 mV and -43.6 mV. This might be the result of longer DNA strands coiled up after hybridization to PNA

probes on the bead. Also, based on Poisson statistics for 10fM DNA concentration 75% of beads has no bound DNA, and therefore we assumed to see two peaks; one with higher percentage of beads population at higher zeta potential value (close to zero) and one with smaller percentage of beads with lower ZP value. However, the measured ZP values failed to illustrate that. To investigate the accuracy of the zeta potential measurements we ran a control experiment with a sample containing 50% of 3µm polystyrene beads with ZP of -77.1mV and 50% of 3µm polystyrene beads with ZP of 1.75mV in DI water (the experiments were repeated 3 times). The result of the first experiment showed that 70.9% of beads have the mean zeta potential value of -38mV and 29.1% of beads have the mean zeta potential of -72.5mV. The second experiment showed one peak at -31mV for 75.6% of beads populations and -67.4mV for only 24.4% of beads. Third experiment illustrated the measured zeta potential value of -30.4mV for 70.2% of beads and -65mV for 29.8% of beads. The value of measured ZP in these experiments not only did not match the average zeta potential of unmixed samples but also the percentage of the beads population did not match the ratio of beads mixture in the solution. One possible reason for this observation could be the aggregation of the beads. To clarify this assumption we measured the size of each bead type as well as the 50/50 mixture of them by DLS. The average diameter of polystyrene beads with -77.1mV ZP was 2254 nm and the average diameter of polystyrene beads with 1.75mV was 3716nm. The average diameter of 50/50 mixture of beads was 4335nm which is larger than the diameter of either of them and it could be the indication of beads aggregation. To reduce the bead aggregation we added 0.1% TritonX in the solution and repeated the zeta potential measurements. However, the results were not significantly different from the experiements without TritonX into the solution. Zeta potential measurements suggest that the Zetasizer is not adequately sensitive for quantitative demonstration of number of charges per

bead. Also, Zetasizer was unable to accurately indicate the percentage of bead populations with various surface charge distributions. It can only illustrate a qualitative charge distribution on beads surface.

4.4 CONCLUSION

As we hypothesized, the detection limit of our device improved from 10 pM to 10 fM with increased DNA length. At DNA concentrations of 1 pM and 100 fM, the 110-mer target was not detectable, while longer 235-mer, 419-mer and 1613-mer targets were detectable. At 10 fM concentration, only 419-mer and 1613-mer targets generated permanent blocks. Also, these results suggest that the position of the complementary target sequence does not impair detection in our platform. Both 419- and 1613-mers, with the target sequence positioned at the middle and end of the strands, respectively, were detectable by our device at 10 fM concentration and above with no false positives. Thus, the complementary probe sequence could be chosen from any position within the nucleic acid target to obtain the highest specificity and capture efficiency. In addition to detecting target sequences in an isolated environment, we demonstrated detection in a simulated real sample with background non-complementary DNA, again with no false positives. These results suggest the potential clinical usefulness of our device to detect larger nucleic acids of length similar to 1613 bases, such as bacterial 16S rRNA. For example, given our ability to detect 1613-mer target NA at ~6×10^5 molecules/100 μL and an average of 10^4 16S rRNA per bacterial cell, our device should be capable of detecting ~60 viable bacterial cells/100 μL (~600 cells/mL), which is well below the clinically important threshold level of 10^5 viable cells/mL in urine that is indicative of infection. In the next chapter we demonstrate the capability of our

sensor to detect *E.Coli* 16S rRNA and we investigate the detection limit of our sensor based on number of cells per milliliter.

CHAPTER 5

DETECTING 16S rRNA SPECIES-SPECIFIC SEQUENCE

5.1 Introduction

A number of *E.Coli* strains are important human pathogens. For instance, *E.Coli* O157:H7 is a well-known contaminant of food and water. The *E.Coli* species alone cause 80-90% of urinary tract infections[118] and each year approximately 93.8 million illnesses and 155,000 death occur worldwide as a result of *Salmonella enteric* species infections[119,120,121].

Traditional methods for detecting the presence of pathogens in a sample entail standard clinical culture plating. After sufficient growth in a selective culture medium, the colonies are tested by PCR or ELISA for identifying the selected pathogen's genes or biomarkers. However, this procedure takes days and requires expensive reagents and bulky instrumentations. Therefore, there is a strong motivation for design and development of low-cost, robust, and portable molecular diagnostics that gives results in minutes.

Essentially, there are two options for pathogen diagnosis: detecting antigens (immunoassays) and detecting pathogen-specific nucleic acid (NA). However, no single antigen or gene sequence is sufficient to confirm an unambiguous detection of a pathogen and often time detection of multiple NA sequences or antigens are required. One of the most commonly used pathogen-specific nucleic acid targets is the 16S ribosomal RNA gene. 16S rRNA is a component of the 30S small subunit of prokaryotic ribosomes which has a role in protein synthesis and it is ~1500 nucleotides in length. The significant advantage of detecting 16S rRNA is that some regions of

it has remained unchanged in all sequenced species and therefore the 16S rRNA can be used as unique target for identifying the pathogen of interest. Besides having a "finger print" characteristics, 16S rRNA has high copy number of 71000 in a viable cell[122] which makes it a potential target for identifying pathogens by PCR-free detection schemes.

The majority of pathogen-specific 16S rRNA detection methods are based on real-time polymerase chain reaction (RT-PCR) technology with impressive detection limit in terms of colony forming units (CFUs). For instance, Yassin and Muller developed a Taq-Man based RT-PCR assay for specific detection of 2.3x 10^5 CFU/mL of *Tsukamurella* among 23 bacteria strains with closely related genes by targeting its 16S rRNA gene after 4 hrs [123]. Wang et al, used a multiplex real-time PCR assay for amplification and rapid detection of 16S rRNA of Methicillin-Resistive *Staphylococci* directly from positive blood cultures with detection limit of 10^3 CFU/mL [124]. In another study by Masek et al, a sensitive 16S rRNA Gene PCR coupled with high-resolution melt analysis was used for differentiation of Typhoidal and Nontyphoidal *Salmonella enteric* species with an impressive detection limit of ~10 CFU/mL[125]**.** Although RT-PCR assay is a powerful tool for detecting 16S rRNA gene, it requires expensive reagents and sizable instrumentation. Therefore, the need remains for development of PCR-independent technologies which has compatible detection limit to RT-PCR method.

In an effort to eliminate PCR, microarray approach has been used in several studies for detecting microbes in environmental samples such as water and soil with detection limits of approximately 10^5 cells [126] and 7.5x 10^6 cells[127]. However, the microarray technology requires labeling and optical readout. There are also few companies that have market clearance and FDA approval for PCR-free *E.Coli* NA detection. For example, AdvandX technology is base on *in situ* hybridization of a fluorophore-tagged PNA probe (PNA FISH) with *E.Coli* 16S rRNA. This

technology has high specificity and selectivity and is capable of resolving microbial population of 10^5 CFU/mL, however, it requires visualization by fluorescent microscopy. Nanosphere Verigene is another PCR-independent technology which is based on a "sandwich" type assay and gold nanoparticles for detection. This technology is capable of detecting multiple NA samples rapidly and simultaneously and it has a low detection limit of approximately 10 fM. However, it requires multiple preparation and detection steps, as well as special reagents and optics. GeneFluidics technology is also based on a "sandwich" type approach and it uses enzyme tagged and electrochemical signal transduction for detection. The detection limit of this technology is 10^4 CFU/mL and it can multiplex and gives results in minutes. However, this technique requires secondary detection probes and additional reagent. Therefore, optimally one would want to avoid the need of extra steps and reagents.

Our nanopore-based sequence-specific NA sensor has substantial potential for detecting species-specific 16S rRNA since it is PCR-independent, optical label free, and cost-effective. Also, it has a potential to be fabricated and packaged as a portable low power device. Furthermore, the size of previously detected ssDNA by our sensor (~1600 nucleotides) is in line with the length of target 16S rRNA at ~1500 nucleotides. Also, we demonstrated the detection of 10fM ssDNA against a background of non-specific genomic DNA to simulate a realistic biological application. To establish the ability of our sensor to discriminate between bacteria strains, we utilized the detection of specific sequence of 16S rRNA genome from an easily cultured non-pathogenic laboratory-strain *E.Coli* (Migula) Castellani and Chalmers (ATCC 25922). This *E.Coli* offers an attractive test system for our technology since its genome has been sequenced and studied thoroughly. Also, the optimal complementary probe sequence to its 16S rRNA has been extensively investigated by other groups[128,129,130]. Here we exhibit the performance of our sensor

for detecting the *E.Coli* (ATCC 25922) 16S rRNA by extracting the total RNA from the viable cells and investigating the detection limit of the sensor in terms of colony forming units. Also, control experiments are conducted by extracting and incubating the total RNA from non-pathogenic Pseudomonas Fluorescents Migula (ATCC 13525) and Pseudomonas Putida (Trevisan) Migula (ATCC 12633) bacteria with closely related genes to target *E.Coli*.

All bacteria were purchased from ATCC, Inc. (Manassas, VA). The detecting PNA probe sequence is NH_2-$(CH_2CH_2O)_{12}$- CTC CTT CCC TCA TTT CA. For positive control experiments, universal PNA probe: NH_2-$(CH_2CH_2O)_{12}$- CTG CCT CCC GTA GGA was used. The sequence of universal PNA probe is complementary to 15 nucleotides of all bacteria's 16S rRNA gene. The PNA detection and universal probes were conjugated to carboxylic acid functionalized 3μm diameter beads as discussed before. The zeta potential after PNA conjugated beads were measured by Zetasizer; and its value was -3.75mV after conjugating the PNA detection probe and -3.27 mV after conjugating universal PNA probes.

5.2 Sample preparation

5.2.1 Cell cultring and counting

Tryptic Soy Medium was prepared for culturing E.*Coli* (ATCC 25922) (15g Tryptic Soy Broth in 500mL DI water, pH 6.8). Nutrient Broth Medium was prepared for culturing Pseudomonas putida(ATCC 12633) and Pseudomonas fluorescens Migula (ATCC 13525) (4g Nutrient Broth in 500mL DI water, pH 6.8). All the culture medium ingredients, Soy Agar and Nutrient Agar were purchased from ATCC, Inc (Manassas, VA). After preparing the culture medium, they were autoclaved at 121°C for 20 min. Bacteria culture plates for colony counting were prepared as follow: 20gr of Nutrient Agar powder and soy Agar powder was dissolved in 250 mL DI

water and was boiled in hot plate and then autoclaved. 10mL of each solution was added into plastic petri dishes and left on a flat surface at room temperature to solidify.

Freshly purchased lyophilized *E.Coli* (ATCC 25922) was mixed with 1mL culture media (Tryptic Soy media) and diluted and incubated in 10 mL culture media and incubated at 37°C, 240 rpm to reach the log phase stage (starter culture). Then 1 mL of starter culture was diluted into 250 mL culture media and incubated at 37°C, 240 rpm to reach the log phase stage. At this stage of bacteria growth, cells are exponentially doubling and therefore there are more viable cells present compare to other stages (lag phase and stationary phase). When cells are dying, for example in stationary phase, their RNA gets enzymatically degraded by RNAses. Therefore, extracted RNA molecules from log phased cells would have better yield and integrity. To accurately culture the bacteria to the log phase stage the optical density was recorded at 600nm wavelength in 30 minutes intervals and then the culture was stopped at OD_{600} (0.4-0.6). The same procedure was repeated for other two control bacteria (ATCC 12633) and (ATCC 13525) in Nutrient Broth media at 26°C, 240rpm. Log phased cells from three different bacteria were initially diluted to 1/100 dilution by transferring 1mL of original culture to 99mL sterile saline blank. The first 10^{-2} dilution was shaken and was serially diluted in 1/10 intervals from 10^{-3} to 10^{-8}. 0.1mL of each dilution (10^{-3} to 10^{-8}) from *E.Coli* (ATCC 25922) was added to Tryptic Soy Agar plates and incubated overnight for cell counting. Same procedure was repeated for control bacteria in Nutrient Agar plates.

Simultaneously, 1mL of each dilution (10^{-2} to 10^{-8}) was prepared for RNA extraction procedure by centrifugation at 25000 x g for 15 min at 4°C. After removing the 1mL supernatant the cell pellets were immediately processed for total RNA extraction as describes below.

5.2.2 RNA extraction and purification

PureLink RNA Mini Kit, PureLink DNase Set, RNAse free water, RNAse-free pipette tips, RNAse-away reagent and RNAse-free Microfuge tubes were purchased from Invitrogen Life Technologies (Grand Island, NY). Total RNA extraction and purification was performed following PureLink RNA Mini Kit and PureLink DNase Set protocols and the total extracted RNA was eluted in 100 μL RNAse free DI water. After RNA extraction from all dilutions of bacteria, 5μL of total RNA from each sample was sent to UCLA microarray core facility for concentration and integrity measurements of the samples by Aligent 2100 Bioanalyzer.

5.2.3 Hybridization assay

High stringency hybridization condition (low salt concentration and high temperature) was used for incubating total RNA samples with PNA-beads. Prior measurements with previously used hybridization buffer (described in previous chapters) and incubation at room temperature resulted in false positive signals observation in case of negative control experiments. In other words, our device was unable to distinguish between target and control samples as a result of non-specific binding of non-complementary RNA to PNA-beads. To reduce the non-specific binding and enhance the selectivity, we used 10 mM NaCl, 25 mM Tris-HCl, pH 7.0 hybridization buffer and incubated the samples with PNA-beads at 68°C overnight. The hybridization condition was carefully chosen based on the study by Li et al. In this study PNA molecular bacons assay was sued for quantitative *D.suillum* rRNA detection with the same optimal hybridization condition[131]. Prior to hybridization, 2.1 x 10^6 PNA-beads were washed twice with wash buffer (10mM CAPSO, 0.2% [vol/vol] Tween 20, pH 10) and once with hybridization buffer (10 mM NaCl, 25 mM Tris-HCl, pH 7.0). RNA samples and PNA-beads

were re-suspended in hybridization buffer in a 100 µl reaction volume at different concentrations and incubated at 68°C overnight.

After hybridization, samples were washed twice in wash buffer and resuspended in 100µL of 1mM KCl, 10mM HEPES pH 7.0 for electrical measurements.

5.3 Results and discussion

Previously our sequence-specific NA detection platform was used to detect ~1600-mer single stranded DNA at 10fM concentration in presence of 30 pM non-complementary DNA background. Here, we investigate the capability of our device to detect non-pathogenic *E.Coli* 16S rRNA gene. The size of 16S rRNA gene is ~1500 nucleotides and its sequence has regions that are unique to the host's genome. Therefore, by detecting the unique sequence of 16S rRNA one can detect the desired bacteria strain.

To design the experiments we used three different bacteria strains: 1) target strain *E.Coli* (Migula) Castellani and Chalmers (ATCC 25922), 2) control strain1 Pseudomonas putida (ATCC 12633), 3) control starin 2 Pseudomonas fluorescens Migula (ATCC 13525). These bacteria strains were chosen based on a study by Stender et al. In this study, 16S rRNA gene of *Escherichia coli* cells in municipal water was rapidly detected by peroxidase-labeled PNA probe and chemiluminescent in situ hybridization technique [132]. They also investigated the sensitivity of two different PNA probe's sequences by dot-blot hybridization to RNA of eight species and concluded that one of the probe sequences has better sensitivity for *E.Coli* 16S rRNA. In our study we used the same sensitive 17-mer PNA probe sequence as a detection probe. For positive control we used the 15-mer universal PNA probe sequence which is complementary to all three bacteria 16S rRNA and has been used by other groups for detecting *E.Coli*[133].

The first set of experiments was intended to investigate the LOD of our sensor based on the concentration of 16S rRNA samples. To assess the LOD of our system, extracted RNA samples were quantified and inspected by Bioanalyzer 2100 instrument and then were serially diluted and measured by our sensor.

The Bioanalyzer measures RNA concentration, size, and integrity number using On-Chip Gel Electrophoresis technique. The concentration of total RNA extracted from target *E.Coli* was 364 ng/µl and the percentage of 16S rRNA was 18.2% of total RNA. Therefore, the calculated concentration of 16S rRNA was 66.248 ng/µl. Using approximate molecular weight of 1500-mer ssRNA (480909 g/mol), concentration of 16S rRNA was calculated in terms of mole per liter to be 137.8 nM. Bioanalyzer measured the size of 16S rRNA to be ~ 1,494 to 1,924 nucleotides. Also, the RNA integrity number of extracted sample was 9.2 (10 represents highest integrity and 0 represents lowest integrity) based on evaluation of the 23S and 16S ribosomal ratios by the Bionalayzer.

Same measurements and calculations were conducted for extracted RNA from two control bacteria. In case of the control1bacteria (ATCC 12633), total RNA concentration was reported as 449 ng/µl and the percentage of 16S rRNA was 25.7%. The size of the 16S rRNA was reported to be ~1260 to 1914 nucleotides and the RNA integrity number was 10. The calculated 16S rRNA concentration was 239nM.

Total RNA concentration of the control 2 (ATCC 13525) was 261ng/µl and the percentage of 16S rRNA was 24.5%. The size of 16S rRNA was between 1294 and 1984 nucleotides and the RNA integrity number was 10. We calculated the 16S rRNA concentration to be 133nM (Figure5.1).

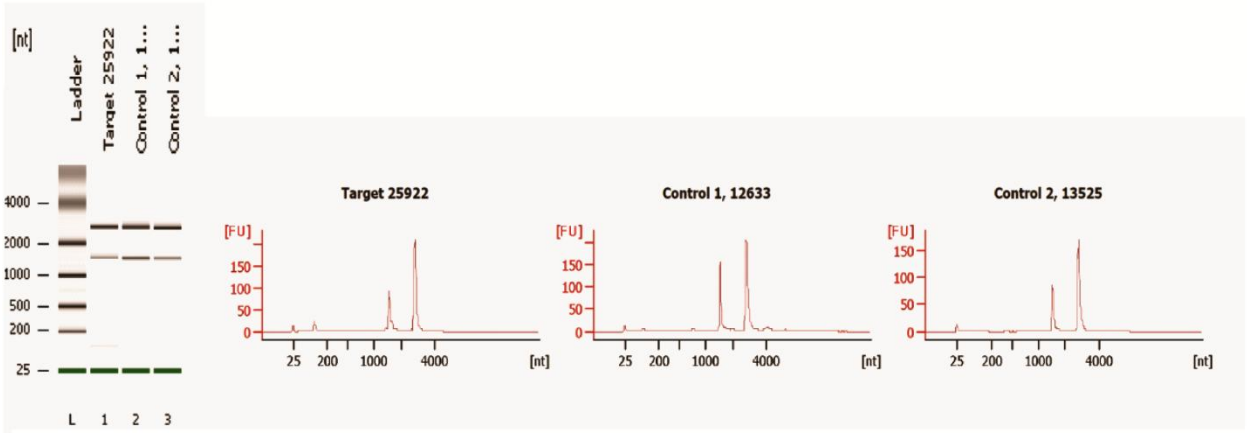

Figure 5.1 Illustrate the chip-gel electrophoresis analysis of target and 2 control bacteria using Bionalyzer 2100. Fluorescent unit versus RNA nucleotides were plotted for 3 samples. The first peack on each graph represents the 16S rRNA and the second peak represents 23S rRNA. When 16S rRNA peak is smaller than the 23S rRNA peak the integrity of RNA is high (around 10).

Following the RNA analysis, extracted RNA from target and control samples were serially diluted based on their 16S rRNA concentrations from 10nM to 1fM and hybridized separately with 2.1 x 10^6 detecting and universal PNA-beads in high stringency condition. The experiments conducted with 10nM and 100pM 16S rRNA samples were hybridized for only 2 hours prior to conductance measurements by our sensor. However, the 10pM 16S rRNA target hybridized for 2 hours with PNA-beads was not detectable by our sensor. This could be the result of insufficient incubation time for PNA-beads to hybridize with RNA molecules at lower concentration and therefore increasing the hybridization duration restored this complication. The hybridization duration was expanded to overnight in case of 10pM to 1fM 16S rRNA experiments and table 5.1 shows the result of the 10pM to 1fM experiments.

Table5.1 Summary of Detection results for target and control samples based on their 16S rRNA concentration. A positive result indicates a blockade measured for > 60 seconds that was reversible. A negative result is indicated when no block or a transient block (<60 sec) was observed.

	Target *E.Coli* (ATCC 25922)		Control bacteria 1 (ATCC 12633)		Control bacteria 2 (ATCC 13525)	
[16S rRNA]	Detection?	Positive control?	Detection?	Positive control?	Detection?	Positive control?
10 pM Expt. 1	Yes	Yes	No*	Yes	No	Yes
10 pM Expt. 2	Yes	Yes%	No	Yes	No	Yes
10 pM Expt. 3	Yes	Yes	No	Yes	No*	Yes
1 pM	Yes	Yes	No	Yes	No	Yes
100 fM	Yes	Yes	No	Yes	No	Yes
10 fM Expt. 1	Yes	Yes	No	Yes	No	Yes
10 fM Expt. 2	Yes	Yes	No	Yes	No	Yes
10 fM Expt. 3	Yes	Yes	No	Yes	No	Yes
1 fM	No	No	No	No	No	No

* Transient block observed

% Transient block observed, followed by permanent block

Our device detected 10pM 16S rRNA of target *E.coli* in three separate experiments. No false positive or negative was observed in these experiments and only few transient blocks were obtained in case of control experiments. Moreover, 1pM and 100fM 16S rRNA of target was detected by the sensor with no false positive and negative. 10fM 16S rRNA of target sample was detected in three separate experiments with no false positive or negative. However, in case of 1fM no detection was observed with detection and universal PNA-beads. Therefore, the concentration detection limit of our sensor for detecting the 16S rRNA is 10fM. This limit is

consistent with the LOD of detecting 1600-mer ssDNA which was previously illustrated by our sensor. In all these experiments, fewer transient blockades were observed compare to previous experiments by the sensor for detecting ssDNAs. This could be the result of hybridization of RNA samples at high stringency condition. The high stringency hybridization condition reduces the non-specific binding of non-complementary RNA samples to PNA-beads and therefore fewer beads with non-specifically bound RNA could reach the sensing zone to block the pore temporarily.

Although the detection limit of our sensor was established in terms of molar concentration of 16S rRNA, we intend to investigate the detection limit in terms of cell numbers (colony forming units (CFU)). In order to exhibit the detection limit base on CFU/mL, bacteria cells were counted at different dilutions and RNA samples were extracted from the corresponding cell dilutions.

The initial attempt was to quantify the original number of cells prior to dilutions in order to roughly estimate the dilution factors and to measure the concentration of 16S rRNA extracted from the original cultured cells. Therefore, after cells were cultured to the log phase, 1mL of the sample was used for RNA extraction and 0.1mL of it was used for counting. We counted the number of *E.Coli* cells to be 2 x 10^9 CFU/ml and the concentration of extracted RNA was 430ng/µl. The RNA integrity number was 9.4, the percentage of 16S rRNA was 15.2%, and therefore the calculated 16S rRNA concentration was 137.7 nM. This value is consistent with our previous calculation of 16S rRNA (137.8 nM) from approximately the same number of cells. Since the original number of cells in culture was ~ 10^9 CFU/ml, in the next set of experiments we roughly estimated the dilution factors in order to extract RNA from ~10^6 to 10^3 CFU/ml. The procedure of these experiments is as follow: cells were cultured to log phase stage and the original cell culture was diluted 1/100 and plated. 10^{-2} dilution was also serially diluted 4 times in

10^{-1} intervals and cells from each dilution were plated and counted the next day. Simultaneously, 1mL of each dilution was centrifuged down for RNA extraction. Number of cells from original culture was counted to be 3.5x 10^8 CFU/mL and therefore the number of cell after 10^{-2} dilution was 3.5x 10^6 CFU/mL , 3.5x 10^5 CFU/mL after 10^{-3} dilution, and so on. The total RNA extraction from 3.5x 10^6 CFU/mL cells (10^{-2} dilution) was 167pg/µl, the percentage of 16S rRNA was 28.2% and the RNA integrity number was 10. The calculated concentration of 16S rRNA was 98pM. However, the concentration of extracted RNA from 3.5x 10^5 CFU/mL, 3.5x 10^4 CFU/mL, and 3.5x 10^3 CFU/mL were below the concentration detection limit (~50 pg/µl) of the Bioanalyzer instrument and therefore we couldn't calculate the concentration of 16S rRNA from those dilutions.

10µL of extracted total RNAs from 3.5x 10^5 CFUs, 3.5x 10^4 CFUs, and 3.5x 10^3 CFUs were hybridized separately with detection and universal PNA-beads suspended in 90µl of hybridization buffer in total volume of 100µl overnight. After the hybridization and samples were resuspended in 1mM KCl and 100µL of each sample was utilized by our sensor to investigate the CFU detection limit. For negative control experiments, same procedure was repeated for two control bacteria; their original number of cells was counted to be 1.02 x 10^8 CFU/mL for ATCC 12633 and 1.1x 10^8 CFU/mL for ATCC 13252.

Table5.2 summarizes the experimental results and each experiment was repeated 3 times (n=3).

Table 5.2. Summary of Detection results for target and control samples based on CFU. A positive result indicates a blockade measured for > 60 seconds that was reversible. A negative result is indicated when no block or a transient block (<60 sec) was observed.

Target *E.Coli* (ATCC 25922)			Control bacteria 1 (ATCC 12633)			Control bacteria 2 (ATCC 13525)		
CFU	Detection ?	Positive control?	CFU	Detection ?	Positive control?	CFU	Detection ?	Positive control?
$3.5x\ 10^5$	Yes	Yes	$1.0x\ 10^5$	No	Yes	$1.1x\ 10^5$	No	Yes
$3.5x\ 10^5$	Yes	Yes	$1.0x\ 10^5$	No	Yes	$1.1x\ 10^5$	No	Yes
$3.5x\ 10^5$	Yes	Yes	$1.0x\ 10^5$	No	Yes	$1.1x\ 10^5$	No	Yes
$3.5x\ 10^4$	Yes	Yes	$1.0x\ 10^4$	No	Yes	$1.1x\ 10^4$	No	Yes
$3.5x\ 10^4$	Yes	Yes	$1.0x\ 10^4$	No	Yes	$1.1x\ 10^4$	No	Yes
$3.5x\ 10^4$	Yes	No	$1.0x\ 10^4$	No	Yes	$1.1x\ 10^4$	No	Yes
$3.5x\ 10^3$	No	No	$1.0x\ 10^3$	No	No	$1.1x\ 10^3$	No	No
$3.5x\ 10^3$	Yes	Yes	$1.0x\ 10^3$	Yes	Yes	$1.1x\ 10^3$	No	Yes
$3.5x\ 10^3$	No	No	$1.0x\ 10^3$	No	Yes	$1.1x\ 10^3$	No	No

As the results indicated, we could successfully detect $3.5x\ 10^5$ CFUs of target *E.Coli* and we observed no false positive or false negative during these experiments. Also, $3.5x\ 10^4$ CFUs were detected by our sensor with no false positive in all three attempts. However, one false negative was obtained in case of detecting target *E.Coli* incubated with universal PNA-beads. No transient blockade was observed by any of the samples as a result of high stringency hybridization condition as we discussed above.

However, in case of samples extracted 16S rRNA sample from $3.5x\ 10^3$ CFUs of target *E.Coli,* only one current block was obtained out of 3 attempts. Also, in one experiment out of three trial false positives were observed in case of detecting $1.0x\ 10^3$ CFUs from Control1 bacteria. Moreover, the positive control using the universal PNA-probe was unsuccessful in the majority of the experiments. These unexpected detection results suggest that the sensor is unable to detect $3.5x\ 10^3$ CFUs and therefore the detection limit of the sensor is $3.5x\ 10^4$ CFUs.

To compare this CFU detection limit with the 10fM 16S rRNA detection limit, we calculated the equivalent number of cells that can be harvest to extract 10fM 16S rRNA in 100µL. Assuming 100% extraction yield and 71000 16S rRNA copy number per cell, the calculated number of cells is ~8. However, experimental results show that the RNA extraction yield was reduced significantly as cells were serially diluted. We calculated the percentage of the RNA extraction yield from 2x 10^9 CFU/mL original culture to be 57.4%. Also, we calculated 16S rRNA copy number per cell after extraction from 2x 10^9 CFUs as follow:

(137.7x10^{-9} 16S rRNA mole/L)/(2x10^9 CFU/mL)= 68.85x10^{-21} mole/CFU

(68.85x10^{-21} mole/CFU)* (6.02x10^{23} number/mole)= (41447.7 number of 16S rRNA/CFU)

However, as cells were diluted 1000 folds the calculated yield was reduced to 23.3% and the number of extracted 16S rRNA per cell was ~17000. This reduction in RNA extraction yield as a function of cell dilutions can justify the higher 3.5x 10^4 CFU detection limit of our sensor in comparison to the calculated 8 CFU detection limit.

The 3.5x 10^4 CFU detection limit is an acceptable range for detecting some pathogens. For instance, a laboratory finding of $\geq 10^5$ CFU/mL in a urine sample generally is accepted as an indicator of infection[134] and the detection limit of our sensor is below the threshold level of 10^5 viable cells/mL. Therefore, our device has a potential application in detecting pathogens in urine.

CHAPTER 6

CONCLUSION AND FUTURE WORK

6.1 Summary

Ultrasensitive, rapid, and cost-effective sequence-specific detection of nucleic acids (NA) is of great significance for pathogen detection, medical diagnostics, drug discovery, and forensic investigations. Many strategies and technologies with high sensitivity and specificity have been developed for NA detection using optical, mechanical, electrochemical and magnetic signal transduction. However, many of these platforms require amplification by polymerase chain reaction, fluorescent or enzymatic labels and expensive instrumentation.

We designed and developed a binary-mode, PCR-independent, optics-free, and potentially low-cost device for sequence-specific NA detection based on conductance measurement of a pore electrophoretically blocked by bead-PNA probe conjugates hybridized with target nucleic acids. The main element of the sensor operation design is PNA probes. In PNA, the negatively charged phosphodiester backbone of DNA/RNA is replaced with repetitive uncharged units of N-(2-aminoethyl) glycine to which the bases are attached with a methyl carbonyl linker, thus enabling the construction of charge-neutral probe-bead conjugates[135]. Introduction of complementary target nucleic acid to these neutrally-charged PNA-bead conjugates resulted in sequence-specific binding of single-stranded DNA or RNA to the PNA, imparting negative charge to the assembly thereby making it electrophoretically mobile. Following placement of these bead conjugates with hybridized target in a conical capillary with tip diameter smaller than the bead diameter, the

beads were electrophoretically driven toward the capillary tip, blocking it and producing a large, easily measureable, and persistent change in electrical current.

In an initial proof of concept study, we showed the proposed sensor operates based on electrophoretic mobility of charged particles. To do so, we utilized two types of charged polystyrene spheres (derivatized carboxylate and derivatized amine) in our detection scheme. At neutral pH and low ionic strength, carboxylic acid beads are negatively charge and under applied electric field they were driven toward the pore and significantly decreased the ionic current across the pore. When switching the polarity of applied voltage, same result was observed in case of positive amine particles. However, in acidic condition, carboxylic acid beads were protonated and were immobile under the applied electric field. Therefore, the current across the pore was not altered. Same result was obtained when amine particles were deprotonated under basic condition. These experiments illustrated that the detection scheme is dependent on particles electric charge.

Following the charged dependency proof of concept, nucleic acid detection was demonstrated using 20-mer PolyA ssDNA as a simple target sequence which hybridized to 12-mer PNA probe conjugates to carboxylic acid beads. Permanent current reduction across the pore was acquired when a target ssDNA-PNA-bead complex blocked the pore. In case of control experiment with non-complementary 20-mer ssDNA (PolyA), no current block or transient blocks were observed as a result of opposing electroosmosis flow. Therefore no false positive was reported in control experiments.

To investigate the selectivity and sequence specificity of the sensor; a 12-mer non-repeating sequence of a gene encoding the anthrax lethal factor was detected as a target oligomer and sequence specificity of the sensor was explored using the anthrax lethal factor with a single-base

mismatch as a control experiment. The sensor showed high sequence specificity by distinguishing between target anthrax lethal factor and control oligomers with single nucleotide polymorphism. In all these experiments the performance of the sensor was as expected with no false positive or false negative response. The concentration detection limit of the sensor for detecting 20-mer ssDNA was reported to be 10pM.

Next we demonstrated the operation of our device with longer DNA strands to reach lower concentration detection limit since there are more charge to the bead per bound DNA strand as the length of the hybridizing DNA increases. We examined the detection of target DNA oligomers of 110, 235, 419, and 1613 nucleotides at 1pM to 1fM concentrations, and finding that the detectable concentration limit decreased as DNA length increased, with 419 and 1613 nucleotide oligomers detectable down to 10 fM. In addition, no false positive responses were obtained with non-complementary, control DNA fragments for similar length. Moreover, since the target sequence positioned at the middle and the end of 419-mer and 1613-mer strand respectively, the complementary probe sequence could be chosen from any position of the nucleic acid sample and therefore the position of the complementary target sequence does not impair detection in our platform. Also, to show the sensor's potential effectiveness to detect biological NA samples with long nucleotide sequences, we successfully detected target fragments at 10 fM concentration against a DNA background simulating the non-complementary genomic DNA present in real sample.

Finally we demonstrated the application of our device for detecting clinically relevance gene such as portion of *E.Coli* 16S rRNA sequence. The detection of species-specific 16S rRNA is commonly used to inform the microbial species in environment and clinical samples. 16S rRNA gene of non-pathogenic *E.Coli* (ATCC 25922) was used as target NA molecule and the 16S

rRNA of two non-pathogenic Pseudomonas putida(ATCC 12633) and Pseudomonas fluorescens Migula (ATCC 13525) bacteria, with closely related gene sequence to target strain, were used as negative control experiments. For positive control experiment, we used PNA-beads conjugates with sequence complementary to all 16S rRNA bacteria. The conductance measurement results showed the species-specific 16S rRNA detection at 10fM detection limit. Also, we demonstrated the detection limit of our sensor in terms of colony forming unit (CFU) to be $3.5x\ 10^4$ CFU. This detection limit is below the threshold concentration limit for detecting the pathogenic *E.Coli* in urine and therefore our device has a potential to be used for detecting the clinically significant pathogens.

In brief, we have developed a binary-mod, PCR-free, optical label free sequence-specific NA detection based on nanopore sensing concept. The sensor mechanically amplifies the signal by relatively large microsphere probe substrate and it has high selectivity and sequence specificity with low clinically significant concentration detection limit. This sequence-specific NA detection platform is cost effective and is easy to operate. Also, it has the capability to detect large nucleic acid oligomers (~1600 nt) at low concentration of 10 fM in presence of non-complementary background genome. Last but not least, this biosensor demonstrated the ability to detect species-specific 16S rRNA gene at meaningful $3.5x\ 10^4$ CFU detection limit.

6.2 Future work

Although the proposed biosensor has substantial properties, it can be improve to become a rapid, portable, compact point-of-care molecular diagnostic device with potentially single molecule detection sensitivity and ability to multiplex. To ultimately reach these criteria and enhance the performance of this technology following future works are suggested.

Device Scale-Down

Scaling-down the device has several advantages such as suitability for multiplexing, faster analysis time and lower concentration detection limits. The lowest detection limits would be achievable if just one or a few target NAs hybridized to a PNA-bead conjugate would make it sufficiently mobile in an electric field to travel toward the lower potential and block the pore permanently. This can be achieved by using beads with smaller diameter and consequently using smaller pore size. To justify the above statement following mathematical relationships can be used: A well-known relationship for electrophoretic mobility, *m* has direct proportionality to diffusivity *D* (Equation 16).

$$m = \frac{D\ z\ F}{RT} \tag{15}$$

On the other hand Diffusivity is inversely proportional to the particle's diameter as shown in equation 17.

$$D = \frac{kT}{3\pi\mu d} \tag{15}$$

Where *k* is Boltzmann's constant, μ is fluid viscosity and *d* is the diameter of particle.

Therefore bead's mobility will increase as its diameter decreases for constant number of bound NA molecule after hybridization. Thus, it would seem that smaller beads would facilitate achievement of lower detection limit. Also, at a constant applied electrophoretic force, the smaller beads have better mobility and therefore, it would travel faster to the sensing zone

compare to the large bead. As a result reducing the bead size and the pore diameter would enhance the detection and analysis time.

The device scale down can be achieved by micromachining silicon-supported silicon nitride (SiN) membrane with single nanometer-to micron-scale-tapered pores.

Integration with microfluidic channels

In order to create a portable and point-of-care (POC) device, micromachined nanopore sensors can be integrated with microfluidic technology. This device can perform the "front end" operations of sample introduction, cell lysis, NA separation and NA hybridization to PNA-bead conjugates as illustrated in figure 6.1.

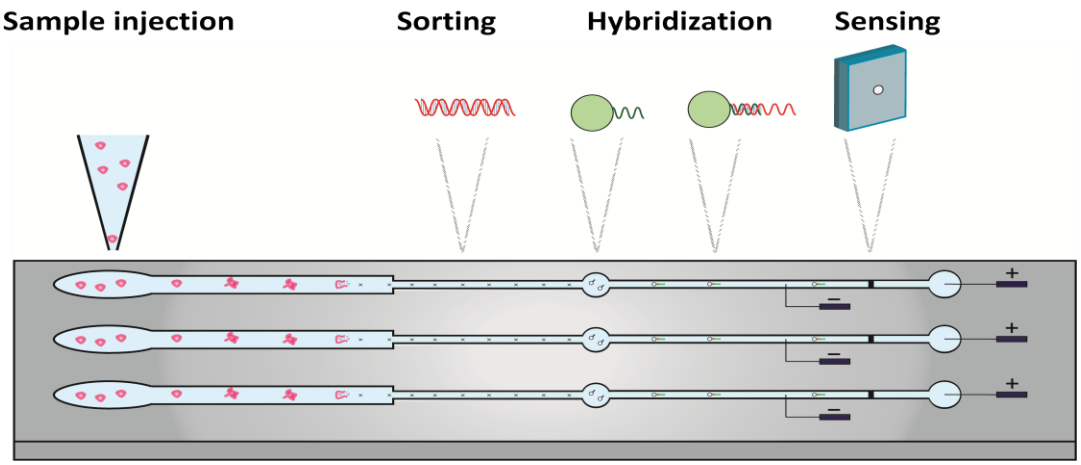

Figure 6.1. Schematic of integrated microfluidic channels with nanopore sensor for "front end" operation and multiplexing.

Microfluidic channels will improve the volumetric limitation of sample preparation, sorting, and hybridization steps. The small incubation volume in channels can enhance the hybridization rate of target NA with complementary PNA-beads which results in faster analysis time. It can

potentially improve the concentration detection limit of the sensor by restoring the small number of samples in preparation steps prior to detection. Moreover, it gives faster analysis time as a result of shorter travel distance to the sensing zone. Also, high-throughput screening can be achieved by combining the microchannels with nanopores.

Probe surface concentration

The probe surface concentration on beads has proved to be an important variable to optimize the sensor sensitivity. A probe concentration that is too high decreases target NA hybridization to PNA-beads conjugates due to electrostatic repulsion and steric hindrance between NA molecules. On the other hand, a low probe concentration reduces the sensor's sensitivity. Studies showed an optimal probe concentration of 10^{12}-10^{13}/cm^2 for flat surface[136]. In the work described in this thesis we saturated the surface of beads with PNA probes. However, the device sensitivity might be enhanced by systematic probe conjugation to beads and quantitatively investigate the probe concentration on the beads.

Device surface chemistry

In order to improve the wettability of the membrane surface, to reduce the nonspecific adsorption, and eliminate the charges on the surface of Si/SiN membrane, we can condition the surface with surface chemistry techniques to reach the optimal surface charge distribution. Si surfaces are expected to be oxidized and to present surface –OH groups in aqueous solution. These –OH groups have the tendency to deprotonate in water and becoming negatively charged. This negative charged surface enhances the opposing electroosmosis flow as previously discussed, which could have a negative effect on sensor operation and detection of target NA-PNA-bead complex. On the other hand, we have shown that the electroosmosis flow is needed to

some extend for removing beads with weakly bound non-complementary NA from the pore. Therefore, the surface charge can be manipulated to reach an optimal electroosmosis flow. For instance, one can enhance the electroosmosis flow by further oxidizing the surface with oxygen plasma to create more negative charges on the Si surface or to reduce the osomosis flow by silanizing the surface with a PEGsilane to cap the surface charges.

REFERENCES

(1) Walker, J. M. *Application of microfluids for molecular diagnostics*; **2013**; pp. 305–334.

(2) Sanger, F.; Air, G.M.; Barrell, B.G.; Brown, N.L.; Coulson, A.R.; Fiddes, J.C.; Hutchison III C.A.; Slocombe, P.M.; Smith, M. *nature* **1977**, *265*, 687–695.

(3) Chee, M.; Yang, R.; Hubbell, E.; Berno, A.; Huang, X. C.; Stern, D.; Winkler, J.; Lockhart, D. J.; Morris, M. S.; Fodor, S. P. *Science (New York, N.Y.)* **1996**, *274*, 610–4.

(4) Maitra, A.; Cohen, Y.; Gillespie, S. E. D.; Mambo, E.; Fukushima, N.; Hoque, M. O.; Shah, N.; Goggins, M.; Califano, J.; Sidransky, D.; Chakravarti, A. *Genome research* **2004**, *14*, 812–9.

(5) Lubin, A. a; Lai, R. Y.; Baker, B. R.; Heeger, A. J.; Plaxco, K. W. *Analytical chemistry* **2006**, *78*, 5671–7.

(6) Lam, B.; Fang, Z.; Sargent, E. H.; Kelley, S. O. *Analytical chemistry* **2012**, *84*, 21–5.

(7) Carey, L.; Mitnik, L. *Electrophoresis* **2002**, *23*, 1386–97.

(8) Hahn, S.; Mergenthaler, S.; Zimmermann, B.; Holzgreve, W. *Bioelectrochemistry (Amsterdam, Netherlands)* **2005**, *67*, 151–4.

(9) Teles, F.; Fonseca, L. *Talanta* **2008**, *77*, 606–623.

(10) Ferguson, J.A.; Boles, T.C.; Adams, C.P.; Walt, D.R.; *Nature biotechnology* **1996,** *14*, 1681-1684.

(11) Yin, M.; Wu, C.; Shao, L.; Chan, W. K. E.; Zhang, a P.; Lu, C.; Tam, H. *The Analyst* **2013**, *138*, 1988–94.

(12) Buhl, A.; Metzger, J. H.; Heegaard, N. H. H.; von Landenberg, P.; Fleck, M.; Luppa, P. B. *Clinical chemistry* **2007**, *53*, 334–41.

(13) Sípová, H.; Zhang, S.; Dudley, A. M.; Galas, D.; Wang, K.; Homola, J. *Analytical chemistry* **2010**, *82*, 10110–5.

(14) Campbell, C. T.; Kim, G. *Biomaterials* **2007**, *28*, 2380–92.

(15) Space, N.; Foundation, G.; Field, M.; Cruz, S. *current opinion in chemical and biology* **2002**, *6*, 816–822.

(16) Nam, J.-M.; Stoeva, S. I.; Mirkin, C. a *Journal of the American Chemical Society* **2004**, *126*, 5932–3.

(17) Kalidasan, K.; Neo, J. L.; Uttamchandani, M. *Molecular bioSystems* **2013**, *9*, 618–21.

(18) Lie, P.; Liu, J.; Fang, Z.; Dun, B.; Zeng, L. *Chemical communications (Cambridge, England)* **2012**, *48*, 236–8.

(19) Liu, J.; Chen, L.; Lie, P.; Dun, B.; Zeng, L. *Chemical communications (Cambridge, England)* **2013**, *49*, 5165–7.

(20) He, S.; Liu, D.; Wang, Z.; Cai, K.; Jiang, X. *Science China Physics, Mechanics and Astronomy* **2011**, *54*, 1757–1765.

(21) Feng, C.-L.; Zhong, X. H.; Steinhart, M.; Caminade, a.-M.; Majoral, J.-P.; Knoll, W. *Advanced Materials* **2007**, *19*, 1933–1936.

(22) Giri, S.; Sykes, E. a; Jennings, T. L.; Chan, W. C. W. *ACS nano* **2011**, *5*, 1580–7.

(23) Zhang, C.-Y.; Yeh, H.-C.; Kuroki, M. T.; Wang, T.-H. *Nature Materials* **2005**, *4*, 826–831.

(24) Drbohlavova, J.; Adam, V.; Kizek, R.; Hubalek, J. *International journal of molecular sciences* **2009**, *10*, 656–73.

(25) Zhang, L.; Li, D.; Meng, W.; Huang, Q.; Su, Y.; Wang, L.; Song, S.; Fan, C. *Biosensors & bioelectronics* **2009**, *25*, 368–72.

(26) Lee, J.-G.; Yun, K.; Lim, G.-S.; Lee, S. E.; Kim, S.; Park, J.-K. *Bioelectrochemistry (Amsterdam, Netherlands)* **2007**, *70*, 228–34.

(27) Xiong, H.; Zheng, X. *The Analyst* **2014**, *139*, 1732–9.

(28) Zhou, H.; Liu, J.; Xu, J.-J.; Chen, H.-Y. *Chemical communications (Cambridge, England)* **2011**, *47*, 8358–60.

(29) Schutzbank, T.E.; Smith, J. *Journal of Clinical Microbiology* **1995**, *33*, 2036-2041.

(30) Hoheisel, J. D. *Nature reviews. Genetics* **2006**, *7*, 200–10.

(31) Wang, L.; Li, P. C. H. *Analytica chimica acta* **2011**, *687*, 12–27.

(32) Abdullah-Sayani, A.; Bueno-de-Mesquita, J. M.; van de Vijver, M. J. *Nature clinical practice. Oncology* **2006**, *3*, 501–16.

(33) O'Sullivan, C. K.; Guilbault, G. G. *Biosensors and Bioelectronics* **1999**, *14*, 663–670.

(34) Chen, S.-H.; Wu, V. C. H.; Chuang, Y.-C.; Lin, C.-S. *Journal of microbiological methods* **2008**, *73*, 7–17.

(35) Dell'Atti, D.; Tombelli, S.; Minunni, M.; Mascini, M. *Biosensors & bioelectronics* **2006**, *21*, 1876–9.

(36) Dell'Atti, D.; Zavaglia, M.; Tombelli, S.; Bertacca, G.; Cavazzana, A. O.; Bevilacqua, G.; Minunni, M.; Mascini, M. *Clinica chimica acta; international journal of clinical chemistry* **2007**, *383*, 140–6.

(37) Thompson, M.; Kiplingt, A. L.; Duncan-hewitts, W. C. *Analyst* **1991**, *116*.

(38) Xu, Q.; Chang, K.; Lu, W.; Chen, W.; Ding, Y.; Jia, S.; Zhang, K.; Li, F.; Shi, J.; Cao, L.; Deng, S.; Chen, M. *Biosensors & bioelectronics* **2012**, *33*, 274–8.

(39) Sakong, J.; Roh, H.; Roh, Y. *Japanese Journal of Applied Physics* **2007**, *46*, 4729–4733.

(40) Janshoff, a; Galla, H.; Steinem, C. *Angewandte Chemie (International ed. in English)* **2000**, *39*, 4004–4032.

(41) Yang, M.; Thompson, M.; Ms, O.; Duncan-hewitt, W. C. *langmuir* **1993**, 802–811.

(42) Hansen, K. M.; Thundat, T. *Methods (San Diego, Calif.)* **2005**, *37*, 57–64.

(43) Fritz, J. *Science* **2000**, *288*, 316–318.

(44) Hansen, K. M.; Ji, H.; Wu, G.; Datar, R.; Cote, R.; Majumdar, A.; Thundat, T. **2001**, *73*, 1567–1571.

(45) Ilic, B.; Yang, Y.; Aubin, K.; Reichenbach, R.; Krylov, S.; Craighead, H. G. *Nano letters* **2005**, *5*, 925–9.

(46) Hwang, K. S.; Lee, S.-M.; Kim, S. K.; Lee, J. H.; Kim, T. S. *Annual review of analytical chemistry* **2009**, *2*, 77–98.

(47) Walter, A.; Surkus, A.-E.; Flechsig, G.-U. *Analytical and bioanalytical chemistry* **2013**, *405*, 3907–11.

(48) Alfonta, L.; Singh, a K.; Willner, I. *Analytical chemistry* **2001**, *73*, 91–102.

(49) Cao, W.; Su, M.; Zhang, S. *Electrophoresis* **2010**, *31*, 659–65.

(50) Wang, C.; Zhou, H.; Zhu, W.; Li, H.; Jiang, J.; Shen, G.; Yu, R. *Biosensors & bioelectronics* **2013**, *47*, 324–8.

(51) Ju, H.; Ye, B.; Gu, J. *Sensors* **2004**, *4*, 71–83.

(52) Takenaka, S.; Yamashita, K.; Takagi, M.; Uto, Y.; Kondo, H. *Analytical chemistry* **2000**, *72*, 1334–41.

(53) Hashimoto, K.; Ito, K.; Ishimori, Y. *Analytical chemistry* **1994**, *66*, 3830–3.

(54) Guiducci, C.; Stagni, C.; Zuccheri, G.; Bogliolo, A.; Benini, L.; Samorì, B.; Riccò, B. *IEEE* **2002**, 3–6.

(55) Hassen, W. M.; Chaix, C.; Abdelghani, A.; Bessueille, F.; Leonard, D.; Jaffrezic-Renault, N. *Sensors and Actuators B: Chemical* **2008**, *134*, 755–760.

(56) Bangar, M. a.; Shirale, D. J.; Purohit, H. J.; Chen, W.; Myung, N. V.; Mulchandani, A. *Electroanalysis* **2011**, *23*, 371–379.

(57) Fan, Y.; Chen, X.; Trigg, A. D.; Tung, C.; Kong, J.; Gao, Z. *Journal of the American Chemical Society* **2007**, *129*, 5437–43.

(58) Gao, Z.; Agarwal, A.; Trigg, A. D.; Singh, N.; Fang, C.; Tung, C.-H.; Fan, Y.; Buddharaju, K. D.; Kong, J. *Analytical chemistry* **2007**, *79*, 3291–7.

(59) Gao, Z.; Agarwal, A.; Trigg, A. D.; Singh, N.; Fang, C.; Tung, C.-H.; Fan, Y.; Buddharaju, K. D.; Kong, J. *Analytical chemistry* **2007**, *79*, 3291–7.

(60) Koh, I.; Josephson, L. *Sensors (Basel, Switzerland)* **2009**, *9*, 8130–45.

(61) Nasirpouri, F.; Nogaret, A. *Nanomagnetisim and Spintronics* **2008**.

(62) Gabig-Ciminska, M.; Holmgren, a; Andresen, H.; Bundvig Barken, K.; Wümpelmann, M.; Albers, J.; Hintsche, R.; Breitenstein, a; Neubauer, P.; Los, M.; Czyz, a; Wegrzyn, G.; Silfversparre, G.; Jürgen, B.; Schweder, T.; Enfors, S.-O. *Biosensors and Bioelectronics* **2004**, *19*, 537–546.

(63) Mulvaney, S. P.; Cole, C. L.; Kniller, M. D.; Malito, M.; Tamanaha, C. R.; Rife, J. C.; Stanton, M. W.; Whitman, L. J. *Biosensors & bioelectronics* **2007**, *23*, 191–200.

(64) Alegret, S.; Aldavert, M.; Mar, S. *TrAC Trends in Analytical Chemistry* **2005**, *24*, 341–349.

(65) Lin, C.; Zhang, Y.; Zhou, X.; Yao, B.; Fang, Q. *Biosensors & bioelectronics* **2013**, *47*, 515–9.

(66) Ma, W.; Yin, H.; Xu, L.; Wang, L.; Kuang, H.; Xu, C. *Chemical communications (Cambridge, England)* **2013**, *49*, 5369–71.

(67) Lee, W.-C.; Lien, K.-Y.; Lee, G.-B.; Lei, H.-Y. *Diagnostic microbiology and infectious disease* **2008**, *60*, 51–8.

(68) Coulter, W.H.; *coulter counter***1953**.

(69) Steinkamp, J. a. *Review of Scientific Instruments* **1973**, *44*, 1301.

(70) Deblois, R A L P H W and Bean, C. P. *Journal of Colloid and Interface science* **1977**, *61*, 323–335.

(71) Kasianowicz, J. J.; Brandin, E.; Branton, D.; Deamer, D. W. *Proceedings of the National Academy of Sciences of the United States of America* **1996**, *93*, 13770–3.

(72) Venkatesan, B. M.; Bashir, R. *Nature Nanotechnology* **2011**, *6*, 615–624.

(73) Saleh, O. A.; Sohn, L. L. *Nano Letters* **2003**, *3*, 37–38.

(74) Shendure, J.; Ji, H. *Nature biotechnology* **2008**, *26*, 1135–45.

(75) Keyser, U. F. *Journal of the royal society interface* **2011,** *9*, 1-10.

(76) Luan, B.; Stolovitzky, G.; Martyna, G. *Nanoscale* **2012**, *4*, 1068–77.

(77) Rosenstein, J.; Ray, V.; Drndic, M.; Shepard, K. L. *2011 IEEE/NIH Life Science Systems and Applications Workshop (LiSSA)* **2011**, 59–62.

(78) Manrao, E. a; Derrington, I. M.; Laszlo, A. H.; Langford, K. W.; Hopper, M. K.; Gillgren, N.; Pavlenok, M.; Niederweis, M.; Gundlach, J. H. *Nature biotechnology* **2012**, *30*, 349–53.

(79) Kowalczyk, S. W.; Wells, D. B.; Aksimentiev, A.; Dekker, C. *Nano letters* **2012**, *12*, 1038–44.

(80) Rosenstein, J. K.; Wanunu, M.; Merchant, C. a; Drndic, M.; Shepard, K. L. *Nature methods* **2012**, *9*, 487–92.

(81) Singer, A.; Wanunu, M.; Morrison, W.; Kuhn, H.; Frank-Kamenetskii, M.; Meller, A. *Nano letters* **2010**, *10*, 738–42.

(82) Balagurusamy, V. S. K.; Weinger, P.; Ling, X. S. *Nanotechnology* **2010**, *21*, 1–9.

(83) Howorka, S.; Cheley, S.; Bayley, H. *Nature biotechnology* **2001**, *19*, 636–9.

(84) Benner, S.; Chen, R. J. a; Wilson, N. a; Abu-Shumays, R.; Hurt, N.; Lieberman, K. R.; Deamer, D. W.; Dunbar, W. B.; Akeson, M. *Nature nanotechnology* **2007**, *2*, 718–24.

(85) Wang, Y.; Zheng, D.; Tan, Q.; Wang, M. X.; Gu, L.-Q. *Nature nanotechnology* **2011**, *6*.

(86) Karhanek, M.; Kemp, J. T.; Pourmand, N.; Davis, R. W.; Webb, C. D. *Nano letters* **2005**, *5*, 403–7.

(87) Steinbock, L. J.; Otto, O.; Chimerel, C.; Gornall, J.; Keyser, U. F. *Nano letters* **2010**, *10*, 2493–7.

(88) Actis, P.; Mak, A. C.; Pourmand, N. *Bioanalytical reviews* **2010**, *1*, 177–185.

(89) Umehara, S.; Karhanek, M.; Davis, R. W.; Pourmand, N. *Proceedings of the National Academy of Sciences of the United States of America* **2009**, *106*, 4611–6.

(90) Fu, Y.; Tokuhisa, H.; Baker, L. a *Chemical communications (Cambridge, England)* **2009**, 4877–9.

(91) Actis, P.; Rogers, A.; Nivala, J.; Vilozny, B.; Seger, R. A.; Jejelowo, O.; Pourmand, N. *Biosensors & bioelectronics* **2011**, *26*, 4503–7.

(92) Berezovski, M.V; Krylov, S.N. Kinetic Capillary Electrophoresis **2008**.

(93) Liu, C. Y. *Electrophoresis* **2001**, *22*, 612–28.

(94) Birtwell, S.; Morgan, H. *Integrative biology : quantitative biosciences from nano to macro* **2009**, *1*, 345–62.

(95) Cao, Y.-C.; Liu, T.-C.; Hua, X.-F.; Zhu, X.-X.; Wang, H.-Q.; Huang, Z.-L.; Zhao, Y.-D.; Liu, M.-X.; Luo, Q.-M. *Journal of biomedical optics* **2014**, *11*, 054025.

(96) Fan, A.; Lau, C.; Lu, J. *The Analyst* **2008**, *133*, 219–25.

(97) Sochol, R. D.; Casavant, B. P.; Dueck, M. E.; Lee, L. P.; Lin, L. *Journal of Micromechanics and Microengineering* **2011**, *21*, 054019.

(98) Hyrup, B.; Nielsen, P. E. *Bioorganic and medical chemistry* **1996**, *4*, 5–23.

(99) Giesen, U.; Kleider, W.; Berding, C.; Geiger, a; Orum, H.; Nielsen, P. E. *Nucleic acids research* **1998**, *26*, 5004–6.

(100) Pellestor, F.; Paulasova, P.; Hamamah, S. *Current pharmaceutical design* **2008**, *14*, 2439–44.

(101) Brandt, O.; Hoheisel, J. D. *Trends in biotechnology* **2004**, *22*, 617–22.

(102) Kerman, K.; Matsubara, Y.; Morita, Y.; Takamura, Y.; Tamiya, E. *Science and Technology of Advanced Materials* **2004**, *5*, 351–357.

(103) Du, D.; Guo, S.; Tang, L.; Ning, Y.; Yao, Q.; Zhang, G.-J. *Sensors and Actuators B: Chemical* **2013**, *186*, 563–570.

(104) Cai, B.; Wang, S.; Huang, L.; Ning, Y.; Zhang, Z.; Zhang, G.-J. *ACS nano* **2014**, *8*, 2632–8.

(105) Ali, M.; Neumann, R.; Ensinger, W. *ACS nano* **2010**, *4*, 7267–74.

(106) Lan, W.-J.; Holden, D. a; Zhang, B.; White, H. S. *Analytical chemistry* **2011**, *83*, 3840–7.

(107) Steinbock, L. J.; Stober, G.; Keyser, U. F. *Biosensors & bioelectronics* **2009**, *24*, 2423–7.

(108) Stober, G.; Steinbock, L. J.; Keyser, U. F. *Journal of Applied Physics* **2009**, *105*, 084702.

(109) Gregg, E. C.; Steidley, K. D. *Biophysical journal* **1965**, *5*, 393–405.

(110) DeBlois, R. W. *Review of Scientific Instruments* **1970**, *41*, 909.

(111) Zohar, H.; Hetherington, C. L.; Bustamante, C.; Muller, S. J. *Nano letters* **2010**, *10*, 4697–701.

(112) Park, Y. D.; Hanbicki, a T.; Erwin, S. C.; Hellberg, C. S.; Sullivan, J. M.; Mattson, J. E.; Ambrose, T. F.; Wilson, a; Spanos, G.; Jonker, B. T. *Science (New York, N.Y.)* **2002**, *295*, 651–4.

(113) Hurst, S. J.; Lytton-Jean, A. K. R.; Mirkin, C. a *Analytical chemistry* **2006**, *78*, 8313–8.

(114) Martins, S. a M.; Prazeres, D. M. F.; Fonseca, L. P.; Monteiro, G. a *Analytical and bioanalytical chemistry* **2008**, *391*, 2179–87.

(115) Xin, Z.; Chen, J. *Plant methods* **2012**, *8*, 26.

(116) Gansauge, M.-T.; Meyer, M. *Nature protocols* **2013**, *8*, 737–48.

(117) Gao, Y.; Stanford, W. L.; Chan, W. C. W. *Small (Weinheim an der Bergstrasse, Germany)* **2011**, *7*, 137–46.

(118) Kudinha, T.; Kong, F.; Johnson, J. R.; Andrew, S. D.; Anderson, P.; Gilbert, G. L. *Applied and environmental microbiology* **2012**, *78*, 1198–202.

(119) Chai, S. J.; White, P. L.; Lathrop, S. L.; Solghan, S. M.; Medus, C.; McGlinchey, B. M.; Tobin-D'Angelo, M.; Marcus, R.; Mahon, B. E. *Clinical infectious diseases : an official publication of the Infectious Diseases Society of America* **2012**, *54 Suppl 5*, S488–97.

(120) Sánchez-Vargas, F. M.; Abu-El-Haija, M. a; Gómez-Duarte, O. G. *Travel medicine and infectious disease* **2011**, *9*, 263–77.

(121) Majowicz, S. E.; Musto, J.; Scallan, E.; Angulo, F. J.; Kirk, M.; O'Brien, S. J.; Jones, T. F.; Fazil, A.; Hoekstra, R. M. *Clinical infectious diseases : an official publication of the Infectious Diseases Society of America* **2010**, *50*, 882–9.

(122) Bremer H.; Dennis, P. Modulation of chemical composition and other parameters of the cell by growth rate **1996**.

(123) Yassin, A. F.; Müller, J. *Diagnostic microbiology and infectious disease* **2012**, *72*, 219–25.

(124) Wang, H.-Y.; Kim, S.; Kim, J.; Park, S.-D.; Uh, Y.; Lee, H. *Journal of clinical microbiology* **2014**, *52*, 1911–20.

(125) Masek, B. J.; Hardick, J.; Won, H.; Yang, S.; Hsieh, Y.-H.; Rothman, R. E.; Gaydos, C. a *The Journal of molecular diagnostics : JMD* **2014**, *16*, 261–6.

(126) Small, J.; Call, D. R.; Brockman, F. J.; Timothy, M.; Chandler, D. P.; Small, J.; Call, D. R.; Brockman, F. J.; Straub, T. M. *small* **2001**.

(127) DeAngelis, K. M.; Wu, C. H.; Beller, H. R.; Brodie, E. L.; Chakraborty, R.; DeSantis, T. Z.; Fortney, J. L.; Hazen, T. C.; Osman, S. R.; Singer, M. E.; Tom, L. M.; Andersen, G. L. *Applied and environmental microbiology* **2011**, *77*, 6313–22.

(128) Noguera, D. R.; Hatice, E. O.; Icrobiol, A. P. P. L. E. N. M. **2006**, *72*, 733–744.

(129) Fuchs, B. M.; Wallner, G.; Schwippl, I.; Ludwig, W.; Wallner, N.; Beisker, W.; Fuchs, B. M.; Schwippl, I.; Ludwig, W.; Amann, R. **1998**.

(130) Nelson, B. P.; Liles, M. R.; Frederick, K. B.; Corn, R. M.; Goodman, R. M. *Environmental microbiology* **2002**, *4*, 735–43.

(131) Li, X.; Morgenroth, E.; Raskin, L. *Applied and environmental microbiology* **2008**, *74*, 7297–305.

(132) Stender, H.; Broomer, A. J.; Oliveira, K.; Keefe, H. P.; Hyldig-nielsen, J. J.; Stender, H.; Broomer, A. J.; Oliveira, K.; Keefe, H. P.; Hyldig-nielsen, J. J.; Sage, A.; Coull, J. **2001**.

(133) Sun, C.-P.; Liao, J. C.; Zhang, Y.-H.; Gau, V.; Mastali, M.; Babbitt, J. T.; Grundfest, W. S.; Churchill, B. M.; McCabe, E. R. B.; Haake, D. a *Molecular genetics and metabolism* **2005**, *84*, 90–9.

(134) Kwon, J. H.; Fausone, M. K.; Du, H.; Robicsek, A.; Peterson, L. R. *American journal of clinical pathology* **2012**, *137*, 778–84.

(135) Nielsen, P. E.; Egholm, M.; Berg, R. H.; Buchardt, O. *Science (New York, N.Y.)* **1991**, *254*, 1497–500.

(136) Thomson, D. a C.; Dimitrov, K.; Cooper, M. a *The Analyst* **2011**, *136*, 1599–607.